Laboratory and numerical modelling studies of sediment flocculation processes in estuaries

Aisha Fowzi Mhashhash

B.Sc., M.Sc.

Cardiff School of Engineering
Cardiff University

Thesis submitted in fulfilment of the requirements for the degree of Doctor of Philosophy at Cardiff University

March 2018

DECLARATION AND STATEMENTS

DECLARATION

This work has not been submitted in substance for any other degree or award at this or any other university or place of learning, nor is being submitted concurrently in candidature for any degree or other award.

Signed ……..…... (candidate) Date…….…….

STATEMENT 1

This thesis is being submitted in partial fulfilment of the requirements for the degree of Doctor of Philosophy (PhD).

Signed ……..…. (candidate) Date…….…….

STATEMENT 2

This thesis is the result of my own independent work/investigation, except where otherwise stated, and the thesis has not been edited by a third party beyond what is permitted by Cardiff University's Policy on the Use of Third Party Editors by Research Degree Students. Other sources are acknowledged by explicit references. The views expressed are my own.

Signed ……..… (candidate) Date…….…….

STATEMENT 3

I hereby give consent for my thesis, if accepted, to be available online in the University's Open Access repository and for inter-library loan, and for the title and summary to be made available to outside organisations.

Signed ……..…. (candidate) Date…….…….

ABSTRACT

Surface water is one of the fundamental parts of the environment and needs to be protected from all pollution sources for human survival. Urban development and human activities have increased the contamination of coastal and estuarine water due to insufficiently treated sewage, runoff from fertilised agricultural area and lawns and releasing industrial pollutant directly into river and estuaries. Cohesive sediment in estuaries can act as either a source or a sink of many pollutants, such as nutrients and heavy metals. Understanding the interactions between sediment and nutrients in water bodies is important because high input rates of nutrients can negatively affect water quality. The prediction of both deposition and the resuspension of cohesive sediment in estuaries supports the understanding of their turbidity, which is important in terms of the biomass of these water bodies and many of the occurring biochemical processes and the morphological processes, which determine the suitability and maintenance of fairways and harbour basins. The complex ways in which hydrodynamic and biochemical parameters affect cohesive sediment are primary reasons for the poor representation of the deposition, erosion and settling of cohesive sediment processes in modelling tools within water estuaries. However, our current understanding regarding the accurate prediction of cohesive sediment transport processes is insufficient because of flocculation processes which occur under certain circumstances (e.g. the increase of salinity in the brackish zone of rivers, which leads to the formation of flocs that are both larger and less dense than individual particles). The phenomenon of flocculation is known to play a significant role in the sediment transport processes of settling, deposition and erosion of cohesive sediment.

There is no unique equation that can be universally used to predict the deposition and suspension rates of cohesive sediment because each estuary is dynamically and physically different from another and this is particularly true for the highly dynamic estuary e.g. Severn Estuary. Therefore, this study focuses on gaining a better understanding of the transport processes of cohesive sediment, including a better inclusion of the flocculation processes by developing a new settling velocity equation for cohesive sediment including flocculation processes as a function of hydrodynamic parameters. It also aims to apply this equation to a numerical model

and to test this refined model by simulating the flocculation phenomenon in the highly dynamic Severn Estuary.

This study employed an extensive experimental setup using a small scale particle image velocimetry (PIV) system. The experimental research was carried out using suspended sediment samples from the Severn Estuary in the UK. A PIV system and an image processing routine were used to measure both floc size distribution and settling velocity. The experimental results indicate that both the floc size and the settling velocity are controlled by the interaction between turbulence and salinity at salinities of less than 10 ppt. At a salinity either equal to or more than 10 ppt, both the floc size and the settling velocity were functions of only turbulent shear stress. The new equations were successfully applied in the Delft3D model; the model results show that they aptly were able to match with observed suspended sediment distributions throughout the estuary. Overall, the developed model can be regarded as a basic tool for being applied to help manage the suspended sediment processes in the Severn Estuary and for assessing the potential impact of climate change and human interference such as tidal renewable energy schemes in this water body.

DEDICATION

Dedicated to my lovely husband for his unconditional love and support

ACKNOWLEDGEMENTS

I would like to take this opportunity to express my deepest gratitude to all those who have made my study is possible.

I would like to express my immeasurable appreciation to my first supervisor, Dr Bettina Bockelmann-Evans, for her support, encouragement and continuous provisions that helped me so much for the completion and success of this study. I could not have successfully finished my thesis without her support.

I would like also to thank my second supervisor, Prof. Shunqi Pan. I appreciate his suggestions and valuable discussions.

I would like also to extend my gratitude to my sponsor, the Libyan Government, for their funding my study.

Further gratitude and appreciation is expressed to Cardiff University technical staff of the Hydraulics Cleer lab and Soil Mechanics Laboratories, for their assistance on technical matters in the laboratory. In particular, I would like deeply to thank Mr Malcolm Seabourne for designing the agitator.

I am also grateful to Dr Adri Mourits and Dr Ellis Penning for their answers about the Delft3D program.

Finally, I would like to thank my mum, brothers and sisters for their continued support, encouragement and love. My warm and special thanks go to my husband (Aasem) and my daughters (Ameera and Tasneim) for their support, encouragement and love. Without all of you, this work would not be finished.

Aisha Mhashhash

LIST OF PUBLICATIONS

- **Papers**
  1. Mhashhash, A., Bockelmann-Evans, B. and Pan, S. 2017. Effect of hydrodynamics factors on sediment flocculation processes in estuaries. *Journal of Soils and Sediments.*
  2. Mhashhash, A., Bockelmann-Evans, B. and Pan, S. 2018. A new settling velocity equation for cohesive sediment based on experimental analysis. *Journal of Ecohydraulics. Accepted for publication.*
- **Papers submitted**
  1. Mhashhash, A. and Bockelmann-Evans, B. 2018. Review of the governing factors controlling phosphorus concentrations in macro-tidal estuaries. *Journal of Continental Shelf Research.*
  2. Mhashhash, A., Bockelmann-Evans, B. and Pan, S. 2018. Modelling cohesive sediment flocculation in macrotidal estuaries. *Journal of Marine Systems.*
- **Publications in Preparation**
  1. Mhashhash, A., Bockelmann-Evans, B. and Pan, S. 2018. Experimental protocol for flocculation processes. *Journal of Visualized Experiments(JoVE)*
- **Conferences**
  1. Mhashhash, A., Bockelmann-Evans, B. N. and Pan, S. 2016. Explicitly salinity and sediment concentration on flocculation processes in estuaries. Presented at: *3rd International Symposium on River Sedimentation*, Stuttgart, Germany, 19-22 September 2016.
  2. Mhashhash, A., Bockelmann-Evans, B. N. and Pan, S. 2016. Effect of hydrodynamics factors on flocculation processes in estuaries. Presented at: *4th IAHR European Congress*, Liege, Belgium, 27-29 July 2016.

TABLE OF CONTENTS

LIST OF FIGURES

LIST OF TABLES

LIST OF SYMBOLS

Symbol	Meaning
$A^{(l)}$	Rouse number
A_i	Total area of the particle at size band i
A_T	Total area of all the particle size band
a	Van Rijn's reference height
a and b	Empirical values
C	Chezy value
$C^{(l)}$	Concentration of sediment fraction (l)
$C_a^{(l)}$	Reference concentration of sediment fraction (l)
$c_b^{(l)}$	Average sediment concentration in the near bottom computational layer
$C_{kmx}^{(l)}$	Average concentration of sediment fraction (l) at the reference layer cell
C_v	K- ε closure constant value
D	Diameter of the beaker
$D^{(l)}$	Deposition flux
$D_s^{(l)}$	Diameter of sediment fraction (l)
d	Floc size
d_i	Particle diameter
d_{50}	Median grain size
davg	Average floc size
dmax	Maximum floc size
$E^{(l)}$	Erosion flux
F_u	Turbulent momentum flux in x direction
F_v	Turbulent momentum flux in y direction
G	Velocity gradient
g	Gravitational acceleration
H	Total water depth

i	Size band
K	Turbulent kinetic energy
L	Mixing length
$M^{(l)}$	erosion parameter
M_u	External sources or sinks of momentum in x direction.
M_v	External sources or sinks of momentum in y direction
m_1	Mass of the density bottle
m_2	Mass of the bottle and dry soil
m_3	Mass of the bottle, soil and liquid
m_4	Mass of the bottle when full of liquid
n	Manning value
n_f	Fractal dimension
P_u	Hydrostatic pressure gradients in x direction
P_v	Hydrostatic pressure gradients in y direction
Q	Discharge
r	Radius
S	Salinity
S_{max}	Maximum salinity
T_S	Turbulent shear stress
T_{cw}	Maximum bed shear stress due to current and waves
$T_{cr,d}$	Critical shear stress of cohesive sediment for deposition
$T_{cr,e}$	Critical shear stress of cohesive sediment for erosion
t	Time
U	Depth averaged velocity in x direction
u	Fluid velocity component in the x direction
u'	Tangential velocity fluctuations
$\bar{u}$	Mean velocity
V	Depth averaged velocity in y direction
v	Fluid velocity component in the y
v'	Vertical velocity fluctuations
Ws	Settling velocity
$Ws^{(l)}$	Settling velocity of sediment fraction (l)
Wso	Median settling velocity

W_{Sf}^{l}	Settling velocity of sediment fraction (l) at fresh water
W_{Smax}^{l}	Settling velocity of sediment fraction (l) at maximum salinity concentration
w	Fluid velocity component in z direction
w'	Radial velocity
ω	Angular velocities
x, y and z	Coordinate system
Z	Elevation above the bed
z_{kmx}	Elevation at the centre of the reference layer cell
α'	Empirical parameter
$\alpha_1^{(l)}, \alpha_2^{(l)}$	Correction factor for sediment concentration
Δρ	Differential density
Δ_t	Difference in the times between the images
Δ_y	Difference between the distances of the front of the cloud on the images
Δz	Difference in the elevation between the centre of the reference layer cell and Van Rijn's reference height
ε	Energy dissipation
$\varepsilon_s^{(l)}$	Sediment diffusion coefficient
η	Kolmogorov microscale
ζ	Water depth above the reference planes
μ	Dynamic viscosity
υ	Water kinematic viscosity
ν_V	Vertical eddy coefficient
ρ	Fluid density
$\rho^{(l)}$	Relative density
ρ_e	Effective density
ρ_f	Flocs density
ρ_p	Particle density
ρ_w	Water density

LIST OF ACRONYMS

Acronym	Definition
CCD	Charge coupled device
EPS	Extra-cellular polymeric substances
ETM	Estuarine turbidity maximum
FSD	Floc size distribution
PIV	Particle image velocimetry
RMAE	relative mean absolute error
RMS	root mean square
SEM	Scanning electron microscope
SPM	Suspended particulate matter
SSCs	Suspended sediment concentrations
XRD	X-ray diffraction

1 Introduction

1.1 Dynamic processes in estuarine waters

Estuaries and coastal areas are defined as the zones between fresh and marine waters that are characterised by complex movement, which are caused by tidal currents and waves (Morris et al. 1995). Estuaries can act as sinks and sources of many pollutants that are related to economic growth and urbanisation, such as the dumping of sewage, rubbish and industrial wastes (Cai 2011; Xu et al. 2013). These pollutants, including nutrients and heavy metals, can accumulate in sediments due to physical, chemical and biological processes; they can also return to the water column after resuspension (Ittekkot 1988; Robins et al. 2016). This is further complicated by the presence of the estuarine front zone, which lies between fresh and saline water (Gebhardt et al. 2005).

The front zone plays a significant role in estuarine circulation, which is the tidal circulation and gravitational circulation due to differences between fresh and salt water, and affect among others sediment grain size distribution (Neill 2009; Robins et al. 2012). In a wide range of macrotidal estuaries, the estuarine turbidity maximum (ETM) zone is at the estuarine front zones (Wellershaus 1981; Burchard and Baumert 1998). The ETM zone is formed by a combination of high suspended sediment concentrations, high settling velocity and resuspension rates of the bottom deposition of suspended sediment (Le Bris and Glémarec 1996). This zone of high suspended sediment concentrations represents a typical area for physical, chemical and biological processes' interactions of dissolved matter, nutrients and suspended sediment (Gebhardt et al. 2005).

Flocculation of suspended sediment has been observed in the ETM zone. Two interpretations are possible due to high sediment concentration in the ETM zone: (1) The flocculation processes are enhanced due to higher concentrations of particles (Nichols 1984; Lang et al. 1989; Lick et al. 1993). (2) Due to sediment flocculation processes, larger aggregates, which have a high settling velocity, are formed. Under changing conditions in shear, these aggregates tend to break down once they reach the estuary's bed. They are also easily resuspended in the water column, which forms part of the turbidity maximum zone (Gebhardt et al. 2005). The intensity and location of ETM zone are affected by highly variable velocity conditions during the tidal cycles, tidal range magnitude, the passing of fresh water flow over a more dense

saline layer, shape, the bathymetry of the estuary and the strength and frequency of the river flow, which is projected to be more variable in the UK with climate change (Uncles and Stephens 1993; Burchard and Baumert 1998; Mitchell 2013; Robins et al. 2016).

Sea level rise as predicted due to climate change could have a significant effect on estuarine functioning (Whitehead et al. 2009). The combination of sea level rise and low river flow could potentially lead to saline intrusion and changes to the ETM zone, which would push them further up the estuary and retain river borne substances in the estuary for extended periods and lead to changes of the bathymetry. By contrast, increased river flows can push the saline intrusion down the estuary, which flushes pollutants and nutrients offshore more quickly (Robins et al. 2014). The reproductive success among other important habitat conditions of estuarine biota is sensitive to saline intrusion and corresponding turbidity maxima, which are projected to gradually shift landwards as a result of sea level rise. Also, the deposition of sediment and the concentration of suspended material in the water may affect the siltation pattern in ports and harbours, and require the need for dredging and the effective disposal of dredged material (Mitchell 2013).

1.2 Classification of sediment transport

Sediment transport by water flow can be classified into suspended and bed load types (Figure 1.1). Suspended load is the transport mechanism in the water column, as the transported particles are small and easily suspended by the water current. Bed load is transported along the bed by the processes of rolling, sliding and hopping (Dyer 1986). Sediment transport can be classified by particle size into cohesive and non-cohesive sediments. Cohesive sediment, such as mud or clay, has a particle size typically ranging from 0.98–63.0 μm. Cohesive sediments are regarded as one of the most important features of estuaries around the world. These sediments consist of organic and inorganic materials, the former including plant and animal detritus and bacteria. These materials alter how particles hold on to each other and how larger particles sometimes form aggregates of up to 1 mm in size by flocculation processes which are discussed in Chapter 2. (Mikes et al. 2004). Non-cohesive sediment, such as sand, has a particle size more than 63 μm and consists mainly of inorganic

materials (Hjulström 1935). This study is focused on cohesive sediment which is universally called mud (a mixture of clay and silt with water).

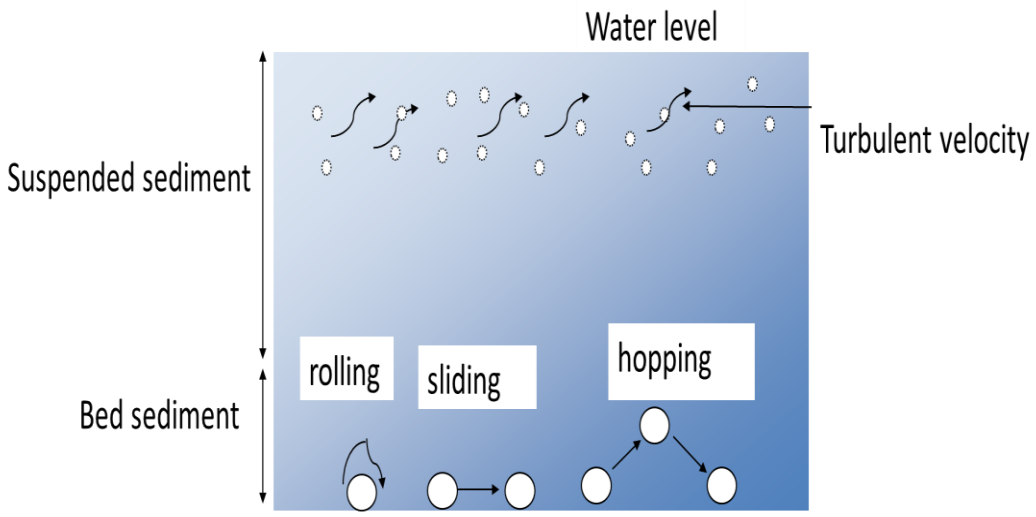

Figure 1.1 Sediment particles' motion, adopted from (Smithson et al. 2002)

1.3 Electrochemical properties of cohesive sediment

The cohesion of fine sediment (clay) is the result of its electrochemical properties. Clay can be described as a specific crystal structure with a high surface area, which can act as an important site for the adsorption of both organic material and metals. The flat side of a clay particle is many times larger than its edges, and it has an excess negative charge (versus the edges, which have a positive charge), which can be chemically balanced by the adsorption of cations from water (Figure 1.2). Isomorphous substitution is an important factor in both the structure and properties of clay minerals. Clay particles usually have a net negative charge. To maintain electrical neutrality, particles attract cations, which are either adsorbed onto the surface or absorbed between the clay layers as they are stacked together. Many adsorbed cations can be replaced by others. Through this exchangeable cation process, clay minerals and particulate organic material can take up cations from a solution and release an equivalent amount of other cations into the solution (Harrison 2007). Clay mineral particles in the water column are flocculated via the ionic

charges on their surfaces and the free ions of dissolved salt that form aggregates of a different size, density, composition and structure. The mechanisms responsible for this dynamic are the flocculation and deflocculation processes, which are treated in greater depth in Chapter 2.

.

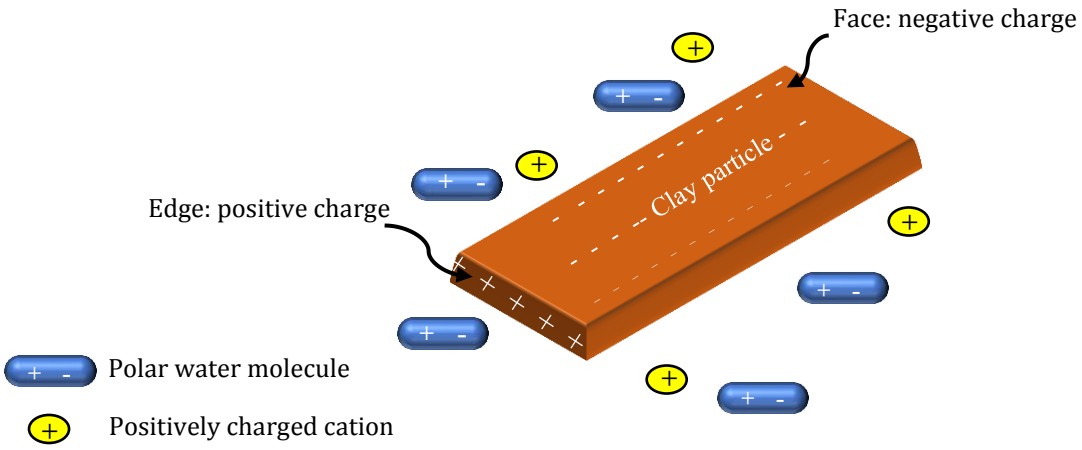

Figure 1.2 Clay particle with water molecules, modified from (Dunn et al. 1980)

1.4 Dynamics of cohesive sediment

The processes of cohesive sediment transport in estuarine waters, including erosion, deposition, resuspension, flocculation and consolidation are illustrated in Figure 1.3. These processes are controlled by physical, chemical and biological processes (Manning et al. 2010b; Wang and Andutta 2013), which are only partly understood (Whitehouse et al. 2000). The quality of the water environment and cohesive sediment concentrations are closely related. High cohesive sediment concentrations in coastal waters are recognised as a worldwide ecological issue (Thompson et al. 2014). In the Severn Estuary, for example, cohesive sediment causes an extremely high suspended sediment concentration in the water column. Parker and Kirby (1982), cited by Manning et al. (2010a), proposed that Bridgewater Bay is the most significant source of fine sediment to the Severn Estuary, which then moves up and

down the estuary with the tides, causing high turbid water. Cohesive sediment can also play an active role in adsorbing and releasing pollutants such as heavy metals and nutrients in the water column (Ackroyd et al. 1986).

A distinctive feature of estuaries is the bed mud layer which forms as a result of deposition of sediment on the bottom. Under different hydrodynamic conditions such as high spring current speed, cohesive sediment can be eroded and deliver nutrients to the system (Gratiot and Manning 2004). This can lead to estuarine eutrophication, which is characterised by reduced dissolved oxygen levels and increased growth of algae. Decomposition of an excessive amount of algae in aquatic ecosystems contributes to the reduction of oxygen levels, which may cause the death of fish and other aquatic organisms and can have a negative effect also on human health (Carpenter et al. 1998).

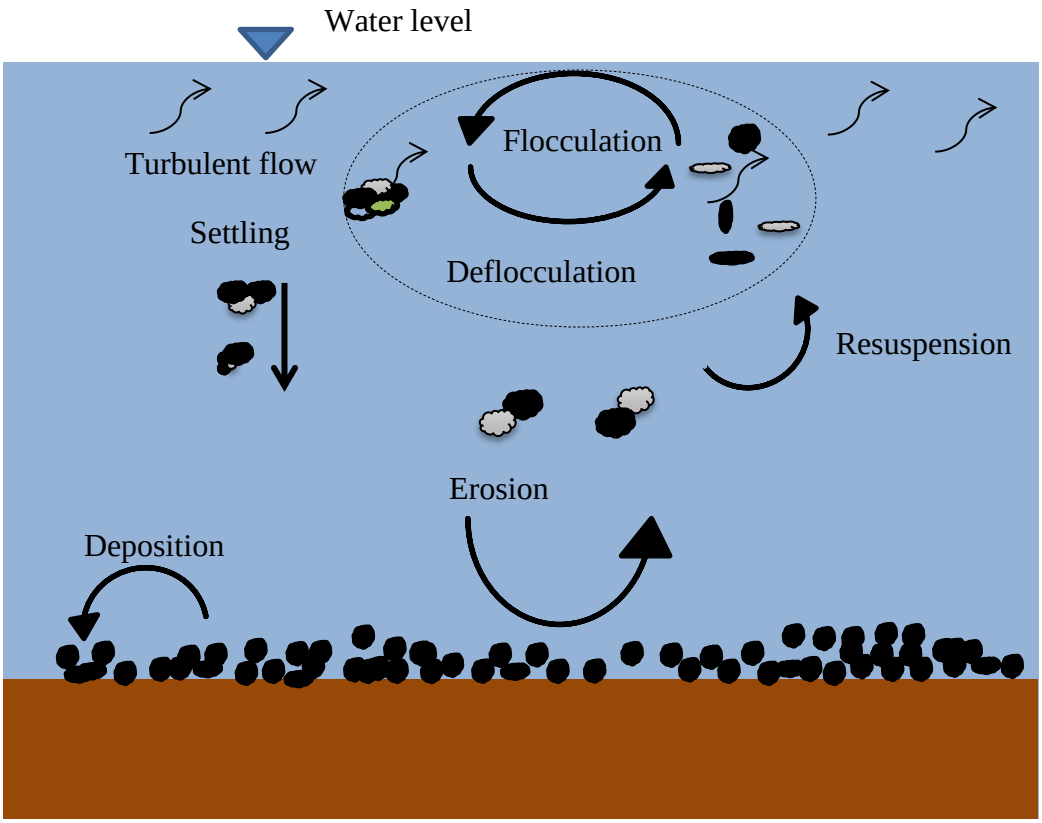

Figure 1.3 Sediment particles' motion, adopted from (Maggi 2005)

The prediction of suspended sediment amounts and the deposition of cohesive sediment in estuaries are key aspects of their management regarding the maintenance

of fairways and harbour basins, their turbidity and water quality and their suitability. In estuaries and coastal areas, cohesive sediments have an ability to form large aggregates, namely flocs, which are larger but less dense than individual particles. The formation of flocs near the surface decreases the penetration of solar radiation in the water column, which constrains the production of plankton. This phenomenon (flocculation) is the most significant process that distinguishes cohesive sediment from non-cohesive sediment transport and it poses a serious complication to modellers of estuarine sediment dynamics.

The settling velocity of cohesive sediment is the main parameter impacting on the fate and transport of the concentration of cohesive sediment (Johansen 1998). In dynamic water environments, such as estuaries, the settling velocity can vary significantly as a result of flocculation processes, which makes estimation of settling velocity and settling rates complicated (Van Leussen 1994). Estimation of the settling velocity of cohesive sediment via Stoke's law is not possible, due to dynamically changing sizes, shapes and densities of cohesive sediments affected by flocculation processes (Geyer et al. 2004). Because the transport of sediment in the Severn Estuary is based on grain size distribution (Manning et al. 2010a), it is necessary to consider the cohesive sediment flocculation processes. Accurate simulations of cohesive sediment processes for scenarios of climate change, global sea level rise and damming projects (e.g. tidal renewable energy schemes) (Etemad-Shahidi et al. 2010) are highly desirable for future management of estuarine and coastal waters.

The international scientific literature contains many laboratory and field studies that focus on flocculation processes in different estuaries. However, among these, few have researched the flocculation characteristics in the highly dynamic macrotidal Severn Estuary (Bryant and Williams 1983; Dyer and Manning 1999); this is an area that is not fully understood. Further investigation is required to determine how sediment flocculation in the Severn Estuary responds to different hydrodynamic parameters, e.g. turbulent mixing (Manning et al. 2010a). Therefore, a good understanding of the sediment transport processes in this type of aquatic coastal environment is essential. The use of laboratory studies can provide a more controlled environment whereby the flocculation phenomena can be researched in greater detail and under controlled conditions.

This project aims to create a flocculation model of highly dynamic estuaries, particularly the Severn Estuary, which could be used to assess the potential impacts of marine renewable energy projects that have been proposed for the Severn Barrage. It also aims to provide robust tools for the accurate prediction of suspended sediment concentrations (SSCs) and deposition to improve our understanding of estuarine bathymetry changes and contaminant transport processes as well as to improve the management of estuarine and coastal waters under future stresses, such as climate change.

1.5 Aims and objectives

The main purpose of this study is to gain a better understanding of the transport processes of cohesive sediments in dynamic estuaries where flocculation processes are occurring by developing a new settling velocity equation for cohesive sediment as a function of hydrodynamic parameters while flocculation processes occur and to refine a numerical model with this equation and use the refined model for the Severn Estuary.

Objectives of thesis

1. To collect and analyse sediment and water samples from the Severn Estuary.
2. To set up, calibrate and validate a Particle Image Velocimetry system (PIV).
3. To mimic the flocculation phenomenon in the laboratory based on field samples.
4. To define the important hydrodynamics factors' effects on the flocculation phenomenon and to measure floc size distribution and settling velocity of cohesive sediment while flocculation occurs.
5. To establish a new settling velocity equation for cohesive sediment while flocculation occurs as a function of the defined hydrodynamics parameters. This task is carried out by analysing the experimental data using Minitab statistical analysis.
6. To set up the numerical model, namely Delft3D.
7. To calibrate and validate the model based on field data.
8. To refine the numerical model to include new settling velocity equations developed from experimental laboratory and field data.
9. To apply and test the refined numerical model in simulating flocculation in the Severn Estuary.

10. To run the numerical model with the original flocculation equations from literature, and compare the results with the new flocculation model's results and field data.

1.6 Outline of thesis

The overall structure of the thesis takes the form of six chapters. Chapter 1 presents a brief background and highlights the aims and objectives of the study. Chapter 2 begins with a comprehensive literature review of the theory of cohesive sediment, flocculation mechanisms and the important techniques for observation of flocculation processes. Chapter 3 describes the study area and field data analysis. Also, it provides experimental setup, the procedure used to mimic the flocculation phenomenon and the effect of hydrodynamics factors on flocculation processes. This chapter has been published as two journal papers and one conference paper. Chapter 4 describes the governing equations of flow and sediment modules within the model used and refined in this study. Chapter 5 describes the model setup, calibration and validation processes. The results of chapter 3 were used in chapter 5 to refine the model to test inclusion of the new settling velocity of cohesive sediment. Chapter 6 represents the main conclusions of the study and recommendations for future research.

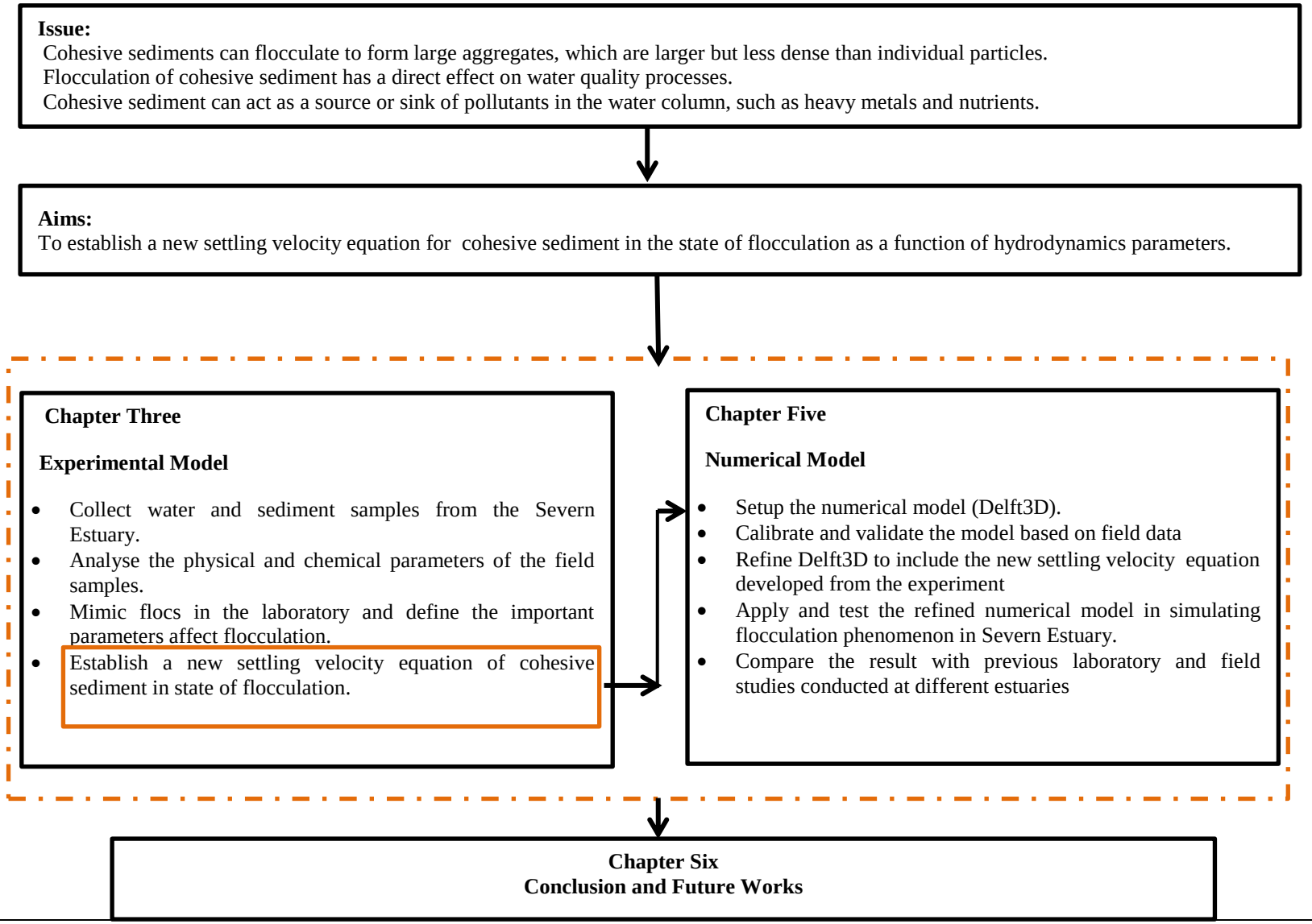
Issue:
Cohesive sediments can flocculate to form large aggregates, which are larger but less dense than individual particles.
Flocculation of cohesive sediment has a direct effect on water quality processes.
Cohesive sediment can act as a source or sink of pollutants in the water column, such as heavy metals and nutrients.
Aims:
To establish a new settling velocity equation for cohesive sediment in the state of flocculation as a function of hydrodynamics parameters.
Chapter Three
Experimental Model
Collect water and sediment samples from the Severn Estuary.
Analyse the physical and chemical parameters of the field samples.
Mimic flocs in the laboratory and define the important parameters affect flocculation.
Establish a new settling velocity equation of cohesive sediment in state of flocculation.
Chapter Five
Numerical Model
Setup the numerical model (Delft3D).
Calibrate and validate the model based on field data
Refine Delft3D to include the new settling velocity equation developed from the experiment
Apply and test the refined numerical model in simulating flocculation phenomenon in Severn Estuary.
Compare the result with previous laboratory and field studies conducted at different estuaries
Chapter Six
Conclusion and Future Works

2 Literature Review

2.1 Introduction

This chapter provides a literature review of previously undertaken research that is relevant to the field of study. The first section reviews the hydrodynamic parameters that affect particle formation and disaggregation, followed by the most recent research regarding flocs' properties, including size, settling velocity and density. Section 2.4 reviews the techniques used to observe the flocculation processes, both in situ and in the laboratory. Section 2.5 presents relevant numerical modelling studies. Finally, section 2.6 reviews the hydrodynamics and sediment transport in the Severn Estuary. The objectives of the reviews are as follows:

1. To collect information from recent studies on the important hydrodynamic parameters that affect flocculation processes (i.e. size, settling velocity and density);
2. To review the important techniques used to observe the flocculation processes; and
3. To identify gaps in the knowledge and consider how the transport processes of cohesive sediment exposed to flocculation processes can be better understood and improved by developing a settling velocity equation.

2.2 Overview of particle formation and disaggregation

Cohesive sediment has the ability to flocculate into large aggregates, namely flocs, which are bigger than individual particles but less dense. These aggregates form when two or more particles collide and stick together, and disaggregation occurs when particles break down into two or more fractions. The two processes can occur in a water body that is exposed to changing physical, chemical and biological parameters (Eisma 1986; Soulsby 1997; Dyer and Manning 1999; Thomsen and Gust 2000; Manning 2001; Spearman et al. 2011; Mohapatra et al. 2012). The collision of sediment particles occurs due to three different mechanisms, as assessed by Van Leussen (1988):

Brownian motion

Brownian motion is defined as the random movement of the particles resulting in the bombardment of flocs by thermally agitated water molecules. This mechanism is affected by temperature, particle size and viscosity. Lick et al. (1993) found that Brownian motion is only effective for particles of less than one micron in size. Floc structures formed by Brownian motion are weak, which means that they are either easily dispersed by shearing or crushed on deposition.

Differential settling

Differential settling is defined as the differential interaction between particles, where larger particles have larger settling velocities; therefore, they can sweep past smaller particles. Lick et al. (1993) found that differential settling mechanisms significantly promote floc growth. Differential settling is only effective during low turbulent conditions, such as in slack water (Van Leussen 1988; Manning and Dyer 1999).

Turbulent motion

Turbulent stress is a dominant mechanism of particle contact due to rapid variation of fluid velocity and pressure. Although quantitative formulations for these mechanisms are described in the literature (e.g. Van Leussen 1988 and Winterwerp 1998), it is recognised that Brownian motion can be negligible in comparison with differential settling and turbulence mechanisms.

In addition, the flocculation mechanism is affected by other parameters such as pH, temperature, sediment concentration, salinity and mineralogical composition (Winterwerp 1999; Mohapatra et al. 2012; Liang et al. 2013), which can alter the suspended sediment particle by modifying its effective particle size, shape, porosity, density and composition. All these parameters are highly variable in estuaries, where tidal forcing induces variations in shear stress, and where fresh water mixes with saline water (Mietta et al. 2009). The most influential parameters of floc size and settling velocity are salinity, suspended sediment concentration (SSC) and turbulence, which have been considered in previous studies and are discussed below.

2.2.1 **Salinity (S)**

As discussed in Chapter 1, clay particles have a net negative charge and a large surface area, which encourage their ability to adsorb organic materials and metals (Harrison 2007). The availability of free ions in fresh water is low, and the clay particles collide when bringing an edge (positive charge) to a negative charge face to allow the Van der Waals force to bind them (face to edge); this is a weak floc structure with large porosity, low density and low strength. As salinity increases in estuaries, the ions increase in abundance, and an ionic double layer is created by binding clay particles (face to face) with larger floc structures, which are stronger than a face to edge connection (Fennessy 1994). However, the double layer's diffusion is suppressed, and it shrinks due to increasing the electrical repulsion force, which occurs because of high ionic concentration (high salinity).

The critical salinity level at which flocculation begins to increase varies from study to study. Verney et al. (2009) studied the effect of turbulence, sediment concentration, salinity, organic matter and diatom bloom on the flocculation processes using suspended sediment from the Seine Estuary using videoing facilities in the laboratory, a similar method to the one used in this study. They demonstrated that salinity's influence on the flocculation process is unclear based on two contrasting salinities of 0 and 20 ppt, whereby diatom blooms, sediment concentration and turbulence are the effective parameters. The sediment concentration and diatom bloom enhance both the flocculation speed and flocculation efficiency. The turbulent shear stress controls the maximum floc size by breaking down flocs larger than the size of the smallest turbulent vortices measured by the Kolmogorov microscale. Other authors did not observe variations in floc size at salinities higher than 10 ppt (Gibbs and Konwar 1986; Sutherland et al. 2015), 2.5 ppt (Wollast 1988) and 15 ppt (Mietta et al. 2009). Nasser and Twaiq (2011) explained that any further increase in salinity level reduces the repulsive force between the face and the edge of the floc, which lead to relatively small, weakly structured flocs. Van Leussen (1999) observed an increase in floc size and settling velocity for increasing salinity within the Ems Estuary. Similar laboratory results were observed by Portela et al. (2013), where increasing salinity enhances the settling velocity by a factor of 6.5 between fresh and high saline water. In addition, laboratory experiments by Burban et al. (1989) showed that for the same floc size,

turbulent shear stress and sediment concentration, the settling velocities of flocs in freshwater are somewhat greater than the settling velocities of flocs in freshwater.

2.2.2 **Suspended sediment concentration (SSC)**

The influence of suspended sediment concentrations (SSCs) on the flocculation processes has been widely studied in both the field and laboratory environments. Many researchers have reported that SSCs have a negative correlation with floc size. The experimental work of Tsai et al. (1987) showed that the equilibrium of the floc size decreases when increasing SSCs from 50 g/m^3 to 800 g/m^3 at a shear stress of 200 s^{-1}. Burban et al. (1989) observed that floc size decreases as the sediment concentration increases in saline water. Similarly, Manning and Dyer (1999) found that floc size decreases with increasing SSCs in the Tamar Estuary by using an in situ settling velocity instrument (INSSEV). After conducting image analysis via a silhouette camera, Berhane et al. (1997) found contrasting in situ results, which revealed that maximum floc size increases with increasing SSCs on the Amazon Shelf.

In terms of settling velocity, the effects of both sediment concentration and salinity on settling velocity were studied in a laboratory using a rectangular tank of 30 cm height by Sutherland et al. (2015). The authors found that increasing salinities above a 20 ppt did not show any appreciable increase in settling velocity. However, the settling velocity depended strongly on SSCs, with the settling velocity decreasing as the SSCs increase (Figure 2.1).

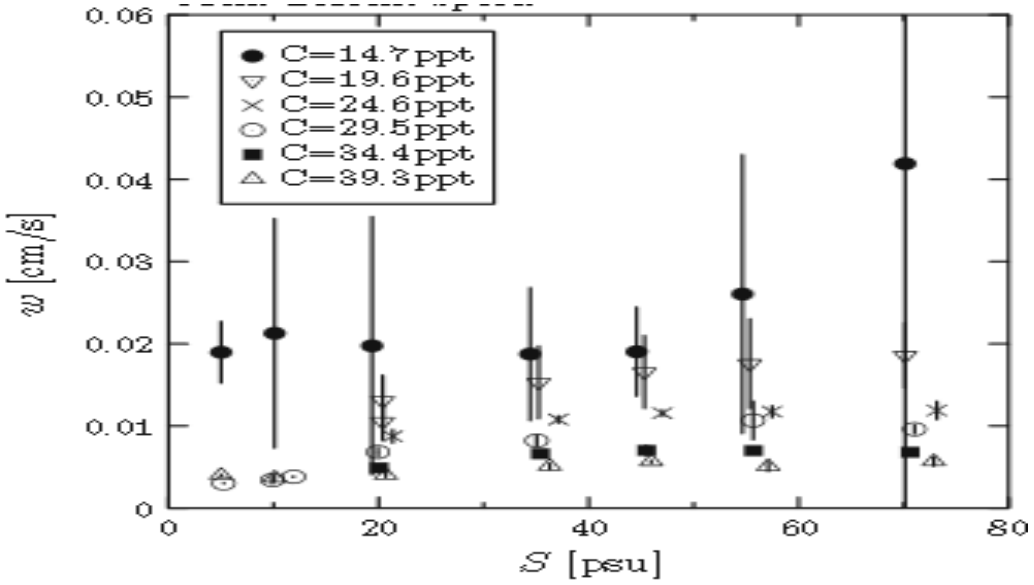

Figure 2.1 Settling velocity as a function of sediment concentration and salinity, different symbols correspond to different clay concentrations as indicated in the legend. Points are drawn at the mean value with vertical lines indicating error estimates (Sutherland et al. 2015)

2.2.3 **Turbulent shear stress (T_S)**

Turbulent shear stress is produced by moving of the water due to tidal regime that contributes to mixing of the fluid in estuaries. Turbulent shear stress has a double role in flocculation processes. It can cause floc growth as well as breakup because low turbulence levels can encourage particles to aggregate by increasing the collision rates between suspended particles. High levels of turbulence can cause a breakup of the flocs due to shear forces, thereby decreasing their size (Van Leussen 1996; Mikes et al. 2004; Manning et al. 2010b; Wang et al. 2011).

A number of authors have conducted both in situ and laboratory experiments to determine how flocculation processes change in turbulent environments. Van Leussen (1999) studied laboratory and field measurements of the Ems Estuary and concluded that floc growth could be affected by both turbulence and sediment concentration through an increased number of particle collisions, whereby the biological and physicochemical parameters affect the efficiency of the collisions. The floc breakup can occur when the local fluid shear stress exceeds the floc shear strength (Winterwerp 1999; Manning 2001). Dyer (1989) found that increasing

turbulent shear stress encourages particles to become aggregates until they reach a maximum size due to the increasing collision frequency between the particles, which in turn increases the settling velocity (Winterwerp 1998). With further increases in turbulent shear stress, the floc size begins to decrease because the internal bonds among the particles are weak and thus break easily. The author summarised that achievement of maximum floc size at low turbulent shear stress depends on the SSC. Therefore, he proposed a schematic description of floc size as a function of both the parameters of turbulent shear stress and SSC (Figure 2.2).

The floc size increases with increasing SSC at low turbulent shear stress; however, after that point, the increasing SSC decreases the floc size because, at a high SSC, the flocs are likely to bump into one another more frequently and subsequently cause a floc to break down. The conceptual model described by Dyer (1989) was confirmed by other authors (e.g. Van Leussen 1998; Manning and Dyer 1999). Manning and Dyer (1999) concluded that flocculation is enhanced at low turbulence and low concentration, whereby high turbulence shear stress above 0.3 N/ m^2 causes a decrease in floc size (Figure 2.3). This was based on experimental laboratory work using SSC from the Tamar Estuary, including SSC ranges of 80–200 g/m^3 and turbulent shear stress ranges of 0.1 N/m^2 – 0.6 N/m^2.

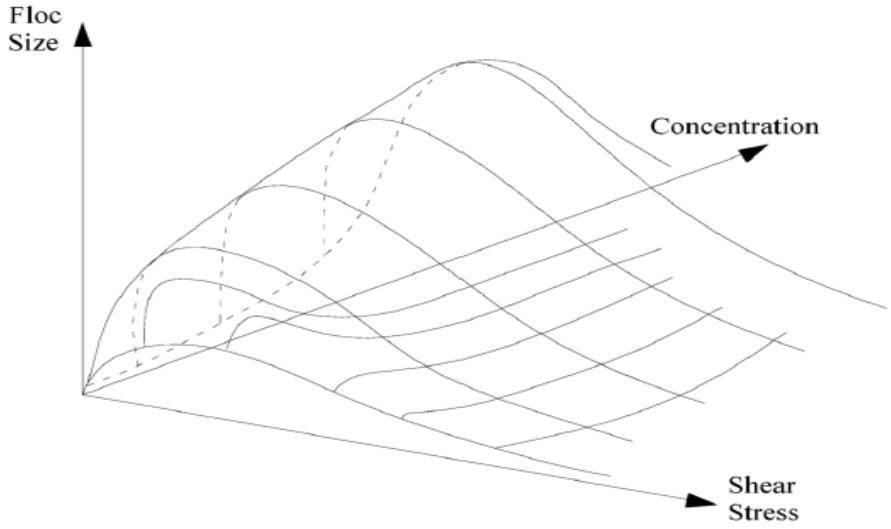

Figure 2.2 Conceptual flocculation diagram showing the relationship between floc size, suspended sediment concentration and shear stress (Dyer, 1989)

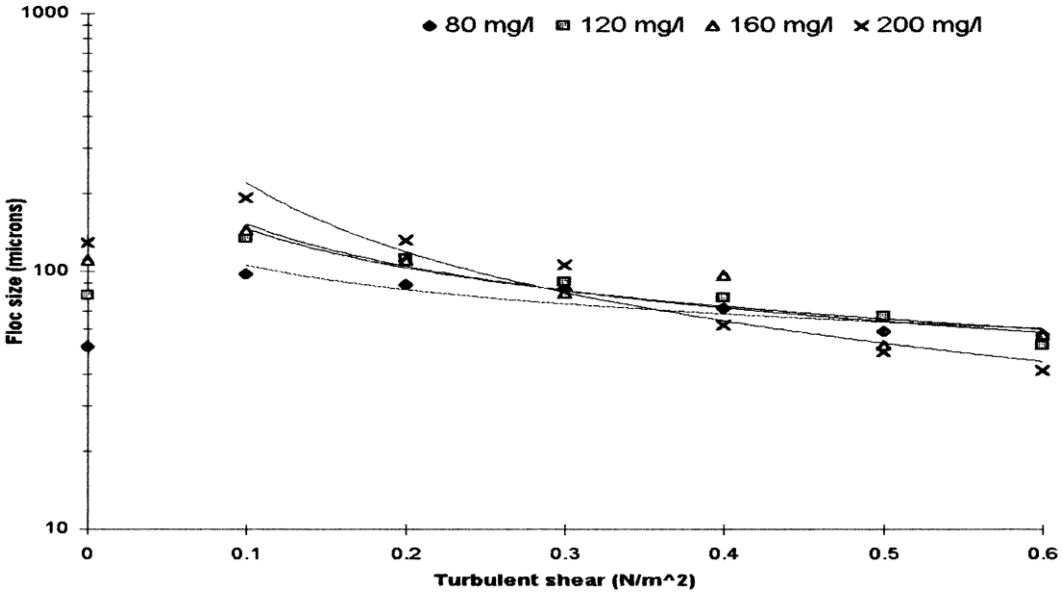

Figure 2.3 Floc size for various concentrations (different symbols) against turbulent shear, derived from laboratory experiments by Manning and Dyer (1999)

Some authors have related turbulent shear stress to the Kolmogorov microscale (η), which defines it as the size of the smallest turbulent eddies. This is further described in Chapter 3 (section 3.4.2). Verney et al. (2009) found that flocs cannot be larger than the Kolmogorov microscale because they would then be broken into small aggregates. By contrast, other studies have shown that flocs can be larger than the Kolmogorov microscale. For example, Berhane et al. (1997) showed that the maximum floc size (dmax) is approximately one and half times that of the Kolmogorov microscale, which ranges from 500–2,000 μm. Manning (2001) observed that, at spring tide, flocs develop and continue to grow in response to increasing SSCs to the point where the maximum floc size is between two to three times that of the Kolmogorov microscale. More recently, in situ results by Cross et al. (2013) observed that flocs exceed the Kolmogorov microscale at the Western English Channel. The authors explained that larger flocs may have formed due to biological activity.

2.2.4 **Other factors**

Other factors could be considered in the flocculation process, such as temperature and biological activity. The latter includes the presence of extra-cellular polymeric substances (EPS). Notably, the sediment can be more cohesive due to sticky EPS,

which is secreted by diatoms that promote the aggregation of particles. These then increase both the size and strength of the flocs (Winterwerp and van Kesteren 2004). When these biological processes bind sediment particles, it allows non-cohesive sand particles to flocculate and thus become part of flocs with cohesive sediment (Spearman et al. 2011). Temperature also affects clay aggregates; however, in estuaries, the temperature effect is considered small (Partheniades 1971). This study focuses on the influence of electrostatic force as the main factor in the formation of mud flocs.

2.3 Floc properties

Flocculation processes pose a serious complication to modellers of estuarine sediment dynamics. Floc size, settling velocity and floc density have been identified as the most important parameters for modelling sediment and contaminant transport (Droppo et al. 1997; Cheviet et al. 2002). A brief description for each of these parameters is discussed below.

2.3.1 **Floc size**

Flocs are marked by complex geometrical features, where two or more particles merge. This repeats several times, resulting in an aggregate that displays a porous cluster structure with properties that differ from the primary particles (Kranenburg 1994). Flocs are composed of up to 10^6 individual particulates. In general, flocs are classified into two types: microflocs and macroflocs (Figure 2.4); cohesive sediment flocculates to form small microflocs, followed by further growth into macroflocs, which are a combination of the microflocs (Eisma 1986). Many authors have offered a wide range of the size that divides microflocs and macroflocs, such as Eisma (1986), who suggested 125 µm, Manning and Dyer (1999) who suggested 160 µm and Lafite (2001), who suggested 100 µm. The state of microflocs continually changes in response to existing hydrodynamic parameters, physicochemical properties and environmental conditions. These microflocs can develop into larger flocs (macroflocs), which behave very differently, examples of real flocs are shown in Figure 2.5.

The majority of the literature agrees that macroflocs have a diameter larger than 100 µm and a settling velocity between 1–15 mm s^{-1}. Macroflocs are unstable structures

with varying shape and density and highly porous structure. Porosities (water content) are commonly 95% for the macroflocs and 90% for the microflocs (Fennessy et al. 1994; Van Leussen 1994; Manning and Dyer 1999; Whitehouse et al. 2000; Lafite 2001; Manning 2001; Manning 2004b; Manning and Dyer 2007; Manning et al. 2010b; Manning and Schoellhamer 2013; Soulsby et al. 2013; Mehta 2014). The highly porous fragile floc structure is easy to break up when water is collected from the estuary by using a traditional sampling method (e.g. use of water bottles) for particle size analysis in the laboratory (Eisma et al. 1983; Eisma 1986; Van Leussen 1988). This decrease of the real floc size contributes to serious implications for the calculation of the settling velocity via the Stokes' law. This is the main problem for the modelling and prediction of estuarine suspended sediment processes. Kranck and Milligan (1992) observed that, in the majority of estuarine conditions, most suspended particulate matter (SPM) within an estuary occurs in the form of flocs.

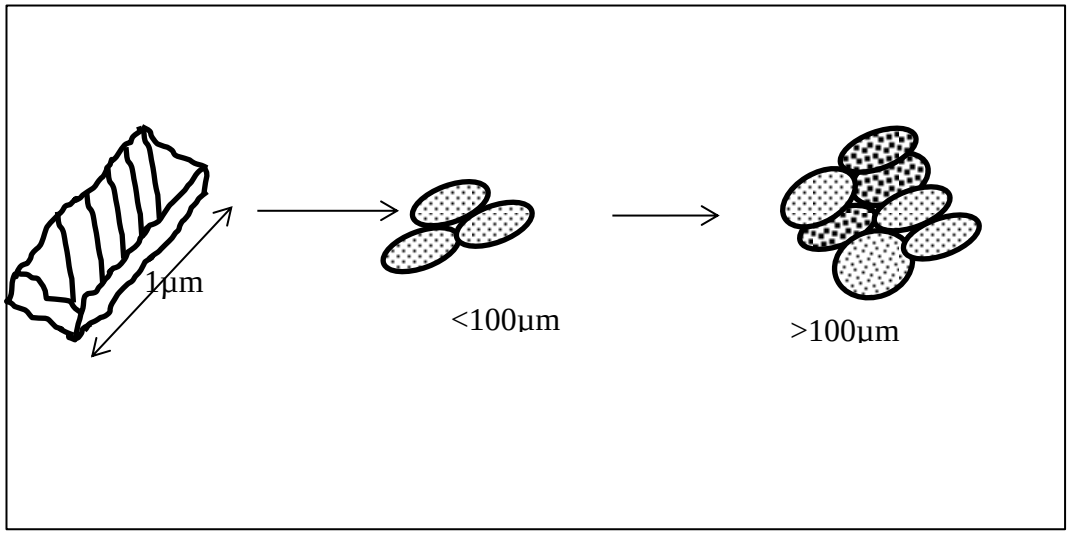

Figure 2.4 Sizes of clay particles, microfloc and macrofloc, adopted from (Manning 2001)

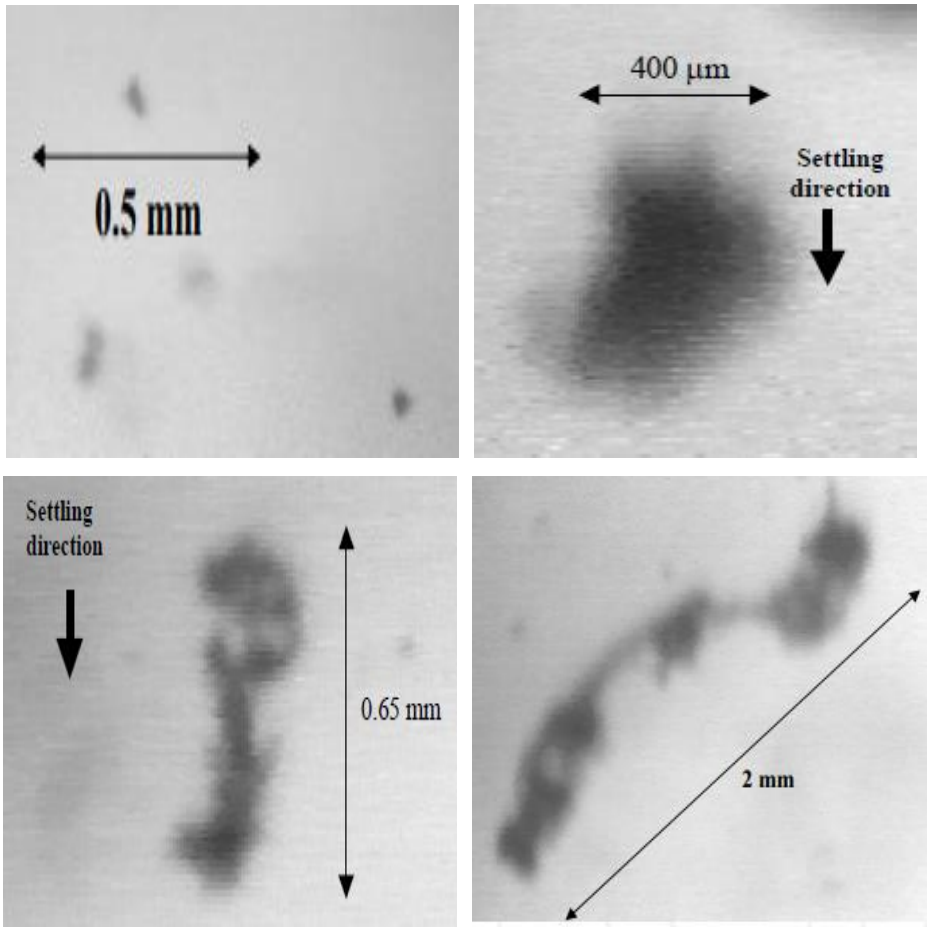

Figure 2.5 A selection of real floc images showing the variability of sizes and shapes, (Manning 2004b)

2.3.2 **Settling velocity**

Settling velocity is one of the main parameters that is used to determine deposition and resuspension rates of suspended sediment in either still or flowing water. The settling velocity of non-cohesive sediment is a simple process and it can be calculated straightforwardly using Stokes' law, which is defined as

$$Ws = \frac{g d_i (\rho_p - \rho_w)}{18\mu} \qquad \textbf{(2.1)}$$

where Ws is settling velocity, ρ_p is particle density, ρ_w is water density, g is gravitational acceleration, d_i is particle diameter and μ is dynamic viscosity.

Stokes' formula is only applicable to spherical particles and when the Reynolds number, which defines as the ratio of the inertia to viscous force, is less than one.

$$\mathrm{Re} = \frac{\rho \bar{u} l}{\mu} \qquad \textbf{(2.2)}$$

Where Re is the Reynolds number, ρ is the fluid density, ū is the mean average velocity and l is the characteristic length scale.

Estimating the settling velocity of cohesive sediment within an estuarine environment is highly complicated because cohesive particles can flocculate and form irregular floc shapes (Manning and Dyer 1999). calculating settling velocity of cohesive sediment from particle size using equation (2.1) is implausible, because settling velocities of fine sediment can vary over a range of several orders in magnitude. This variation is caused by different parameters such as sediment concentration, turbulence and salinity, as discussed early in this chapter (Krone 1962; Van Leussen 1997; Van Leussen 1999; Mikes et al. 2004; Manning et al. 2010b; Pejrup and Mikkelsen 2010). Three decades ago, an attempt was made (using an Owen tube) to measure settling velocity of cohesive sediment in situ as a function of SSC ranging up to 10 kg/m^3 (Owen 1976), which led to the development of the following equation

$$\mathrm{Wso} = \mathrm{a}\ \mathrm{SSC}^{\mathrm{b}}, \qquad \textbf{(2.3)}$$

where Wso is the median settling velocity, SSC is suspended sediment concentration and a and b are empirical values.

Another mathematical model including the effect of turbulence has been proposed by Van Leussen (1994), which can be expressed as

$$\mathrm{Ws} = \mathrm{Wso}\ \left(\frac{1 + \mathrm{aG}}{1 + \mathrm{bG}^2}\right) \qquad \textbf{(2.4)}$$

where Ws is the settling velocity, a and b are empirical values and G is the velocity gradient, which can be determined by taking the square root of turbulent energy dissipation rate divided by kinematic viscosity.

More recently, Winterwerp (1998) has modified the Stokes' law to include the fractal dimension (n_f), as:

$$\mathrm{Ws} = \alpha' d_i^{3-nf} \frac{(\rho_s - \rho_w)}{\mu} d^{nf-1} \quad \textbf{(2.5)}$$

Where α' is empirical parameter, μ is molecular viscosity, n_f is fractal dimension, further described in the next section, ρ_s and ρ_w are sediment and water density, respectively. d_i is diameter of primary particle and d is equivalent spherical floc diameter.

Table 2.1 summarises the settling velocity equations of cohesive sediment, as developed from previous experimental and field data. The parameters included in these equations are suspended sediment concentration, turbulence and floc size. some of them have been applied in numerical models. Although many equations are available in the literature to calculate the settling velocity (Figure 2.1), the applicability of these equations may vary from one estuary to another due to different availability of suspended sediment, estuary topography and mineralogy and biological properties of the particles (Manning and Dyer 1999).

Settling velocity can either be measured directly in a settling column or calculated indirectly by knowing the size and density of the particle. Different instruments have been developed, both for in situ and laboratory measurements, to determine settling velocity of cohesive sediment. These will be described in section 2.4.

Table 2.1 Settling velocity of cohesive sediment from previous experimental and field data, (d: floc size, Ws: settling velocity, SSC: suspended sediment concentration, T_S: turbulent shear stress, G: velocity gradient, Δρ: differential density, r: radius)

Reference	Equation	Type of study (laboratory or field study) and location
(Gibbs 1985)	Ws $= 1.73\ d^{0.78}$, $\Delta\rho = 0.00019 d^{-0.97}$ d: (cm), Ws (cm/s), Δρ: (g/cm^3), $R^2 = 0.99$	• Laboratory study, Susquehanna River • Field study, Chesapeake Bay
(Sternberg et al. 1999)	Ws $= 0.0002\ d^{1.54}$, d (μm), Ws (mm/s), $R^2 = 0.61$	• Field study, Northern Californian continental shelf
(Agrawal and Pottsmith 2000)	Ws $= 0.45X10^{-3}$ r$^{1.17}$, r: (μm), Ws (cm/s)	• Field study, New Jersey coast
(Mikkelsen and Pejrup 2001)	Ws $= 0.00026\ d^{1.53}$, d (μm), Ws (mm/s), $R^2 = 0.925$	• Field study, Danish coastal waters
(Shi et al. 2003)	Ws $= 2.37\ SSC^{-0.84}$, SSC: (kg/m^3), Ws (mm/s), $R^2 < 0.3$	• Field study, Changjiang Estuary
(Manning 2004c)	Ws $= 0.718 + 8.33\ T_S - 12\ T_S^2 + 0.000938\ SSC$, SSC: (g/cm^3, T_S: (N/m^2), Ws (mm/s), $R^2 = 0.91$, SSC < 8 kg. cm^{-3}, $0.04 < T_S < 0.7$	• Field study, Tamar, Gironde and Dollard Estuaries

Reference	**Equation**	**Type of study (laboratory or Field Study) and Location**
(Manning 2004a)	• Microflocs (d < 160μm) $Ws = 0.244 + 3.25\ T_S - 3.71\ T_S^2$, T_S (0.04-0.55 Pa), R^2=0.75 $W_S = 0.65\ T_S^{-0.541}$, T_S (0.5-10 Pa), R^2=0.73 • Macroflocs (d > 160μm) $W_S = 0.644 + 0.000471\ SSC + 9.36\ T_S - 13.1\ T_S^2$, T_S (0.04-0.7 N/m^2), R^2 = 0.93 $W_S = 3.96 + 0.000346\ SSC - 4.38\ T_S + 1.33\ T_S^2$, T_S (0.6-1.5 N/m^2), R^2 = 0.9 $W_S = 1.18 + 0.000302\ SSC - 0.491\ T_S + 0.057\ T_S^2$, T_S (1.45-5 N/m^2), R^2 = 0.99 Valid for SSC = <8.5 kg/m^3	• Field study, Tamar, Gironde and Dollard Estuaries

2.3.3 **Floc effective density**

Effective density, which is also referred to as either excess density or bulk density, can be defined as the difference between the floc's bulk density and the water's density ($\rho_e = \rho_f - \rho_w$). It is the most practical value related to particle aggregates. Typically, when flocs increase in size, they demonstrate a lower effective density. However, their settling velocity tends to decrease due to the high porosity of the flocs (Van der Lee 2000). Effective density can be calculated theoretically based on Kranenburg (1994) model as

$$\rho_e = \rho_f - \rho_w = (\rho_p - \rho_w)(\frac{d}{d_i})^{n_f-3}, \quad \textbf{(2.6)}$$

where ρ_f is the flocs density, ρ_w is the water density, ρ_p is the sediment density, d is the equivalent spherical floc diameter, d_i is the diameter of the primary particle and n_f is the fractal dimension, which is defined as the measurement of the flocs' effectiveness regarding filling space as a function of the floc size.

The fractal dimension of flocs (n_f) can be determined theoretically using the Winterwerp model (Winterwerp 1999). This model was developed based on published field and laboratory data from the North Sea, Chesapeake Bay, Ems and Tamar Estuary. For floc size ranges from 20 to 1000 µm and settling velocity ranges from 0.04 to 10 mm/s. By knowing the value of n_f, the effective density can be calculated using equation (2.6) which has been widely used byDyer and Manning (1999); Mantovanelli and Ridd (2008) and also in this study.

Figure 2.6 shows two dimensional projections of typical three dimensional aggregates with different fractal dimensions ranging from n_f = 1.2 to n_f = 2.5. Typical values for the fractal dimension in estuarine and coastal water range from 1.7 to 2.2 (Maggi et al. 2007). It is difficult to measure the n_f value directly; therefore, an indirect approach, such as plotting of the data (floc size and settling velocity) applying the Winterwerp (1999) model as shown in Figure 2.7 is used. A fractal dimension of 2.3 is an indication of the presence of strong flocs, while an n_f of 1.4 represents weak estuarine flocs. The highest fractal dimension value of 3 represents a uniform floc structure.

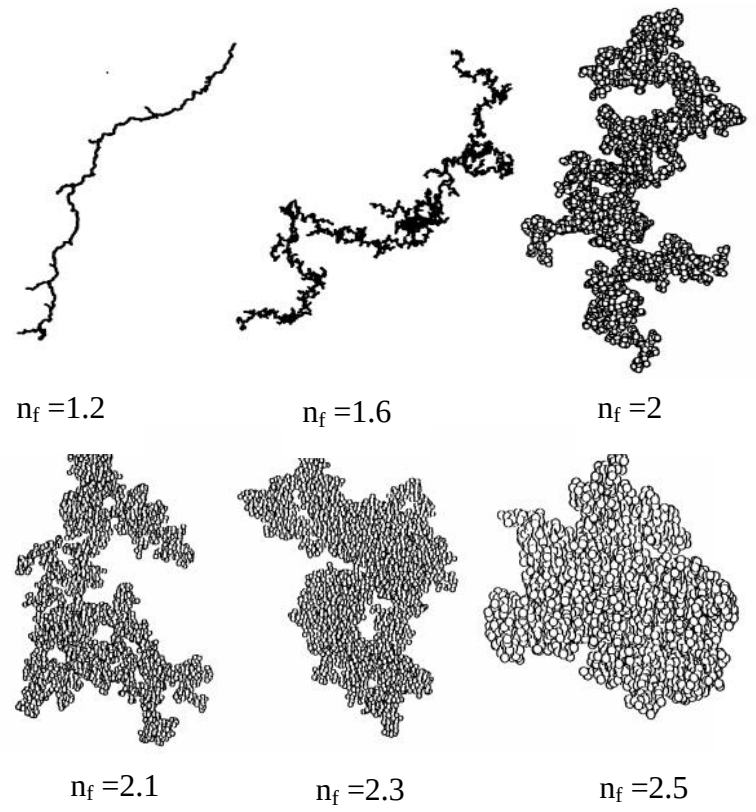

Figure 2.6 Two-dimensional projections of typical three-dimensional aggregates with fractal dimensions ranges from n_f = 1.2 to 2.5 ((Thouy and Jullien 1996)

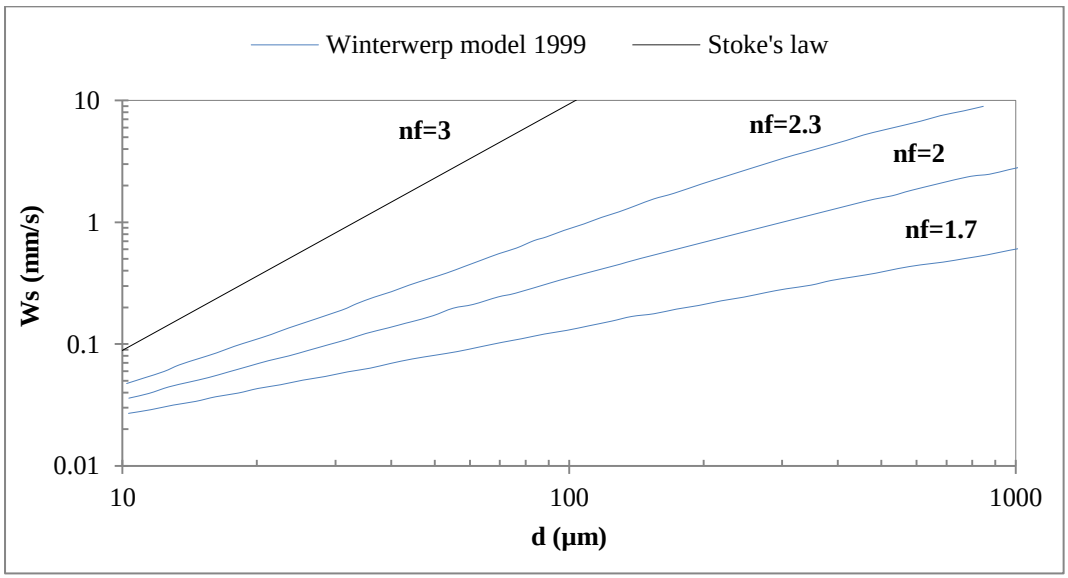

Figure 2.7 Winterwerp's model, redrawn from Winterwerp (1999)

The general trends exhibited by the flocs effective densities from literature sources over three decades are shown in Figure 2.8. Some of these studies use a variation of Stokes' law to estimate the effective density based on the floc size and settling velocity. However, others use equation (2.6) by determining the fractal parameters after plotting the floc size and the settling velocity with Winterwerp's model of Figure 2.7. A decrease in density and increase in particle size were observed by all authors, yet with a varying slope. For example, for the same aggregate size, very different effective densities were found ranging over more than three orders of magnitude between Fennessy (1994) and Manning (2004a). This variability can be explained by the different conditions under which the measurements were carried out: either in situ observation or flocculation in the laboratory, the mineral nature of the particle, the sample location, the sediment concentration, the history of the flocs structure etc. (Verney 2006).

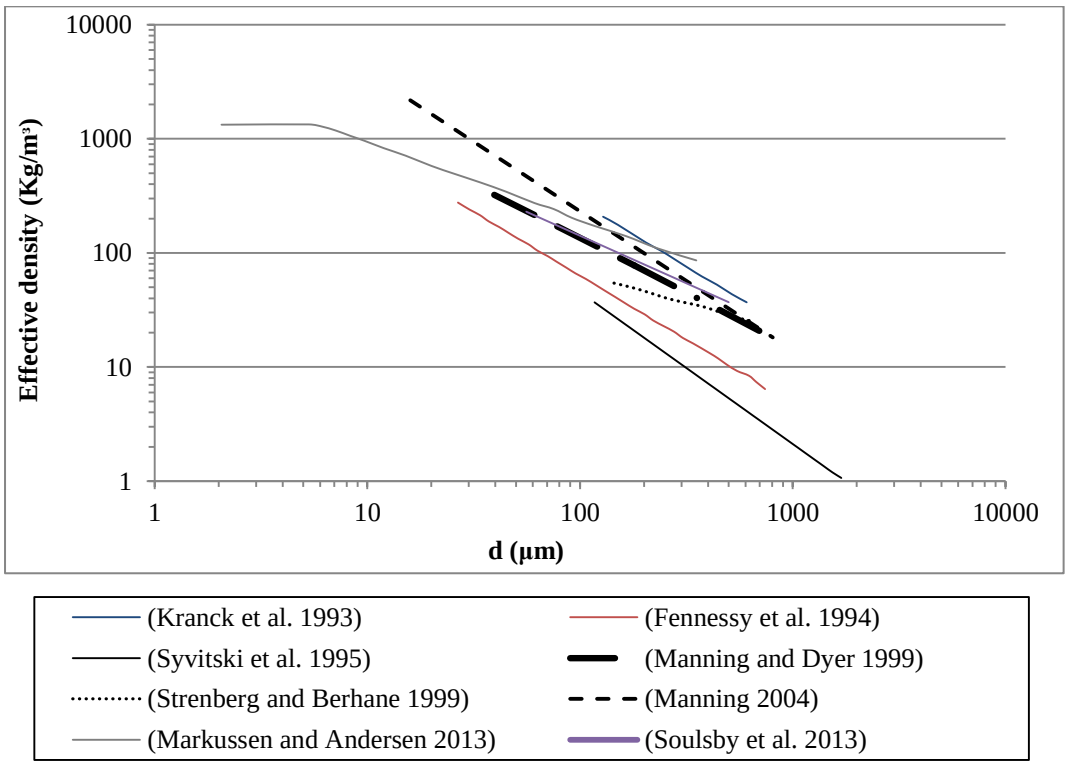

Figure 2.8 Relationship between floc size and effective density from previous studies

2.4 Technique observations of the flocculation processes

Numerous attempts were made to observe and study the flocculation processes occurring in different estuaries both in situ and in the laboratory. Many of these studies focused on observing and quantifying the particles in suspension and in their settling velocities according to the physicochemical parameters of the water column. The next two subsections summarise the findings of these studies.

2.4.1 **In situ studies**

Assessment of an in situ photograph was the first technical attempt to measure individual floc diameters (Eisma et al. 1990). Over time, this technique has been improved to include video equipment and computer imaging analysis to provide more accurate data analyses (Fennessy et al. 1994; Syvitski et al. 1995; Maldiney and Mouchel 1996; Milligan 1996; Van Leussen and Cornelisse 1996; Sternberg et al. 1999). An advantage of in situ studies is that it is possible to quantify the properties of natural particles (size, density and settling velocity). However, in situ studies fail to understand the complex interactions between the processes of flocculation and natural variables (Verney 2006). Moreover, most of these studies were carried out at a fixed point, and they did not follow the movements of the particles in the water column, which reinforce the complex interpretation of a tidal cycle. The particles are passing from one point to another in the estuary, and they will have been subjected to different forces of nature, such as different salinity and turbulence intensity; therefore, their properties may not have the same origin. Different devices have been developed to measure both the particle distribution and the settling velocity of the particles in situ, as briefly described in Table 2.2.

Table 2.2 In situ devices for measuring and observation of particles' properties

Reference	Instrument name	Research Institute	Name of Site	Measurement parameters
(Eisma et al. 1990)	Camera System	Netherlands Institute for Sea Research	Scheldt River and Estuary	Particle size of suspended sediment
(Van Leussen and Cornelisse 1993)	Video In situ (VIS)	National Institute for Coastal and Marine Management (RIKZ) of Rijkswaterstaat and Delft Hydraulics-Netherlands	The Ranselgat (mouth of the estuary) and the River Ems	Floc size and settling velocity of suspended sediment
(Fennessy et al. 1994)	In situ Settling Velocity Instrument (INSSEV)	Institute of Marine Studies, University of Plymouth	Tamar and Elbe Estuaries	Floc size and settling velocity spectra
(Syvitski et al. 1995)	Floc Camera Assembly (FCA)	Atlantic Geoscience Centre	Halifax Inlet Estuary	Floc size, shape, concentration and settling velocity
(Milligan 1996)	Benthos 373 Plankton Silhouette	Bedford Institute of Oceanography	Elbe River	Floc size spectra
(Maldiney and Mouchel 1996)	Endoscopic Photographs	No	Elbe Estuary	Particle size

Reference	Instrument name	Research Institute	Name of Site	Measurement Parameter
(Knowles and Wells 1998)	In situ Aggregate Analysis Camera (ISAAC)	Institute of Marine Sciences, University of North Carolina	Columbia and Hudson Rivers	Quantitative analysis of fine suspended particles
(Sternberg et al. 1999)	Video-trap System	School of Oceanography, University of Washington	Northern California continental shelf	Particle size, shape and settling velocity of SSC
(Mikkelsen et al. 2007)	In situ Size and Settling Column Tripod (INSSECT)	Department of Fisheries and Ocean, Bedford Institute of Oceanography	Po, Chienti and Pescara Rivers (Italy)	Floc size and settling velocity
(Mantovanelli and Ridd 2008)	Sedimentation Velocity (SEDVEL)	James Cook University, School of Mathematics and Physics, Townsville, Australia	Cleveland Bay (Australia)	Mass concentration and mass distribution of settling velocities of SPM
(Davies et al. 2017)	Submersible Digital Holographic Particle Imaging System (LISST holo)	Marine Institute of University of Plymouth (UK)	Norwegian Fjord	Particle size and shape.

2.4.2 **Laboratory studies**

Natural flocculation processes, including the measurement of sedimentation, resuspension, erosion and turbulence intensity, are difficult to reproduce in laboratory experiments due to their complexity. However, laboratory experiments are valuable for systematically investigating the effects of specific parameters, such as salinity, SSC and turbulence, under controlled conditions (Manning 2004c; Manning et al. 2004; Mikes et al. 2004). Many simplifications are made in laboratory studies to control the different variable parameters in the flocculation process. Four different devices, namely the jar test (Mikes et al. 2004), the Couette device (Serra et al. 1997; Serra and Casamitjana 1998), the sedimentation column and turbulence grid (Maggi 2005) and the annular flume with a video camera system (Dyer and Manning 1999) have been used to both generate turbulence and study flocculation processes in laboratory experiments. The development of video technology has allowed researchers to obtain both floc size and settling velocity spectra.

Video in Lab (VIL)

Video in the lab has been used to measure floc size (Mikes et al. 2004). The advantages of this instrument are that it requires little equipment cost and it is easy to implement. It consists of a glass bowl, a charge coupled device (CCD) camera and a variable speed agitator (Figure 2.9), which is used to control the turbulence level inside the bowl. Floc size can be measured for varying parameters, including turbulence level, salinity and SSC. This device is limited to sediment concentrations below 0.35 kg/m^3 (Verney et al. 2009).

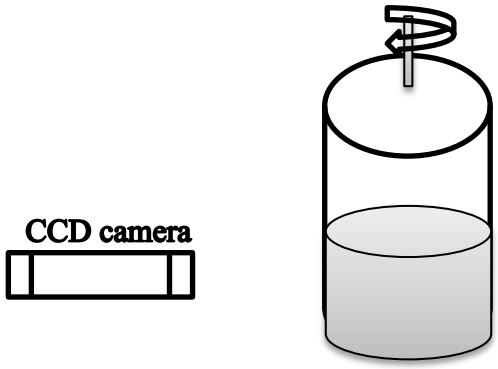

Figure 2.9 Schematic diagram of Video in Lab

Couette flow system

The Couette flow system was developed at the Geophysical Fluid Dynamics Laboratory, University of Girona. The device consists of two cylinders: an outer fixed cylinder with two lateral openings for sampling and an inner rotated cylinder (Serra et al. 1997; Serra and Casamitjana 1998). A camera is used to measure particle size distribution (Figure 2.10). The main advantage of this device is that it generates more isotropic turbulence when compared with blades in a jar test, and the turbulence intensity is known and controlled.

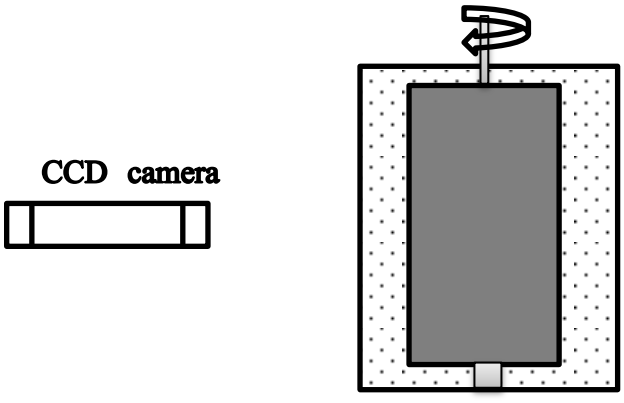

Figure 2.10 Schematic diagram of couette flow system

Sedimentation column and turbulence grid

The sedimentation column and turbulence grid method was developed at Delft University (Maggi 2005). The instrument consists of five elements: a climatized room, a sedimentation column and grid, a sedimentation injection system, a measuring system and an overflow tank (Figure 2.11). Unlike the previous devices where the flow is permanent, the advantage of this device is that both the size and settling velocity of flocs can be quantified. Also, it can simulate real environmental conditions by controlling temperature, concentrations and turbulence.

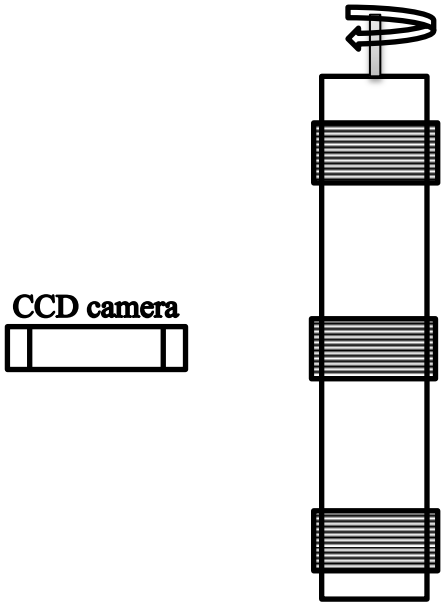

Figure 2.11 Schematic diagram of sedimentation column and turbulence grid

Annular flume with a video system

The method based on the annular flume linked to a video system was developed at the Institute of Marine Studies, University of Plymouth (Manning and Dyer 1999) to measure settling velocities and floc diameters under various sediment concentrations and turbulent shears. The device consists of an annular flume with a diameter of 1.2 m and a channel depth and width of 0.15 m and 0.1 m, respectively. A ring is

suspended from the roof as the annular ring rotates; flow is induced, which creates a velocity gradient, and a video camera measures both the settling velocity and floc size (Figure 2.12). The instrument has an upper viewing turbidity limit of 210 g/m^3. This device is more suited to investigations of the dynamic cohesive sediment, as the flocculated particles are not disrupted by recirculating pumps and filters.

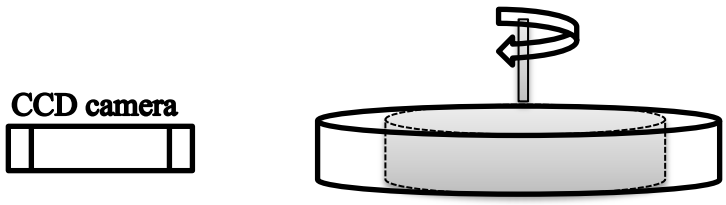

Figure 2.12 Schematic diagram of annular flume with a video system

2.5 Numerical modelling studies

During the recent decades, numerical modelling has become increasingly a useful tool in cohesive sediment transport management. Flocculation processes can significantly alter the hydrodynamic characteristics of the SSC. There are a few studies reported in the literature, in which implementation of the flocculation formula in three dimensional numerical models. Some of these studies are briefly described in this section.

The floc aggregation and breakup was included in 1DV Reynolds stress model by Villaret and Davies (1995). The model was applied to analyse the sediment turbulent flow interaction by studying the effect of the floc size distribution over the water column. There was no experimental data which can be used for the model validation. Bungartz and Wanner (2004) used SEDFLOW model to simulate SSC and the particle settling velocity frequency distribution in Spree River, Germany. The model includes advection transport, K-ε turbulence model and gravitational settling as a basic formula. The sediment transport was modelled as multiple sediment

fractions with corresponding multiple deposition behaviour. The model was evaluated by comparing the results with field data. The results demonstrated that the model is capable to predict the suspended sediment transport and deposition. The simulation results indicated that the sediment aggregation can not be neglected in cohesive sediment modelling studies considering that there is a potential error in cohesive sediment modelling if aggregation is not taken into account.

The Manning model described in Table (2.1) was implemented into TELEMAC3D by Baugh and Manning (2007). The model was applied to simulate the flocculation processes in Thames Estuary, UK. The simulation results indicated that Manning's model could produce 93% of the total mass settling flux. Whereas, sediment modelling without flocculation processes estimated 15% of the total mass. The Manning model proved able to reproduce observed SSC with a fairly high degree of reliability.

2.6 Hydrodynamic and sediment transport in the Severn Estuary

The Severn Estuary, which is located between South East Wales and the northern coast line of South West England, is the largest tidal estuary in the UK. The river system has a total catchment area of approximately 25,000 km^2 (Jonas and Millward 2010), and the estuary has a total channel length of 137 km. The catchment area supplies a total fluvial input of nearly 375 m^3/s. The estuary is macrotidal, with a tidal range of 7–12 m during mean spring tides (Uncles et al. 2002). It is characterised as one of the most dynamic estuaries in the world due to its large tidal range of up to 14.7 m (Kadiri et al. 2014). The average tidal currents in the estuary range from 0.6 m/s–1.5 m/s. The maximum spring tidal velocity is 2 m/s in the inner channel and lower estuary. In the narrow, deep channel, the tidal currents exceed 5.5 m/s (Manning et al. 2010a). The Severn Estuary, which is a mixed sediment system, consists of a wide range of different particle sizes, from coarse materials (gravel and sand) to fine materials (silt and clay) (Manning et al. 2010a). The estuary has extremely high suspended concentrations of 1,000 g/m^3 at spring tide (Gao et al. 2011).

The source of fine sediment in the Severn Estuary is summarised in Figure 2.13. The drainage area receives approximately 1.9 x 10^9 kg/y of fine sediment from the fluvial tributaries (Allen 1990; Winterwerp 1999), with the main contributors coming from the rivers Severn, Wye and Bristol Avon. This value contributes to approximately 77% of the total annual sediment load (Collins 1983). Some fine sediment is delivered by the bedrock cliffs on the margins of the Bristol Channel and Severn Estuary at the rate of 5 x 10^8 kg/y. The areas of subtidal mud in the inner Bristol Channel and lower estuary conceal about 2.7 x 10^{11} kg/y of settled mud. However, the largest area of post-glacial fine sediment is preserved beneath the wetland environment. The water body of the inner Bristol Channel and the Severn Estuary receives approximately 1.13 x 10^{13} kg/y from the preserved sediment beneath the salt marsh wetland. At spring tide, the fine sediment load in suspension is almost 1.3 x 10^{10} kg/y; by contrast, at neap tide, the fine sediment load is about 9 x 10^9 kg/y, which is approximately 40% less than the value at spring tide. Therefore, the total fine sediment from the water body, subtidal mud areas and wetlands is 1.16 x 10^{13} kg/y (Allen 1990).

Fine sediment in the water estuary is affected by seasonal cycles and the tidal cycle (semi-diurnal or diurnal). For example, during the summer season, the SSCs are lower due to increasing temperatures, reduction in wind, less sediment being discharged from tributaries and less wave energy, all of which lead to the net deposition of fine sediment on the bed. After cohesive sediment settles in the bed and forms a fluid mud layer, it gradually consolidates. This layer resists erosion with increasing water depth. Spring tides have higher tidal speeds and variable shear stress, which maintain fine sediment suspension in the water column and cause the resuspension of fluid mud by erosion of flocs from the mud-bed layer. During neap tides, the tidal current speed reduces, which contributes to a smaller amount of sediment in suspension. This causes it to settle back onto the estuary bed (Whitehouse et al. 2000; Kirby 2010).

The settling velocity of cohesive sediment is enhanced due to its ability to flocculate, which then forms a steep gradient change in the concentration profile in the near-bed region (Manning et al. 2010a). Whitehouse et al. (2000) measured the turbidity depth profile in the Severn Estuary and found variable concentration profiles. There was a fluid mud layer seen close to the bed in some profiles, whereas others showed

smooth concentration profiles. The authors suggested that a single formula cannot reproduce the conditions in each profile.

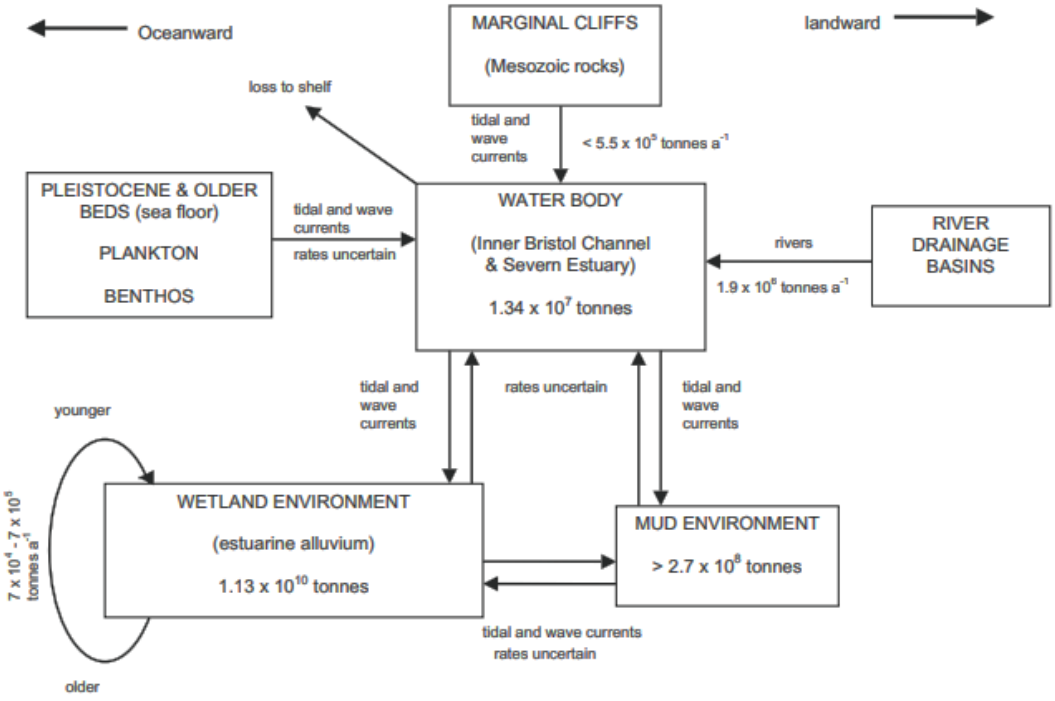

Figure 2.13 Summary of movement and exchanges of fine sediment in the inner Bristol Channel and Severn Estuary, (Allen 1990)

2.7 Summary

Cohesive sediment transport in estuaries and coastal areas is one of the most important processes for controlling its morphological evolution and its water quality. An accurate determination is required for the settling velocity of the suspended material to predict the transport of cohesive sediments. Flocculation significantly affects both the transport and fate of cohesive sediment through slowly turning and sinking primary particles into large, rapidly sinking flocs (Winterwerp, 1998). The dynamic and physical properties of flocs are different from the primary particles, and they strongly influence settling, deposition and other sediment transport processes. Understanding and predicting settling velocity while flocculation occurs is key to predicting deposition and resuspension of cohesive sediment in estuaries. From the

literature, the effect of salinity on floc size and settling velocity varies from estuary to estuary. It is understood that salinity variations are also affected by variations in shear stress, sediment concentration and organic carbon; therefore, it is difficult to study each parameter independently (Mietta et al. 2009). The variation in floc size and settling velocity under controlled parameters must be understood regarding a particular estuary because each one is dynamically and physically different from another. The effects of sediment concentration on floc size and settling velocity are associated with other parameters, such as salinity and turbulence. In addition, it is not possible to measure settling velocity as a function of sediment concentration and ignore the other physicochemical parameters. It is evident that the effects of turbulence on floc size and settling velocity are dependent on turbulence intensity and the methods employed (either laboratory or in situ) in studies as well as the variances from one estuary to another.

2.8 Identified research gap

Although some flocculation experiments have been performed on natural sediment at different salinities, SSCs and turbulences (e.g. Manning 2001, Manning et al. 2004, Mikes et al. 2004, Sutherland et al. 2015, Verney et al. 2009), there is still a lack of understanding regarding the flocculation phenomenon in the Severn Estuary (Manning et al. 2010a), which is one of the highly dynamic estuaries in the world due to its large tidal range of up to 14 m. It also has a substantial surface area, which makes it an ideal estuary for tidal energy projects and water quality processes. The flocculation processes need to better understood in order to be able to assess the impacts these changes might have in future water quality processes. Based on the literature review, only one in situ study has examined the flocculation of suspended sediment. This study was carried out in Portishead (in the Severn Estuary) Twenty-eight samples were analysed and large flocs (with a diameter of 800 µm) with low density were found, while both high and low densities were observed in small flocs (150 µm) (Manning and Dyer 1999). This study attempted to gain a better understanding of the flocculation processes of cohesive sediment in the laboratory using sediment samples from the Severn Estuary with variations of salinity ranging from 0 to 30 ppt, turbulence intensity ranging from 0.57 to 8.5 N/m^2 and suspended sediment concentration of 0.1, 0.15 and 0.2 Kg/m^3.

3 Settling velocity of suspended sediments

3.1 Introduction

This chapter presents the laboratory experiments that were conducted in this study. The collection and storage of the water and sediment samples are described, followed by the experiments, which consist of two different parts. The first part deals with the analysis of the water and sediment field samples. The second part mimics the flocculation phenomenon and measures the flocs size and their settling velocity as functions of the hydrodynamic and physicochemical parameters.

3.2 Study area

Water and sediment samples were collected from different points along the upper Severn Estuary approximately one metre from the shore (see Figure 3.1). The data were collected on 16 June 2014. Samples were taken at the spring high tide mark of 9.5 m at Sharpness Dock, England. Samples were collected from three different sites. The first site, Slipway, is located upstream at Lydney with coordinate $2^{\circ}30`00.67``\mathrm{N}, 51^{\circ}42`52.12``\mathrm{W}$. The second location, Gatcombe, is nestled in a wooded valley with coordinate $2^{\circ}27`68.27``\mathrm{N}, 51^{\circ}44`05.10``\mathrm{W}$ The third location, Beachley, is located on a peninsula at the confluence of the rivers Wye and Severn, where the Severn Bridge ends with coordinate $2^{\circ}64`92.79``\mathrm{N}, 51^{\circ}62`47.63``\mathrm{W}$. These locations are characterised with more cohesive sediments which are affected by flocculation processes. The fine sediments in the Severn are coming from the fluvial tributaries (Allen 1990; Winterwerp 1999), with the main contributors coming from the rivers Severn, Wye and Bristol Avon. This value contributes to approximately 77% of the total annual sediment load (Collins 1983). They would be directly affected by the construction of a marine renewable energy device. The samples were kept in a cool box and then returned immediately to the laboratory where they were stored in a refrigerator to minimise biological activity.

This Chapter has already been published as two journal papers: 1. Mhashhash, A., Bockelmann-Evans, B. and Pan, S. 2017. Effect of hydrodynamics factors on sediment flocculation processes in estuaries. *Journal of Soils and Sediments*. 2.Mhashhash, A., Bockelmann-Evans, B. and Pan, S. 2018. A new settling velocity equation for cohesive sediment based on experimental analysis. *Journal of Ecohydraulics. Accepted for publication.*

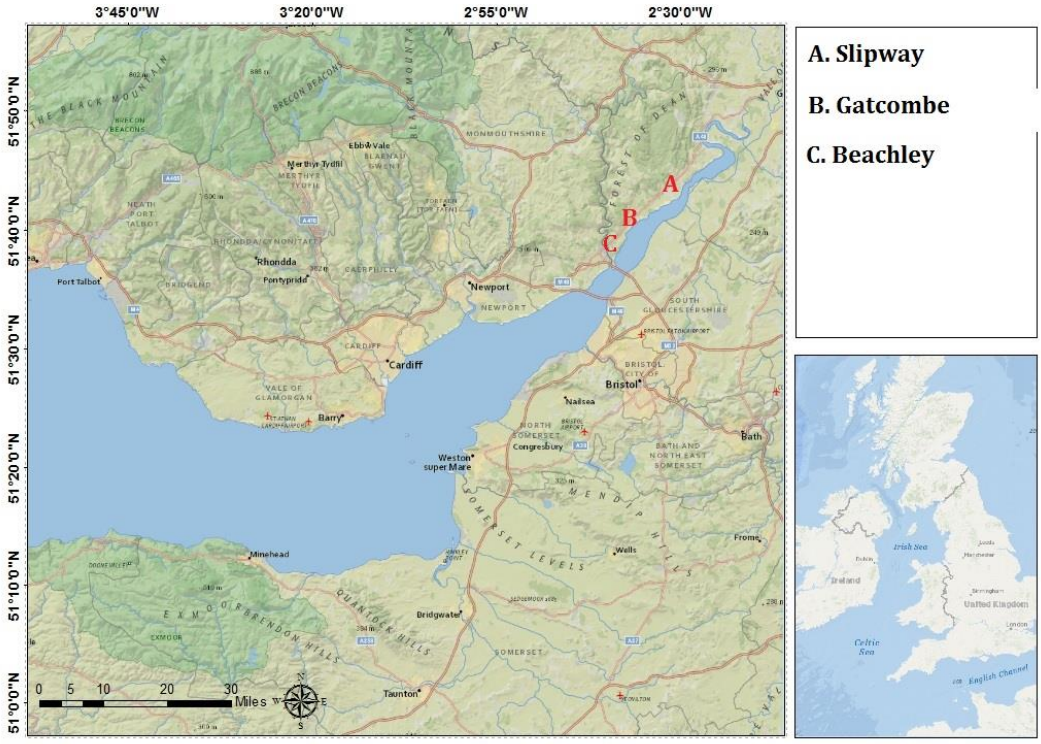

Figure 3.1 Map of Severn Estuary showing the location of three sampling sites (Slipway, Gatcombe and Beachley)

3.3 Part 1: Sediment and water analysis

This section describes the water and sediment properties. The water analysis is described in sections 3.3.1 and 3.3.2. The sediment analysis is described in sections 3.3.3, 3.3.4 and 3.3.5. The physicochemical parameters of the estuary water (salinity and pH) were measured in samples collected at each site. The results are shown in Table 3.1.

3.3.1 **pH**

The pH of the water was determined using an electronic pH meter. The probe was immersed in the sample bottle after allowing the meter to stabilise before the reading was taken. The pH meter was calibrated with two calibration solutions at pH 4 and pH 9 prior to use. The probe was rinsed with deionised water and wiped dry between sample readings.

3.3.2 **Salinity**

Salinity is measured in part per thousand (ppt) by the degree of concentration of the dissolved salt. Since salts form ionic particles when dissolved, salinity is a strong component of conductivity. Usually, salinity is estimated using algorithms based upon conductivity, which is much easier to measure. In this study, an electronic conductivity meter was used to measure the salinity. Prior to use, the salinity probe was calibrated using a calibration solution at the conductivity of 1,413 ms/cm. The probes were rinsed with deionised water after each use to ensure that no cross-contamination occurred between samples.

Sediment characteristics play an active role in the sediment transport processes in the water ecosystems by affecting nutrient and other pollutants adsorption and desorption as well as the resuspension and deposition of sediment particles and thus string bathymetric changes. The apparatus and procedures for analysis of the suspended sediment characteristics, such as particle density, mineral composition and particle size distribution are described in this section.

3.3.3 **Particle density**

The empty glass bottle was weighed (m_1). The sediment sample then was dried overnight in an oven at 105^0C. The bottle and 5-10 g of the dry sample were weighed (m_2). The weight of the sample was calculated as the difference between (m_1) and (m_2). Sufficient air-free distilled water was added in three stages until the bottle was filled with the water. Between each stage, the bottle and its content were placed in a vacuum desiccator. The desiccator was evacuated gradually, reducing the pressure to about 20 mm of mercury. Care was taken during this operation to ensure that air trapped in the soil did not bubble too violently, which could have led to small drops of the suspension being lost through the mouth of the bottle. The bottle in the evacuated desiccator was left for at least one hour until no further loss of air was apparent. The bottle and its contents were then weighed (m_3). The bottle was cleaned and filled completely with air-free distilled water, wiped dry and then weighed (m_4). This procedure was repeated twice. Therefore, two values of particle density were obtained. The average of the two results was calculated. If the difference between the two results was more than 0.03 mg/m^3, then the test was repeated. The particle density was calculated using the following equation:

$$\rho_p = \frac{\rho(m_2 - m_1)}{(m_4 - m_1) - (m_3 - m_2)} \quad \textbf{(3.1)}$$

where ρ is the density of the liquid used at the constant temperature (in kg/m^3), ρ_p is the particle density, m_1 is the mass of the density bottle (in g), m_2 is the mass of the bottle and dry soil (in g), m_3 is the mass of the bottle, soil and liquid and m_4 is the mass of the bottle when full of liquid only (in g).

3.3.4 **X-ray diffraction analysis (XRD)**

Before the particle size was determined, X-ray diffraction analysis was carried out using a Philips PW 3830 X-ray instrument to analyse and determine the dominant minerals present in the solid sediment samples (Figure 3.2). The samples were dried at 105°C for 24 hours. A small amount of the dried sample was then placed on the sample holder in the X-ray sample chamber, and the scan was run. After completing the scan, the data were exported and analysed using the software X'Pert High Score. The composition of the crystalline minerals was then identified by searching and matching the sample peaks with the known mineral peaks. The sensitivity of the XRD was 0.1%.

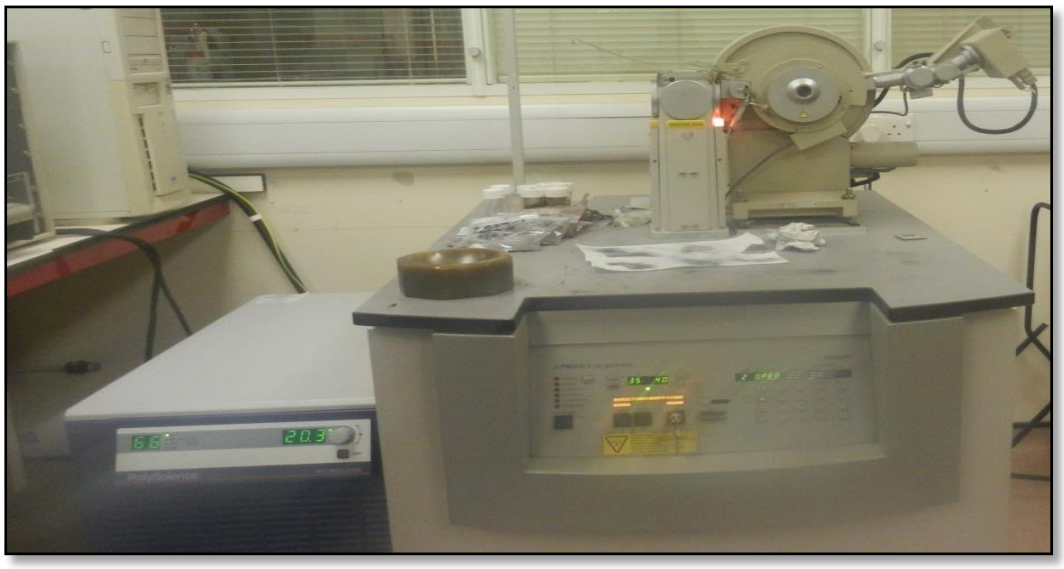

Figure 3.2 X-ray diffraction instrument for determining the dominant minerals present in the samples

3.3.5 **Particle size distribution**

The particle size distribution of the suspended sediment samples was analysed using a Malvern Master Sizer 3000 (Figure 3.3). Before the particle size analysis of samples, specific information is needed such as particle density of the suspended sediment and the chemical composition of the suspended sediment. These parameters were measured previously (see sections 3.3.3 and 3.3.4). The Malvern Master Sizer uses a rapid technique that detects a wide range of particle sizes (from 0.02 μm to 2000 μm) with an accuracy of ± 1% on the d_{50} (median grain size). The Malvern Master Sizer uses laser diffraction to measure the size of the particles. The particle density value and the information about the chemical composition of the sediment were then entered into specialist computer software. The intensity of the light scattered is measured as a laser beam passes through a dispersed particulate sample. These data are then analysed using specialist computer software to calculate the particle size distribution.

Figure 3.3 Malvern master sizer instrument for measuring particle size distribution

3.4 Part 2: Flocculation phenomenon

Monitoring flocculation behaviour of cohesive sediment in situ is difficult and costly. Previous researchers have investigated the behaviour of cohesive sediment in the laboratory and carried out numerical modelling that can be used to simulate the natural condition. It is difficult to produce the correct detail of natural flocculation processes in the laboratory due to the complexity of processes involved such as sedimentation, resuspension, erosion and turbulence intensity. However, laboratory experiments are valuable for systematically investigating the effects of specific parameters, such as salinity, SSC and turbulence, under controlled conditions (Van Leussen 1999; Manning 2004c; Manning et al. 2004; Mikes et al. 2004). The ability to determine floc size and settling velocity in hydrodynamic estuarine waters and to represent these accurately in numerical models could contribute to the better understanding and knowledge of managing estuarine and coastal waters under future stresses such as climate change. In addition, flocculation mechanisms (i.e. floc size and settling velocity) can be more accurately represented in numerical models at the field scale, and direct effects on morphological and water quality processes can be better investigated.

Part 2 of the experiments was carried out to address the following two main aims:

1. To study the effects of the hydrodynamic parameters of sediment concentration, salinity and turbulence shear stress on floc size and settling velocity using a particle image velocimetry (PIV) system.
2. To derive a new regression equation for predicting the settling velocity as a function of the hydrodynamic parameters using Minitab and the PIV system.

3.4.1 Experimental setup

Flocculation experiments were conducted in a 1L glass beaker of 11 cm diameter. It was equipped with a variable speed agitator to control turbulence of the flow inside the beaker. This device was prepared by adapting the method used by Mikes et al. (2004). A settling column with a diameter of 5 cm and a height of 40 cm was used to measure the flocs' settling velocities. Flocs were introduced from the top of the settling column filled with water, where the falling flocs were filmed using a PIV system, as shown in Figure 3.4. The PIV system consists of a backlight which is

positioned opposite the CCD camera to provide a uniform black background upon which particles appear as white. The CCD camera had 1392X1040 pixel sensitivity, focal length, f, of 9mm and a maximum frequency of 30fps (Δt= 1/30 s), a Polytec BVS-11 Wotan flash stroboscope and trigger box, fibre optic cable and linelight (Harries et al. 2013).

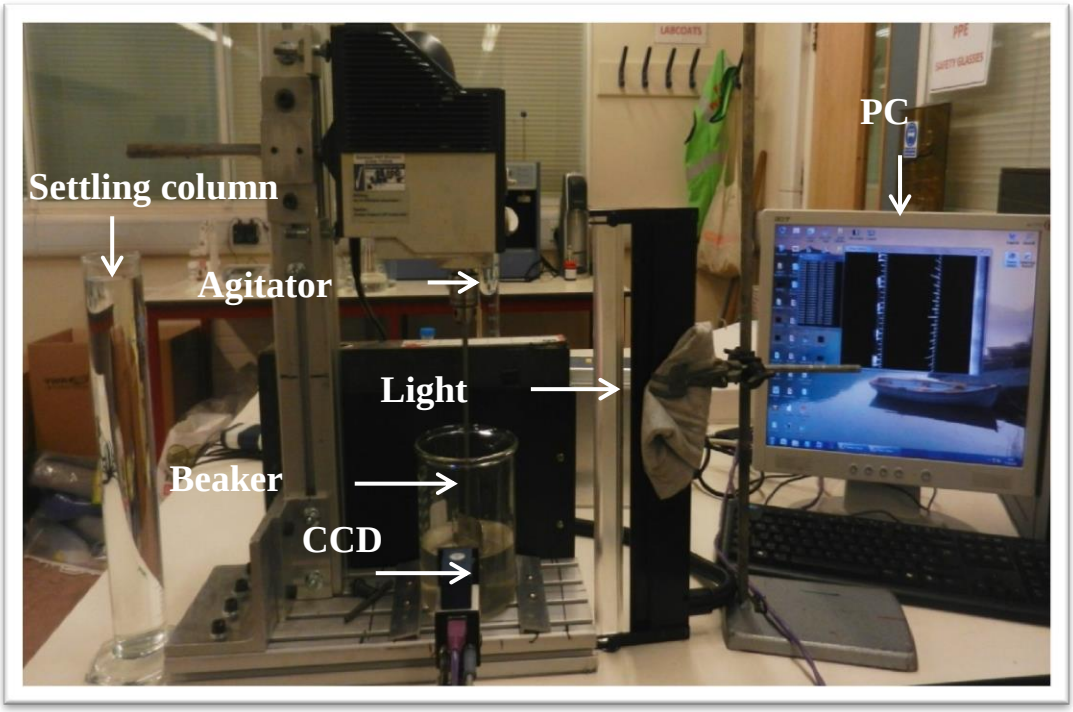

Figure 3.4 PIV set-up in the laboratory (Mhashhash et al. 2017)

3.4.2 **Instrument calibration**

The hydrodynamic shear stress inside the beaker was quantified by measuring the velocity. The angular velocities (ω) of the agitator were set at 37, 50, 70, 90 and 110 rpm. Turbulence is typically obtained from three velocity components (u', v' and w'), but the radial velocity (w') was found to be so small that it could be neglected. Therefore, at each rotational speed, the turbulent kinetic energy (K) was calculated from the measurements of the tangential and vertical velocity fluctuations ($u'$and v'). Turbulent kinetic energy (K) was defined as follows:

$$K = \frac{1}{2}(\overline{u'^2} + \overline{v'^2}) \quad \textbf{(3.2)}$$

Figure 3.5 shows the top view of the beaker with a diameter (D) of 11 cm. The light was at a distance (y) of 2 cm from the centre of the beaker. Because the fluctuation velocity is a function of the flow velocity, it could not be calculated directly using the PIV camera. In Figure 3.5, the green arrow shows the flow velocity (u) and the red arrow shows the fluctuation velocity (u', v'), which was calculated as follows:

$$u' = u\cos\phi \quad \textbf{(3.3)}$$

$$v' = v\sin\phi \quad \textbf{(3.4)}$$

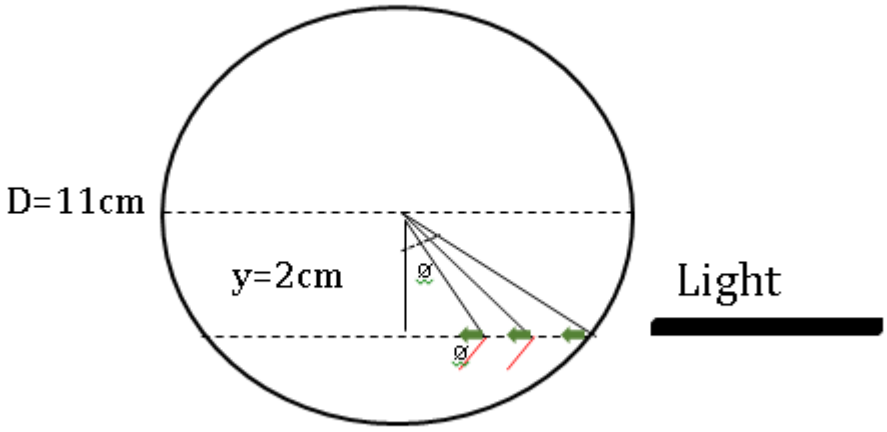

Figure 3.5 Top view of the beaker

Equation 3.5 was used to determine the turbulent shear stress (T_S) in N/m^2 (Manning 2004b):

$$T_S = 0.19\rho_w K \quad \textbf{(3.5)}$$

where ρ_w is the water density and which was assumed to be 1000 kg/m^3, 0.19 is an empirical value and K is the turbulent kinetic energy.

The flow velocity, u, was also calculated theoretically by conversion of the angular velocity into the linear velocity.

$$u = \frac{\pi D \omega}{60000} \quad \textbf{(3.6)}$$

where D is the diameter of the beaker (mm), and ω is the angular velocity (rpm).

Also, the turbulent shear stress was classified in units of length using the Kolmogorov (1991) microscale (η):

$$\eta = \left(\frac{\upsilon^3 . L}{K^{\frac{3}{2}} . C_v}\right)^{\frac{1}{4}} \quad \textbf{(3.7)}$$

where C_v is a K- ε closure constant value set at 0.09 (Manning and Dyer 1999), L is the mixing length, which corresponds to the diameter of the beaker (0.11m), K is the turbulent kinetic energy and υ is the water kinematic viscosity ($1.15 \text{ X } 10^{-6}$ m^2/s).

3.4.3 **PIV system validation**

The PIV system was validated by measuring the settling velocities of artificial sand of four different sizes (63, 150, 212 and 300 μm). Before measuring the settling velocity, sand samples were prepared for the experiment. The particle size was measured by using a set of sieves of known mesh size. Dry sand samples were passed through the set of sieves, which were arranged in decreasing mesh diameters, and the sieves were mechanically vibrated for twenty minutes (Figure 3.6).

After sieving the sand sample, the settling velocity of each size fraction was measured. There are several different methods available for measuring the fall velocities of particles within a water column. In the technique used here, particles were introduced from the top of a settling column that was 5 cm in diameter, 40 cm in length and filled with de-aired water. The tap water was left for one day in the water tank. This step is essential to remove dissolved air in the water and to obtain a

clear picture when taking pictures of the samples. The settling velocity was measured by recording both the travelling time and the distance of particles via a particle image velocimetry (PIV) camera. The experiments were conducted at room temperature of 20°C ± 0.5°C. All experiments were performed under quiescent conditions without shear. The particles were introduced from the top of the settling column into the water and allowed to settle approximately 13 cm by the force of gravity prior to switching the camera on to allow any activity from the introduction method to be damped out. The PIV system proved to work well and be method of recording the measurement of particles >60 μm.

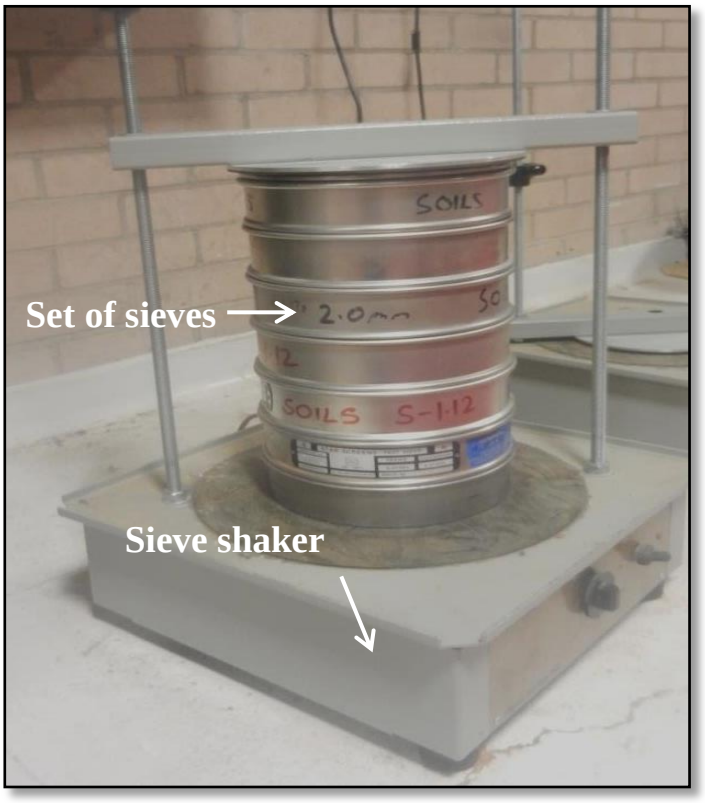

Figure 3.6 Vibratory sieve shaker for analysing sand size

3.4.4 Experimental procedures for measuring the effects of hydrodynamic parameters on the flocculation processes

A set of laboratory experiments was conducted to investigate the effects of salinity (S), turbulent shear stress (T_S) and suspended sediment concentration (SSC) on the flocculation processes. The first subsection describes the settling velocity of the samples collected from the Severn Estuary under different conditions: dry, wet, semi-wet and fully mixed samples. The following subsection describes the flocculation phenomenon and the effects of hydrodynamic parameters on the floc size and the flocs settling velocity.

3.4.4.1 Settling velocity of cohesive sediment

The settling velocity of the sediment particles without flocculation was measured in order to calibrate the numerical model which is discussed in Chapter 5. The settling velocity of Severn Estuary samples was measured using four different conditions: dry, wet, semi-wet and fully mixed sampling procedure in order to improve our understanding of particles behaviour under these different conditions. All experiments have been duplicated.

Dry sample procedure

A well mixed one-litre estuarine water sample was filtered through 0.45 μm cellulose filter paper. The filter with the wet sample was left in the oven for 24 hours at 105°C. The weight of the dry sample was then calculated as the difference between weight of the filter with the dry sediment and the empty filter paper. Next, 0.5 g of the dry sediment sample were introduced from the top of a one-litre water column, and the PIV camera was then used to capture images over a period of 50 seconds.

Wet sample procedure

The field sample was lifted into the bottle to allow the sediment to settle under the force of gravity. The water above it was carefully removed, and 3 ml of the settled sample from the bottom was introduced into the top of a one-litre water column. The sample was cloudy, and its settling velocity was measured manually by dividing the difference between the distances of the cloud front from two camera images over time. The settling velocity can be calculated as

$$\mathrm{Ws} = \frac{\Delta_y}{\Delta_t} \quad \textbf{(3.8)}$$

where: Δ_y is the difference between the distances of the front of the cloud on the images, and Δ_t is the difference in the times between the images.

Semi-wet sample procedure

A small amount of water was added to 1 g of the dry sample and mixed gently. The sample was introduced into the settling column from the top. The settling velocity of the semi-wet sample was then measured via analysis of the camera images.

Fully mixed sample procedure

The field sample in the bottle was shaken gently, and the sediment then settled under the force of gravity. The settling velocity was measured every 15 min by dividing the clear front settled distance in the water over time.

3.4.4.2 Influence of hydrodynamic parameters on the floc size and settling velocity

The replication of natural flocculation processes in laboratory experiments is challenging because of the complexity of the processes involved such as hydrodynamic processes, ionic interaction and adsorption of chemical components and contaminants (McCave 1984; Droppo 2001; Tombácz and Szekeres 2004; Mietta et al. 2009). Nevertheless, laboratory experiments are valuable because they systematically investigate the effects of specific parameters, such as salinity, suspended sediment concentration and turbulence, under controlled conditions (Manning 2004c; Manning et al. 2004; Mikes et al. 2004). This study focuses on investigating the influence of salinity, suspended sediment concentration and turbulence on floc size and settling velocity. The experiments were carried out in two main steps. In the first step, the highest tested shear stress of 60 N/m^2 was applied to break down any potential macroflocs in suspension. In the second step, the agitator was run at the lowest turbulence level of 0.57 N/m^2 for a duration of 120 min as recommended by Mikes et al. (2004) and Verney et al. (2009). Correspondingly, in a tidal cycle, two hours is the typical period of time available for flocculation to occur at favourable conditions present during the slack water period. Le Hir et al. (2001)

stated that the average floc size no longer changes after two hours and flocs have to settle in throughout the tidal cycle, which is around low and high tide. Consequently, there is no need to examine a longer period.

Effect of S on floc size and settling velocity

The formation of aggregates at different salinity ranges was chosen to simulate the natural processes of cohesive particles in the estuary as they pass from fresh water into highly saline marine waters. To explore the effects of salinity variation on floc size and settling velocity, a set of laboratory experiments with salinity levels of 0, 0.5, 1, 2, 2.5, 5, 7.5, 10, 20, and 30 ppt were conducted at suspended sediment concentration (SSC) and a turbulence level (T_S) of 100 g/m^3 and 0.57 N/m^2, respectively.

Effect of SSC on floc size and settling velocity

The formation of aggregates at different SSC was chosen in this study as the important variable which governs the collision rate and subsequent degree of flocculation of particles in estuarine waters. To determine the effect of sediment concentration variation on flocs size and settling velocity a set of laboratory experiments with SSC of 100, 150 and 200 g/m^3 were conducted at two different salinities of S 2.5 and 20 ppt and at turbulent level of 0.57 N/m^2.

Effect of T_S on floc size and settling velocity

Turbulence plays a major role in the flocculation mechanism. The formation of aggregates at different T_S was chosen in this study as one of the important variables which governs the collision rate and subsequent degree of flocculation of particles in estuarine water. To investigate the effects of turbulent shear stress variation on floc size and settling velocity, a set of laboratory experiments with turbulent shear stresses of 0.57, 1.7 and 3.8 N/m^2 were conducted for SSC of 100 g/m^3 and S of 2.5, 5 and 20 ppt.

In each test, the flocs were carefully extracted from the glass beaker with a syringe, and they were gradually introduced into the settling column. The diameter of the syringe was sufficiently large to minimise floc breakage. This sampling protocol (syringe sampling) was successfully used and validated against in situ floc

observations (Gratiot and Manning 2004; Manning et al. 2010c; Manning and Schoellhamer 2013). Following the introduction of the sample into the water column, the flocs were allowed to settle by gravity over a distance of nearly 13 cm prior to switching the camera on to permit the damping out of any activity caused by the introduction method of the flocs into the settling column.

Mimicking of the natural journey of a particle in estuarine water

Two additional experiments were conducted in this study to investigate the effects of turbulence and salinity on particle size over time. In natural estuarine waters, turbulence varies during the tidal cycle (Zhu et al. 2015). This study explored this phenomenon to identify the effects of turbulence on FSD over time. In estuarine areas, particles that issue from catchment areas move through the salinity gradient of the estuary (Mikes et al. 2004). The effect of the salinity gradient on floc size over time was considered in order to mimic the natural journey of a particle in estuarine water. In each experiment, only one parameter was varied at a time, while the other was kept constant. The first experiment was commenced at an S of 2.5 ppt, SSC of 100 g/m^3 and T_S of 0.57 N/m^2 and run for 2 hours to allow the flocs to develop from the initial state to an equilibrium state (Le Hir et al. 2001; Mikes et al. 2004). Then the turbulent shear stress was increased hourly until it reached 8.5 N/m^2. The second experiment was conducted at an SSC of 100 g/m^3, T_S of 0.57 N/m^2 and S of 2.5 ppt and run for 2 hours. Then the salinity was increased every hour until it reached 30 ppt. The agitator was stopped for 3–5 seconds to take the PIV images for use in the analysis of the size of the flocs. Pictures were taken over a period of 50 seconds.

3.4.5 PIV camera data analysis

The experiments were aimed to measure the floc size and settling velocity of individual flocs occurring at different dynamic parameters. This section describes the data analysis techniques that were applied to data recorded with the PIV camera (Verney et al. 2009; Keyvani and Strom 2014; Zhu et al. 2015). The ImageJ program was used to calculate floc properties, including area, location and circularity. This method generally uses sequences of floc images taken at two-second intervals. The floc size distribution and settling velocity were both obtained from floc image recording and processing. There were five main steps in the image processing: (1) selecting the flocs manually at the start and at the end of the sequence by opening

images using image editor and paint program; (2) enhancing background (brightness and contrast); (3) removing any noise to make sure the flocs appear in all of the sequential images by opening images using an image editor and the paint program; (4) removing all flocs which are touching the image boundary and are not in focus; and (5) calculating the features of flocs, including sectional area and location, by using the "ImageJ" software. As this method is interactive, the risk of errors being made in the determination of the floc paths is very low.

ImageJ was used to detect particles larger than 60 μm; below this limit, the pixel resolution of the floc measurement was not consistent. Hence, the smallest microflocs (< 60 μm) were not accounted for in the description of the floc population during the experiment. Floc size was obtained using the contrast between the dark background and the white silhouette of each floc. The surface equivalent diameter d was calculated by converting particle area (A) into an equivalent circular diameter (Flory et al. 2004; Mikes et al. 2004; Verney et al. 2009) as follows:

$$d = \sqrt{\frac{4A}{\pi}} \qquad \textbf{(3.9)}$$

3.5 Results and discussion

3.5.1 Physicochemical water parameters of field samples

The physicochemical parameters of the water samples collected at the three sites namely, Slipway, Gatcombe and Beachley, on 16th June 2014 at spring tide condition are presented in Table 3.1. The physicochemical water parameters pH and salinity (S) were measured for six water samples at each site.

Slipway

The pH at Slipway was found to range from 6.9 to 7.42. The salinity was found to range between 14.60 ppt and 14.74 ppt.

Gatcombe

The pH at Gatcombe was found to range from 6.99 to 7.83. The salinity was found to range between 18.06 ppt and 18.39 ppt.

Beachley

The pH at Beachley was found to range from 7.08 to 7.79. The salinity was found to range between 19.27 ppt and 19.37 ppt. The average salinity range increased by 25% from upstream to downstream from 14.57 ppt to 19.33 ppt.

Table 3.1 Physicochemical parameters of water samples collected at three different sites (Slipway, Gatcombe and Beachley)

Samples	Slipway		Gatcombe		Beachley	
	pH	S (ppt)	pH	S (ppt)	pH	S (ppt)
S1	7.01	14.67	6.99	18.14	7.54	19.34
S2	7.42	14.60	7.83	18.06	7.55	19.27
S3	7.01	14.72	7.81	18.12	7.61	19.39
S4	7.32	14.74	7.52	18.14	7.79	19.32
S5	6.90	14.62	7.70	18.39	7.66	19.37
S6	7.28	14.63	7.62	18.18	7.08	19.32
Average	7.15	14.57	7.58	18.17	7.53	19.33

3.5.2 **Sediment characteristics of sediment samples**

The results of the suspended sediment characteristics are shown in this section including particle density and particle size distribution.

Particle density

Measurement of particle density is important for the analysis of particle size distribution. The particle density of the Severn Estuary samples was measured in the laboratory and was found to be 2433.28 kg/m^3. Also, the particle density of the artificial sand sample was measured in order to validate the particle image velocimetry (PIV) system. The sand density was 2650.94 kg/m^3.

Particle size distribution

The suspended sediment in the Severn Estuary from the three sites Slipway, Gatcombe and Beachley comprised to 95 % of cohesive sediments (Figure 3.7), with a d_{50} of 11.4, 11.2 and 11.1 µm, respectively.

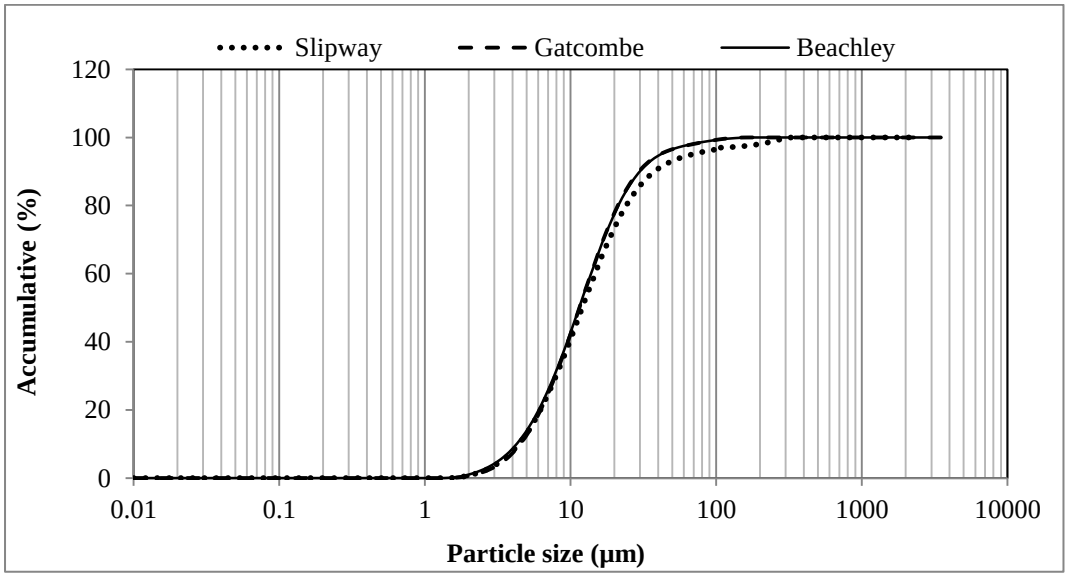

Figure 3.7 Particle size distribution of the Severn Estuary sediment samples at sites Slipway, Gatcombe and Beachley

3.5.3 **PIV system calibration and validation**

The results of the comparison between the experimental flow velocity (calibration flow velocity in the beaker) and the theoretical flow velocity are shown in

Figure 3.8. The theoretical flow velocity was calculated by converted the rotation speeds from (rpm) into the linear velocity (m/s) using equation (3.6). The flow velocities were found to correlate well at a R^2 value of 0.98. This result confirms the accuracy of the PIV camera and the suitability of this method to this novel type of application, which supports its previous application by Maggi (2005). Table 3.2 presents the calculated turbulent shear stresses that correspond to all of the rotational speeds and the experiment (measured) and theoretical (calculated) average flow velocity values.

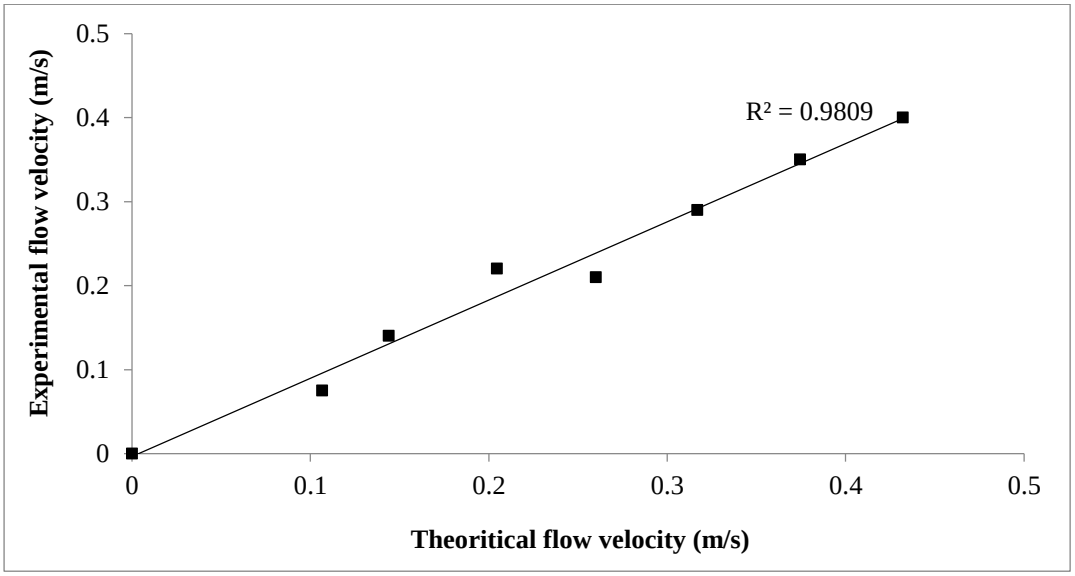

Figure 3.8 Comparison between experimental and theoretical flow velocities.

Table 3.2 Shear flow parameters with respect to different angular velocities

Angular velocity	Flow velocity		Turbulent shear stress
	Measured	Calculated	
rpm	m/s	m/s	N/m^2
37	0.10	0.08	0.57
50	0.14	0.14	1.70
70	0.20	0.22	3.80
90	0.26	0.21	6.00
110	0.32	0.29	8.50

The PIV system was validated by measuring the settling velocities of artificial sand of four different sizes (63, 150, 212 and 300 μm) in the settling column. The settling velocities of the differently sized artificial sand particles were measured theoretically by using Stokes' law equation (2.1). This equation is a function of sand size and sand density which has been measured in the laboratory (see section 3.5.2 for the result). The results of using the PIV camera compared well with the theoretical results of using Stoke's law (Figure 3.9). For particles with diameters less than 212 μm, the results showed reasonable clustering around the 1:1 line. The results for particles of 300 μm were in agreement within a factor of two of the theoretical value (Figure 3.9). The results showed an accuracy of 90% in estimating the size and settling velocity of all the differently sized sand samples. These results confirmed the accuracy of the PIV camera and the suitability of this method for measuring the settling velocities in this experimental setup (Mhashhash et al. 2016). Due to the optical limitations, using a 1L glass beaker in the laboratory to mimic floc behaviour is operational only for sediment concentrations below 0.35 kg/m^3 (Verney et al. 2009). The results showed that the main limitation of the PIV experiments carried out in this study was the light source, which was not strong enough to operate with sediment concentrations above 0.25 kg/m^3. Financial restrictions prohibited the purchasing of a stronger light source as part of this project.

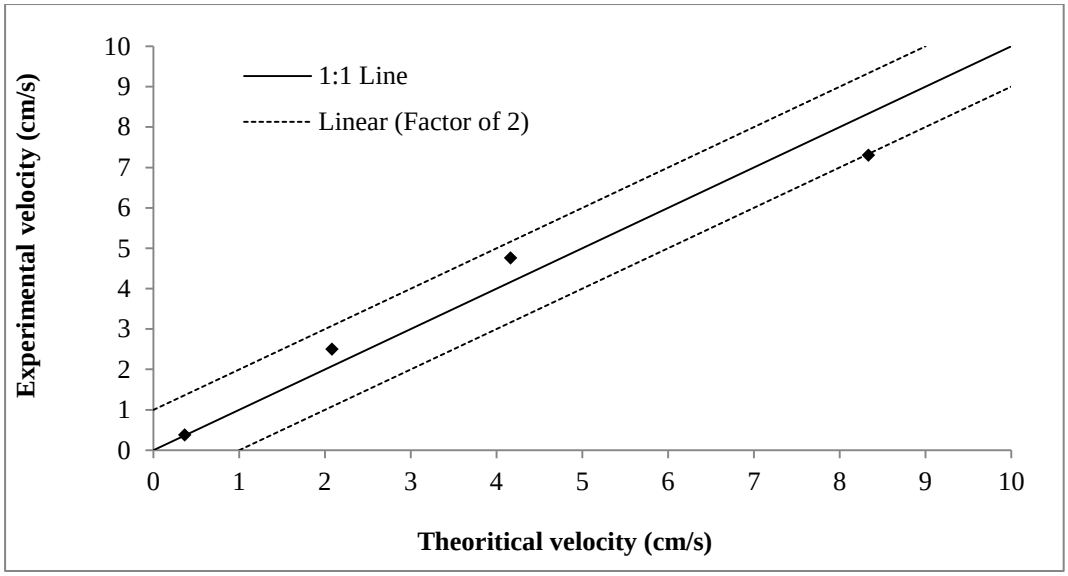

Figure 3.9 Comparisons of theoretical settling velocities with velocities measured in the laboratory using PIV camera

3.5.4 **Settling velocity of cohesive sediment**

The settling velocities of the field samples were measured under four methods of dosing the settling column with the samples: dry, wet, semi-wet and fully mixed. The aim was to study the sediment settling behaviour. The results of these methods are explained in the following:

Dry sample

The settling velocity of the dry sample as function of time was measured by analysing the PIV images. The ImageJ software was used to analyse the images and calculate the settling velocity. The settling velocity resulting for the dry sampling method is shown in Table 3.3.

Wet sample

The settling velocity resulting from the wet sample method was measured by using equation (3.8) as the difference between the distances of the front of the cloud on the images over time (see Figure 3.10). The settling velocity of the wet sample was calculated for ten pictures, and then the average of settling velocity of all pictures was calculated. The result is described in Table 3.3.

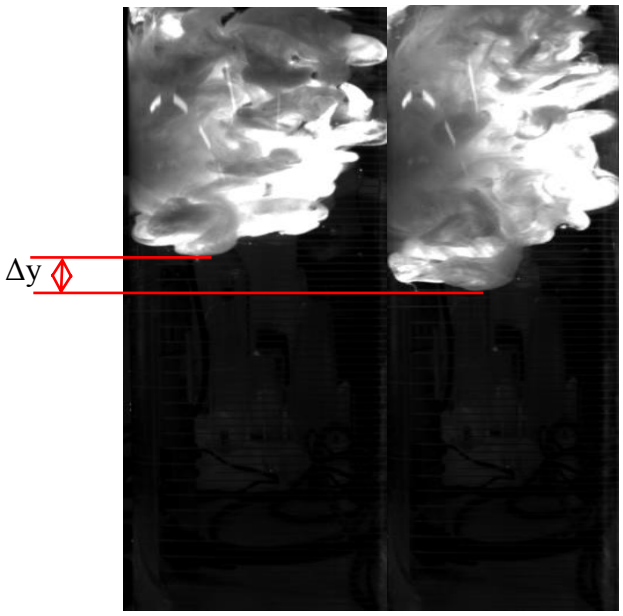

(a) **(b)**

Figure 3.10 PIV images of the settling of the wet suspended sediment sample at different time steps

Semi-wet sample

The settling velocity of the semi-wet sample was calculated by analysing PIV images. The average settling velocity of semi-wet sample was calculated for ten pictures, and then the average of settling velocity of all pictures was calculated. The result is described in Table 3.3.

Fully mixed sample

The settling velocity of the fully mixed sample was measured using the traditional method by dividing the clear front settled distance in the water over time for twelve hours. Figure 3.11 shows the settling velocity of the fully mixed sample, which had a maximum of < 0.35 mm/s, as a function of time. The average settling velocity was calculated by averaging all the data points. The result is described in Table 3.3.

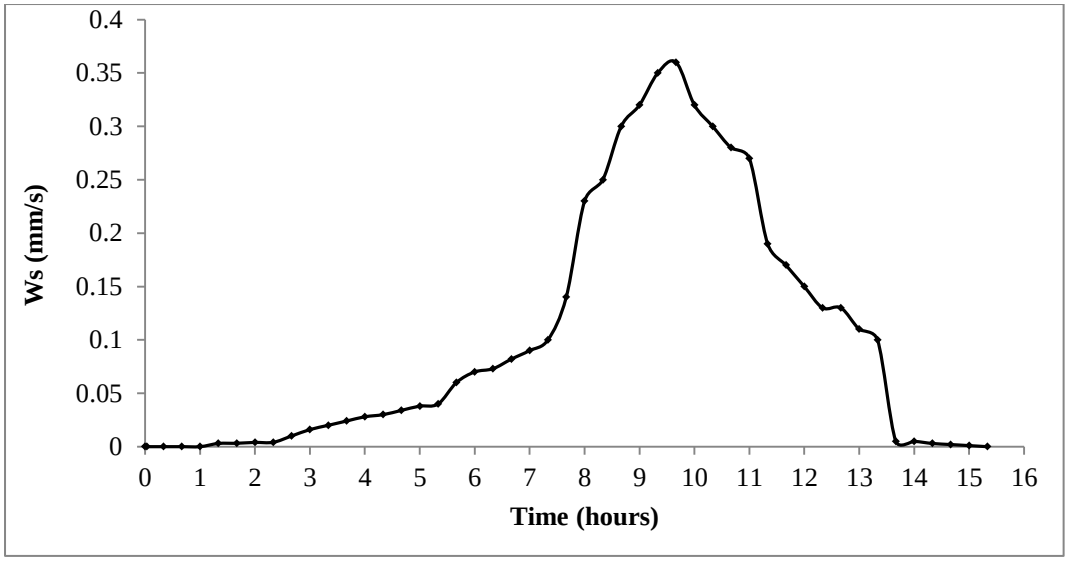

Figure 3.11 Settling velocity of the fully mixed sample as a function of time.

The settling velocities of the field samples were calculated for the four sampling different conditions (dry, wet, semi-wet and fully mixed). Comparisons between the different sampling conditions are presented in Table 3.3. The fully mixed sampling conditions presented results with very slow settling velocities resulting from particles that were too fine, while the settling velocity of the wet sample conditions caused the presence of bigger distance with much larger settling velocities in the Severn Estuary sample. Notably, the settling velocities of both the dry and semi-wet samples were approximately the same. It is recommended that using the fully mixed sampling is a proper method to describe the settling velocity of a single particle size.

Table 3.3 Settling velocity of Severn Estuary sample (Ws: settling velocity)

Sampling condition	Ws (mm/s)	Measure method
Fully mixed sampling	0.100	Using traditional method of measuring distance over time of clear front settling down
Wet sampling	35.00	Using photo analysis
Dry sampling	11.20	Using photo analysis
Semi-wet sampling	11.87	Using photo analysis

3.5.5 **Flocs size distribution (FSD)**

In each test, ten images were analysed to produce the FSD (Maggi 2005). The particle sizes were primarily divided into eight size bands. Band 1 consists of floc sizes below 100 μm, while band 8 consists of floc sizes higher than 700 μm. Other size ranges with increasing floc sizes starting from range 1 and going up to 8 of the flocs were represented by bands 2 to 7. The floc size was transformed to a particle area (A%) based on a FSD according to the following equation

$$\%A_i = \frac{A_i}{A_T} X\ 100 \quad \textbf{(3.10)}$$

where i is the size band. A_i is the total area of the particle at size band i, and A_T is the total area of all the particle size band.

3.5.5.1 **Effect of salinity on FSD**

The spherical equivalent FSDs as a function of S (0, 0.5, 1, 2, 2.5, 5, 7.5, 10, 20 and 30 ppt) are shown in Figure 3.12. The results are classified according to the shape of the histograms in four graphs: 1) Figure 3.12a shows the salinities of 0, 0.5 and 1 ppt; 2) Figure 3.12b shows the salinities of 2 and 2.5 ppt; 3) Figure 3.12c shows for the salinities of 5 and 7.5 ppt; 4) Figure 3.12d shows the salinities of 10, 20 and 30 ppt. The distribution of floc sizes demonstrates that the particle sizes ranging from 70 μm (detection limit) to 941.6 μm (maximum floc size). The largest overall area was for floc size ranging from 100–250 μm. The largest floc sizes (>700 μm) were detected only at the S of 2.5 ppt, whereas no particles less than 100 μm were detected for this salinity. The area of floc size (600-700) μm decreased by 3% with increasing salinity from 2.5 to 5 ppt.

The maximum and average floc sizes (dmax and davg) exhibited variability that increased as the salinity increased from 0 to 2.5 ppt. The variability then decreased to an almost constant value of 504 μm at S larger than 5 ppt. The floc size indicated that dmax at S of 2.5 ppt (941 μm) produced approximately double the floc size displayed in fresh water and higher saline water of S >7.5 ppt. Compared to the dmax, the area of the floc size (100–200) μm increased by 15% from very low salinity to a high salinity of 30 ppt. The process can be observed in the laboratory, at low salinity rates the water became less turbid as a result of the particles that were involved in flocculation processes.

In fresh water, the positive charge on the edge of the flocs is low. Subsequently, the flocs are small in size. This result has been reported by different authors (Dorich et al. 1984; Droppo and Ongley 1994). When the amount of sodium chloride (NaCI) and other salt water ions was increased the positive charge on the floc edge gradually increased until it is big enough to induce flocculation, and the flocs are bigger at S of (2–2.5) ppt. The onset of flocculation occurred under low salinity conditions, which was found to be the best environment for the flocs to reach the maximum size greater than 700 μm.

This result was in good agreement with the findings of previous studies. Dobereiner and McManus (1983) found that coagulation increased at low salinities (1–2) ppt based on data from the Tay Estuary. Gibbs and Konwar (1986) found that the aggregate size in the Amazon Shelf depended on salinity when it was less than 10 ppt. Wollast (1988) found that intense flocculation occurred as soon as the salinity level was increased to about 1 ppt and was complete when it reached values above 2.5 ppt. Krone (1962); Allersma et al. (1967); Migniot (1968); Lintern (2003) and Thill et al. (2001) showed that salinity variation affected flocculation up to a threshold beyond which no significant effect was observed.

Any further increase in the level of salinity reduced the repulsive force between the face and the edge of the floc and led to weakly structured flocs that were relatively small (Nasser and Twaiq 2011). This finding demonstrates that the aggregation effect is dominant at the low salinities because of the shortage of large flocs. Over time, breakage becomes competitive when sufficient number of large and fragile flocs exists in the system. The increase in the percentage of small flocs with increasing salinity could be caused by collisions. This result corresponds with the results of a field study by Van Leussen (1999) carried out in the Ems Estuary. The findings showed that a floc size of less than 160 μm increased strongly from low salinities toward the seaward boundary, whereas the overall area of floc sizes larger than 160 μm increased in the low salinity region.

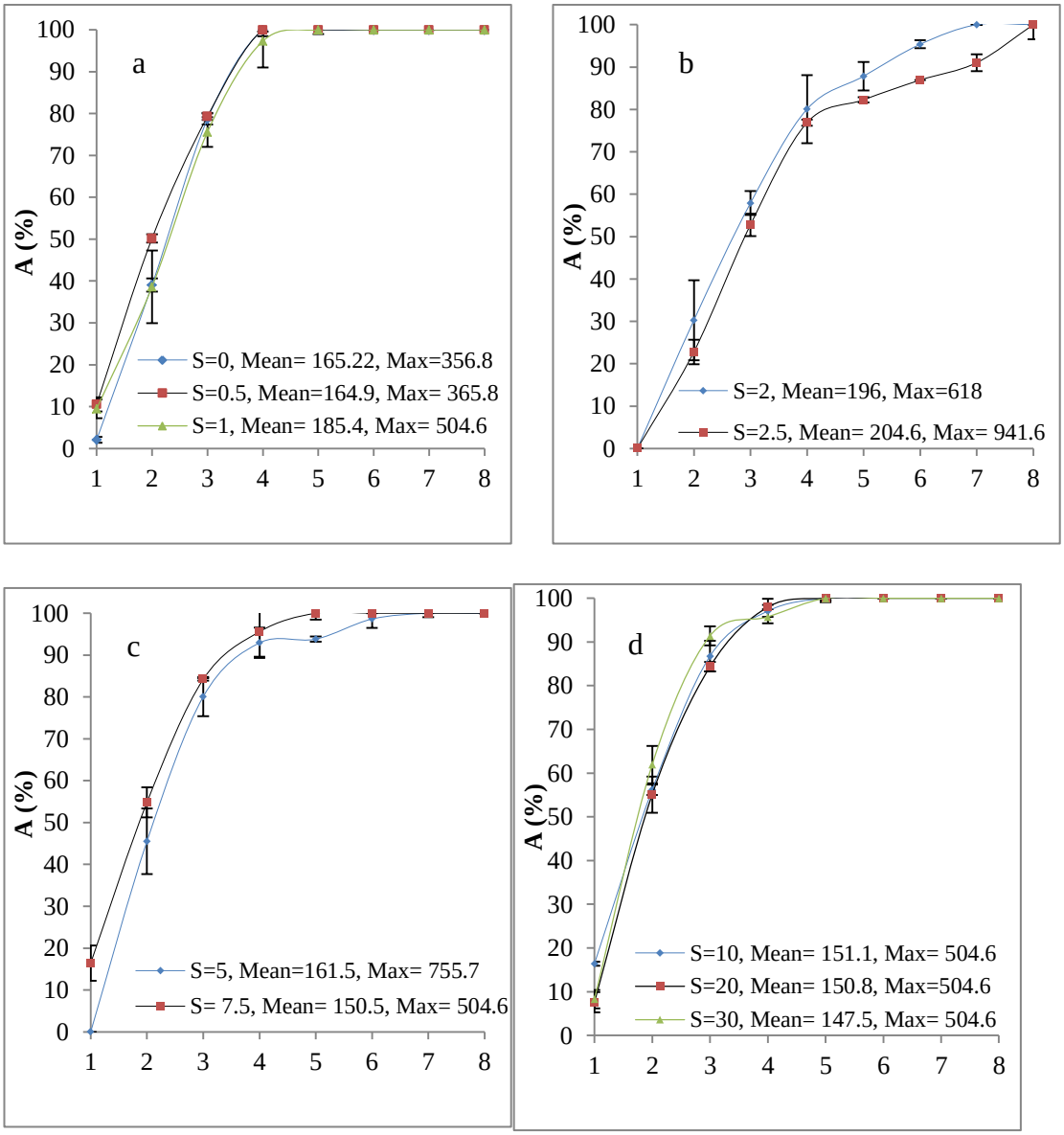

Size band	**1**	**2**	**3**	**4**	**5**	**6**	**7**	**8**
Floc size (µm)	**<100**	**100-200**	**200-300**	**300-400**	**400-500**	**500-600**	**600-700**	**>700**

Figure 3.12 The size band distribution of floc area against salinity; the ranges represent the standard deviations between two runs

3.5.5.2 **Effect of suspended sediment concentration on FSD**

The floc size distributions as a function of SSC (100, 150, and 200) g/m^3 at both salinities of 2.5 ppt and 20 ppt are displayed in Figure 3.13. Floc size exhibits variability that increases with increasing SSC at both salinities of 2.5 ppt and 20 ppt. The floc size distribution for the data shows that particle sizes ranged from 75 μm to 941.6 μm, with the greatest numbers of flocs being in the 150-250 μm range. The percentage of large flocs (>700 μm) at S 2.5 ppt decreases from 9% to 2% with increasing sediment concentrations from 100 to 200 g/m^3 as shown in Figure 3.13 a. This result is in good agreement with the results obtained by Manning and Dyer (1999), who worked at the Tamar Estuary with in situ settling velocity (INSSEV). This decrease in the percentage of large flocs with increasing sediment concentration could be a result of the disruption caused by collisions (with an increase in collision frequency as SSC increase), whereas aggregation at low sediment concentrations and salinity of 20 ppt is less than that at low sediment concentration and salinity of 2.5 ppt.

The flocculation onset can occur at low salinity and low concentration. This is the best environment for floc size to reach the maximum size of more than 700 μm as discussed previously in section 3.5.5.1. With increasing SSC at low salinity, the flocs are more likely to bump into each other more frequently which subsequently can cause flocs' breakdown. In this situation, the floc size is still larger than 700 μm but the percentage of the large flocs is decreased by 7% (Figure 3.13 a). Figure 3.13 b indicates that at a high salinity of 20 ppt the particles do not exceed 500 μm at SSC of 100 mg l^{-1}. This stage might be transitory until a specific amount of sediment is attained, which gives particles a higher chance to bump into each other and reach sizes in excess of 700 μm at SSC of 200 g/m^3 (see Figure 3.13 b). At S of 20 ppt, the peak at SSC of 100 and 150 g/m^3 is almost the same, for floc sizes (100 – 200 μm). The position of the peak moved with increasing SSC to 200 g/m^3 from smaller floc size towards larger floc size. At the same salinity range of (20 ppt), the maximum floc size increases with increasing SSC. A possible reason is that at high salinities of 20 ppt the probability of collision between particles is enhanced with increasing SSC. Consequently, the floc sizes increase with increasing SSC (Figure 3.13 b). Eisma et al. (1991) found that the increase in SSC will have an influence on reducing the turbulent level and are contributing to increasing the frequency of particle

collisions and hence causing enhanced flocculation. Tsai et al. (1987) conclude that increased sediment concentration may enhance flocculation by increasing particle size due to increased frequency of particle collisions with increased SSC and reduction of inter-particle space.

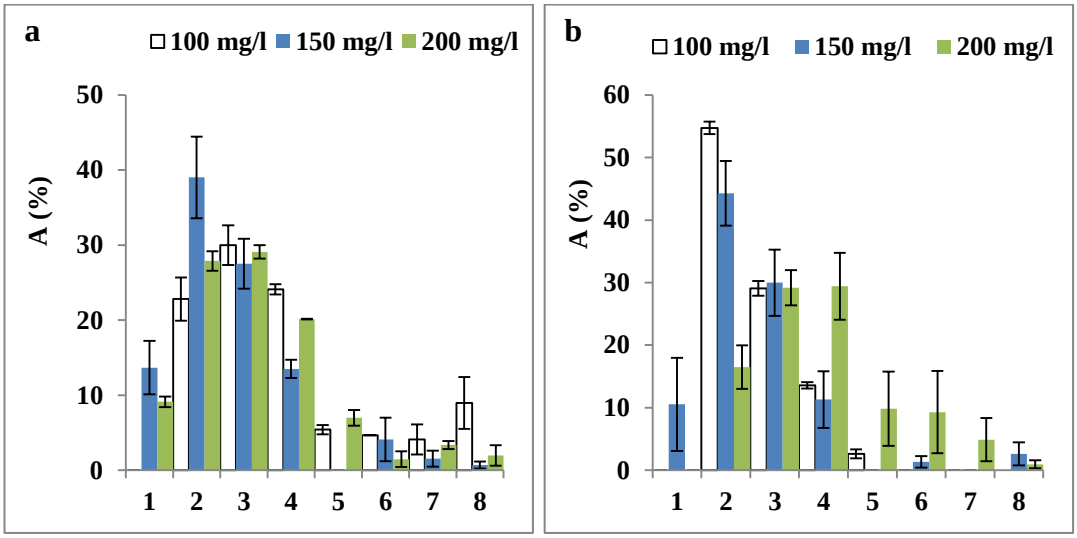

Size band	1	2	3	4	5	6	7	8
Floc size (µm)	<100	100-200	200-300	300-400	400-500	500-600	600-700	>700

Figure 3.13 Floc size distribution at various concentrations for a) S=2.5 ppt and b) S=20 ppt

3.5.5.3 Effect of turbulence on FSD

The FSDs as a function of the turbulent shear rate at salinity of 2.5 ppt are shown in Figure 3.14. At the smallest shear stress (0.57 N/m^2), no particles smaller than 100 µm were detected, but particles larger than 500 µm were observed. However, at the highest shear stress of 8.5 N/m^2, 50% of the floc area was made up of particles less than 100 µm, and no particles larger than 400 µm were detected. This finding indicates that the range of turbulent shear stresses (0.57–8.5 N/m^2) is causing the aggregate to break up instead of enhancing the flocculation process. The average floc size ranged between 204 µm to 135 µm (Figure 3.14). There was a decrease in the average floc size as well as the maximum floc size as the turbulent shear stress increased.

The Kolmogorov microscale values used for the experimental work exhibited good correspondence with the maximum floc size. The maximum floc size (dmax) was approximately two-and-half times the length of the Kolmogorov scale (η).

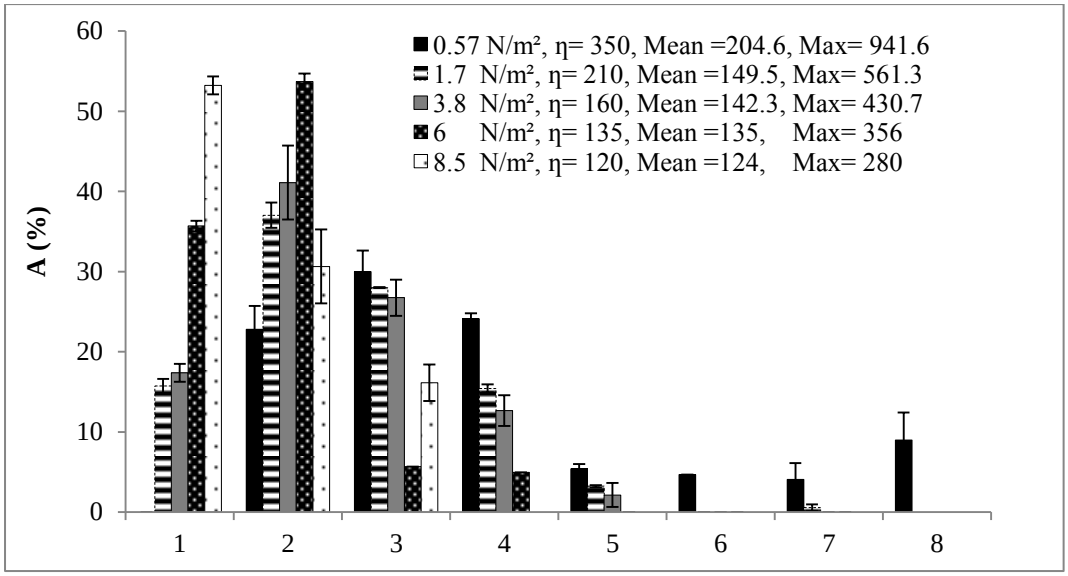

Figure 3.14 Floc size distribution under different turbulent shear stresses and at S of 2.5 ppt including the standard deviations between two runs.

Figure 3.14 indicated that the largest Kolmogorov microscale value is 350 μm and once this value was decreased, which means the turbulent shear stress increased, this was causing aggregate breakup as opposed to the enhancement of flocculation process.

3.5.5.4 Effect of salinity changes over time with a constant agitator speed on FSD

During the test and the following subsequent image analysis, it became apparent that increased salinity did not improve the flocculation phenomenon as discussed previously in section 3.5.5.1. As mention above in section 3.5.5.1, the floc size decreased as the salinity increased from 2.5 to 7.5 ppt. It is believed that flocculation is enhanced by increasing salinity up to a definite threshold, above which an additional increase would have no effect (Krone 1962; Allersma et al. 1967; Lintern 2003). The results of this experiment showed that the relationship between floc size

and salinity was independent of the history of the floc formation. At all salinity ranges, the maximum floc size of the tests with constant salinity throughout was approximately the same as tests in which salinity changed over time (Figure 3.15). This result means that the relationship between floc size and salinity was independent of the history of the floc formation.

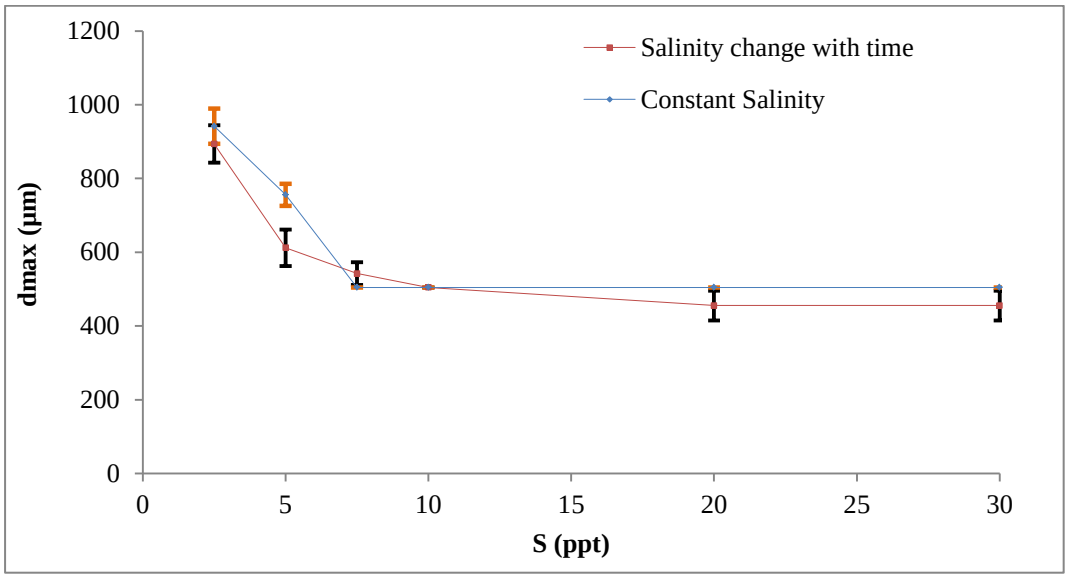

Figure 3.15 Variation in maximum floc size versus salinity gradient for two scenarios (salinity changing over time during the test and constant salinity). The ranges represent the standard deviations between two runs

3.5.5.5 Effect of turbulence change with time on FSD

Figure 3.16 shows the relationship between the maximum floc size and the variation in the turbulent shear stress over time. The results show that turbulent shear stress increased from 0.57 N/m^2 to 8.5 N/m^2, which caused an increase in the breaking up of the flocs. The maximum diameter decreased from 941.6 µm at T_S = 0.57 N/m^2 to 280 µm at T_S = 8.5 N/m^2 (approximately 67.6%) (Figure 3.16). This observation is similar to that of Manning and Dyer (1999), who found a decrease in floc size with an increase in the shear velocity of up to 0.3 N/m^2 in their laboratory flume experiments with sediment samples from the Tamer Estuary with sediment concentrations ranging from 80 g/m^3 to 200 g/m^3. In the present experiment, the maximum floc size was found to be similar in both sets. As shown in Figure 3.16, in one set, five different turbulent shear stresses were tested of 0.57, 1.7, 3.8, 6 and 8.5

N/m^2, which represented the variations among the maximum floc size of the tests with constant T_S throughout.

In addition, the other set, as described above, was tested at an initial turbulence of 0.57 N/m^2 for two hours. Subsequently, the turbulence was increased to 1.7, 3.8, 6 and 8.5 N/m^2 in one-hour intervals. The results of this experiment showed that the relationship between floc size and turbulent shear stress was independent of the history of the floc formation. At all turbulent shear stress levels, the maximum floc size of the tests with constant T_S throughout was approximately the same as tests in which T_S changed over time (Figure 3.16). As known that in natural estuarine waters, turbulence varies during the tidal cycle, this result means that the relationship between floc size and turbulent shear stresses was independent of the history of the floc formation.

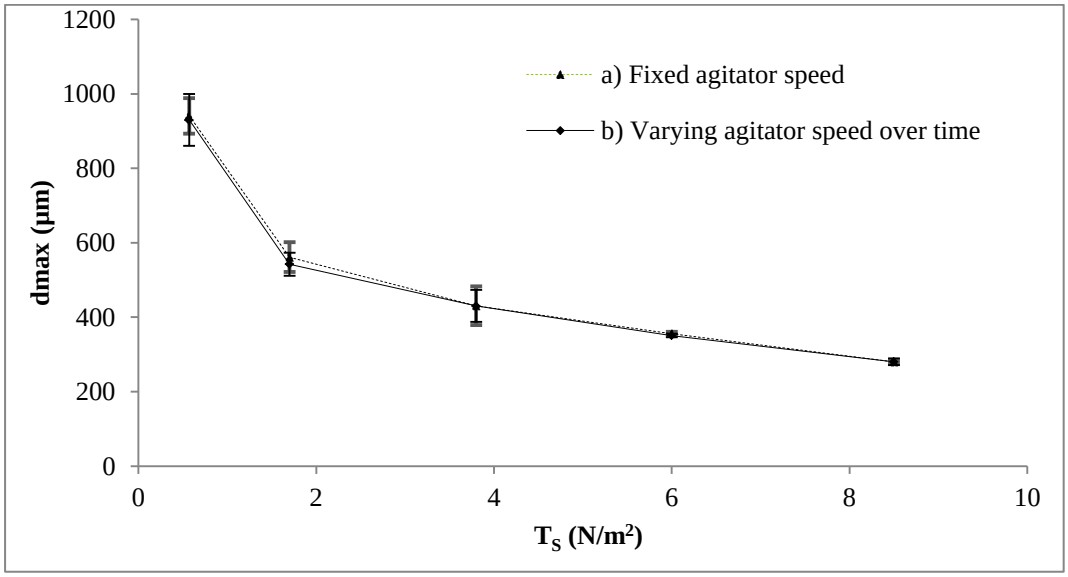

Figure 3.16 Maximum floc size for a) fixed agitator speed and b) varying agitator speed over time. The range shows the standard deviation between two runs.

3.5.6 **Settling velocity**

3.5.6.1 **Effect of suspended sediment concentration and salinity on settling velocity**

The relationship between the average floc size and settling velocity for a specific suspended sediment concentration (SSC) for both salinity ranges of 2.5 and 20 ppt (Figure 3.17 a and b). In this figure, the floc distribution was split into four components, each with their own mean floc size and settling velocity as suggested by Dyer et al. (1996). The authors suggested that an accurate representation of floc settling velocity can be derived by splitting the floc distribution into two or more components, each with their own mean settling velocity. Figure 3.17 illustrates that the settling velocity changes from 0.4 to 1.2 mm s^{-1} and 0.2 to 1.1 mm/s for salinities of 2.5 and 20 ppt respectively. The settling velocity at salinity 2.5 ppt, displays a similar trend to experimental data presented by Burban et al. (1989), and the field data recently reported by Manning (2004c), where, at low shear stress the settling velocity was smaller at lowest SSC and increases with increasing SSC. This could be due to the floc density, which will be examined in the next section, the slow settling floc being of low density and low SSC, whereas, the fast settling values were a result of more dense flocs. Also, Pejrup and Mikkelsen (2010) found that the settling velocity increases with increasing SSC from 20 ppt to 200 g/m^3 under fresh water conditions, based on data collected by Pejrup et al. (1997). This can be explained by the fact that at low salinity and high sediment concentration, the particles start bumping into each other which leads to a decrease of the flocs' surface area and the floc becomes denser.

The collision frequency appeared to stimulating the increase of the settling velocity. Whereas, at high salinity of 20, this situation is reversed and the faster settling velocity was found to occur at lower SSC. This could be the result of floc structure, which will be discussed late in section 3.5.8. The settling velocity at the concentration of 200 g/m^3 and both salinity ranges of 2 and 20 ppt is interesting (Figure 3.17 a and b). The sediment settling velocity at S of 20 ppt was 0.37 mm/s which was 54% or 0.43 mm/s slower than the settling velocity of flocs generated at low salinity (2.5 ppt). This could be the result of floc structure and density. The

decrease in the settling velocity with increasing salinity is perhaps due to the formation of flocs with lower densities in the high salinity range (Johansen 1998).

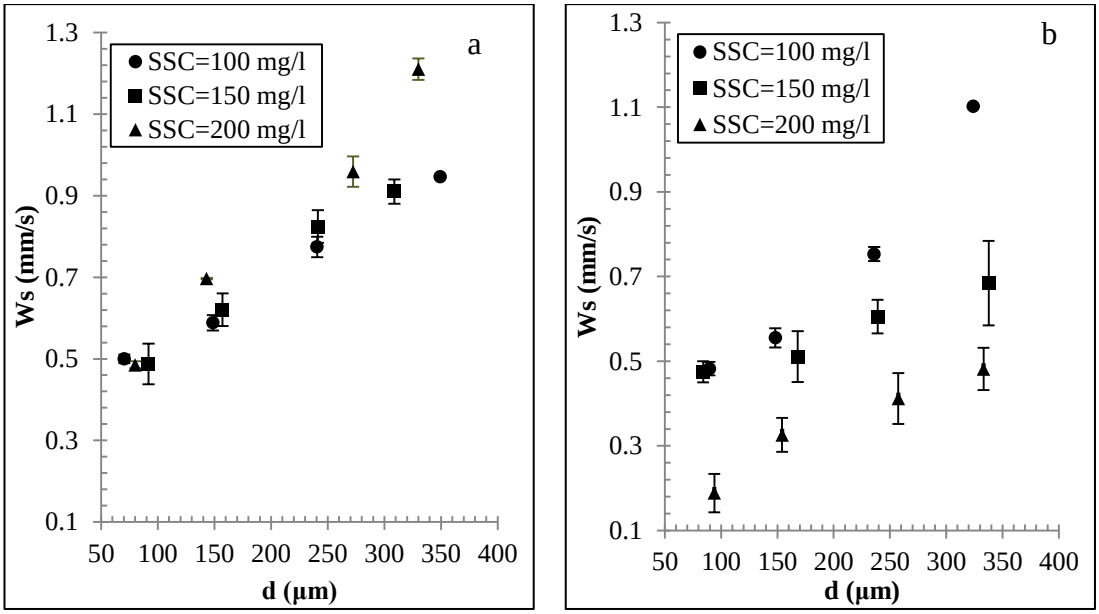

Figure 3.17 Settling velocity for various concentrations (different symbols) against floc size at a) S=2.5 and b) s=20. The range shows the standard deviation between two runs

3.5.6.2 **Effect of turbulent shear stress and salinity on settling velocity**

Data analysis was performed using Minitab statistical analysis to determine the regression equation between settling velocity and the physiochemical and hydrodynamic parameters (S, SSC and T_S). There was not enough data to include all these three parameters on the regression equation. The statistical analysis indicated that the correlation between settling velocity and SSC is not strong enough compared with S and T_S. Therefore, only S and turbulence (N/m^2) represented the average settling velocity value. Figure 3.18 shows the settling velocity plotted against salinity (2.5–30 ppt) at different turbulent shear stresses (0.57, 1.7 and 3.8). Figure 3.18 indicates that the average settling velocity varied from 0.54 to 0.86 mm/s. The regression line shows that the average settling velocities depended on both salinity and turbulent shear stress. The average settling velocity increased by nearly 27% as the turbulent shear stress increased from 0.57 N/m^2 to 3.8 N/m^2. Similar results were obtained by Manning et al. (2007) where high turbulence levels caused an increase in settling velocity as observed in the field study at Scheldt

Estuary. The settling velocity decreased by 21% as the salinity increased from of 2.5 to 7.5 ppt.

The settling velocity then began to increase to reach almost a constant at S of 10 ppt and higher. This finding has been previously observed by different authors (i.e. Gibbs and Konwar 1986, Verney et al. 2009, Sutherland et al. 2015) where the settling velocity did not change for S higher than 20 ppt. In developing a settling velocity equation as a function of salinity and turbulent shear stress, it was not possible for a single fitted line to include the experimental range of the salinity (Mhashhash et al. 2018). Therefore, the graph was split into two zones, as presented in Figure 3.18. For salinity less than 10 ppt, the settling velocity was dependent on both parameters of salinity and turbulence. Over 10 ppt, only turbulence affected settling velocity.

The Minitab 17 statistical package was used to model the experimental data and perform a multiple regression analysis, which showed a statistical confidence level of 95%. These equations were developed for a sediment concentration of 100 g/m^3. The experimental data were firstly modelled to find the relationship between floc size and the parameters of salinity and turbulent shear stress. Then, the settling velocity as a function of flocs size was developed. The regression equations are expressed as follows:

For S less than 10 ppt

$$\text{davg} = 245.8 - 10.88\,\text{S} - 40.67\,\text{T}_\text{S} + 4.62\,\text{T}_\text{S}^2 \quad \textbf{(3.11)}$$

$$\text{Ws} = 1.464 - 0.0758\,\text{S} - 0.00289\,\text{davg} \quad \textbf{(3.12)}$$

Equations (3.11) and (3.12) can be combined together to form equation (3.13) for calculating the settling velocity as a function of turbulent shear stress and salinity.

$$\text{Ws} = 0.75 - 0.045\,\text{S} + 0.117\,\text{T}_\text{S} - 0.0133\,\text{T}_\text{S}^2 \quad \textbf{(3.13)}$$

For S more than and equal 10 ppt

$$davg = -14.70\ T_S + 154.2 \quad \textbf{(3.14)}$$

$$Ws = -0.0031\ davg + 1.15 \quad \textbf{(3.15)}$$

Equations (3.14) and (3.15) can be combined together to form equation (3.16) for calculating the settling velocity as a function of turbulent shear stress at high salinity.

$$Ws = 0.623 + 0.0866\ T_S \quad \textbf{(3.16)}$$

The regression equations indicate that the correlations between S, T_S and Ws are essential with R^2 of 0.9 with a statistical significance of P <0.01. These equations have been applied to the Delft3D model and were tested using the model for the Severn Estuary (Chapter 5).

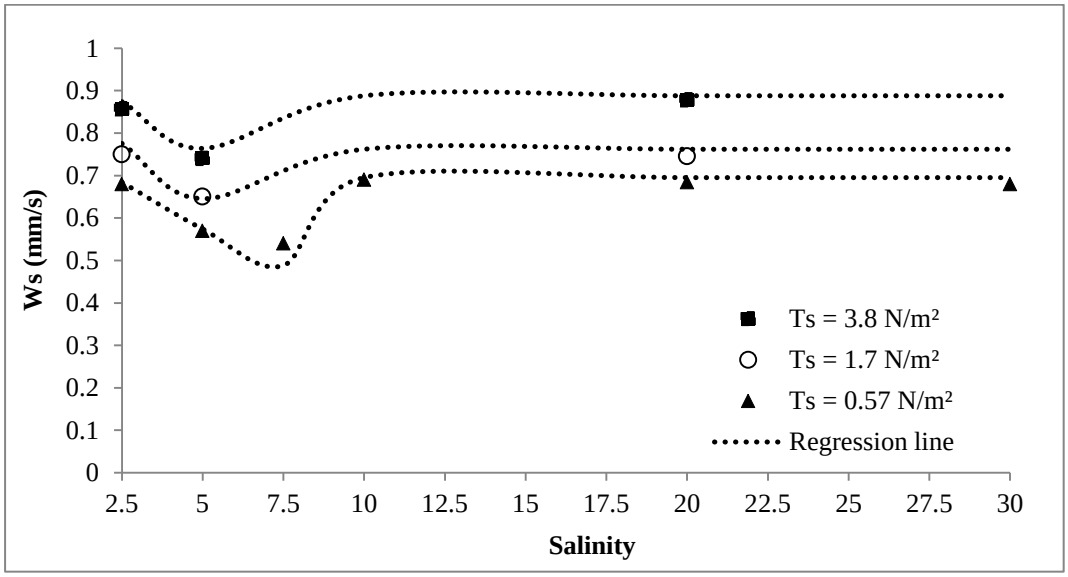

Figure 3.18 The average settling velocity over the experimental salinity ranges for different turbulent shear stresses

3.5.7 Comparison of experimental measurement data with other published experimental studies

The average settling velocity as a function of average floc size for different SSC, S and T_S was plotted and compared with those in previous experimental studies, as shown in Figure 3.19. The magnitudes of the Ws values observed during the present study were found to be higher than those seen in the laboratory by Verney et al. (2009) and smaller than those found by Lick et al. (1993), which could be a result of the method used to analyse the data. In Figure 3.19, floc distribution was split into eight size bands; each band has a specific mean floc size and settling velocity. However, Verney et al. (2009) and Lick et al. (1993) utilised the mean floc size to compute the floc settling velocity. The experimental results of this study are similar to those of Manning and Dyer (1999) in the region of d (70–140) μm, but were slightly lower in the region of d = 140–200 μm. The trend of the settling velocities was similar to the findings of an experimental study conducted by Sternberg et al. (1999) with only the gradient being lower.

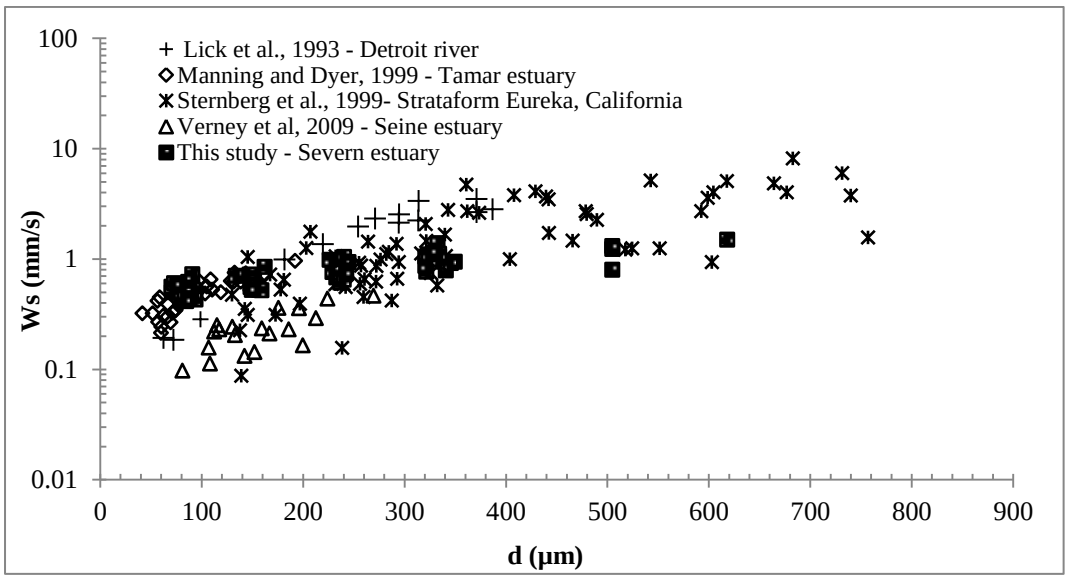

Figure 3.19 Comparison of floc sizes and settling velocities in different estuaries

3.5.8 **Analysis of floc structure**

The variability of floc size and settling velocity relationships results of the difference in composition and structure of the flocs. Because the floc structure could not be measured directly using the PIV camera, the fractal dimension of flocs (n_f) was determined theoretically using the Winterwerp model (Winterwerp 1999). This model was developed based on published field and laboratory data from the North Sea, Chesapeake Bay, Ems and Tamar estuary. For floc size ranges from 20 to 1000 µm and settling velocity ranges from 0.04 to 10 mm/s.

The experimental data at different salinity ranges are plotted with the Winterwerp model, as shown in Figure 3.20. The results show that the experimental data adequately matches the Winterwerp model. The overall trend of the experimental data was slightly steeper than the fit at n_f = 2 for the different salinity ranges. However, when the individual data sets were studied, the slope was in agreement with an n_f of between 2 and 2.3 for low salinity levels and an n_f of between 1.7 and 2 for high salinity levels of from 7.5 ppt to 20 ppt (Figure 3.20c). This result is shown in the scanning electron microscope (SEM) photographs provided in Figure 3.21 a and b. In this figure, the floc structure is shown at low and high salinities of 2 and 20 ppt, respectively. This result indicates that the floc size becomes increasingly irregular in shape and its structure becomes unstable and fragile (less dense) as S increases (Figure 3.21 b).

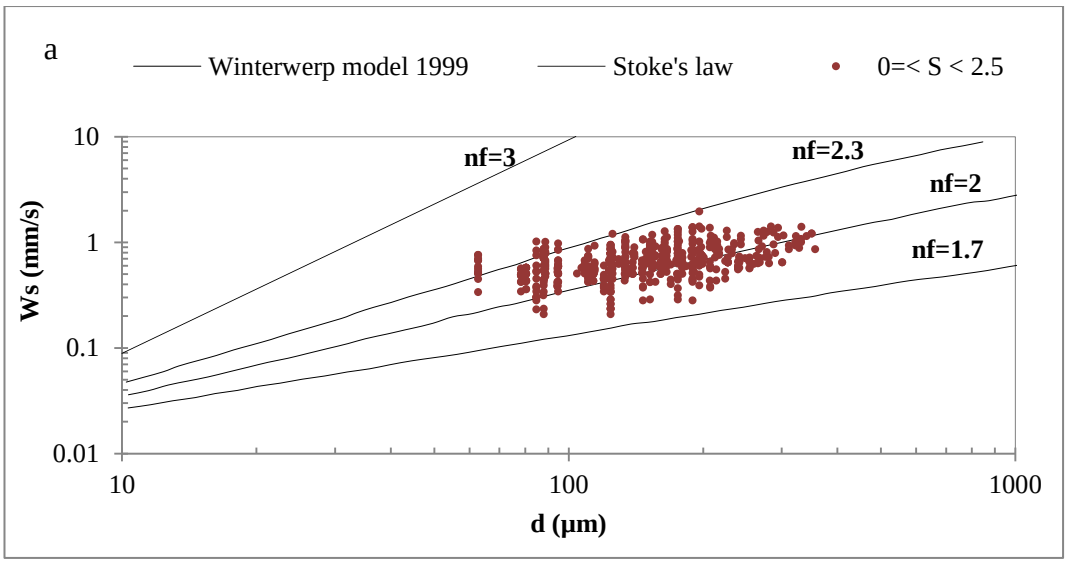

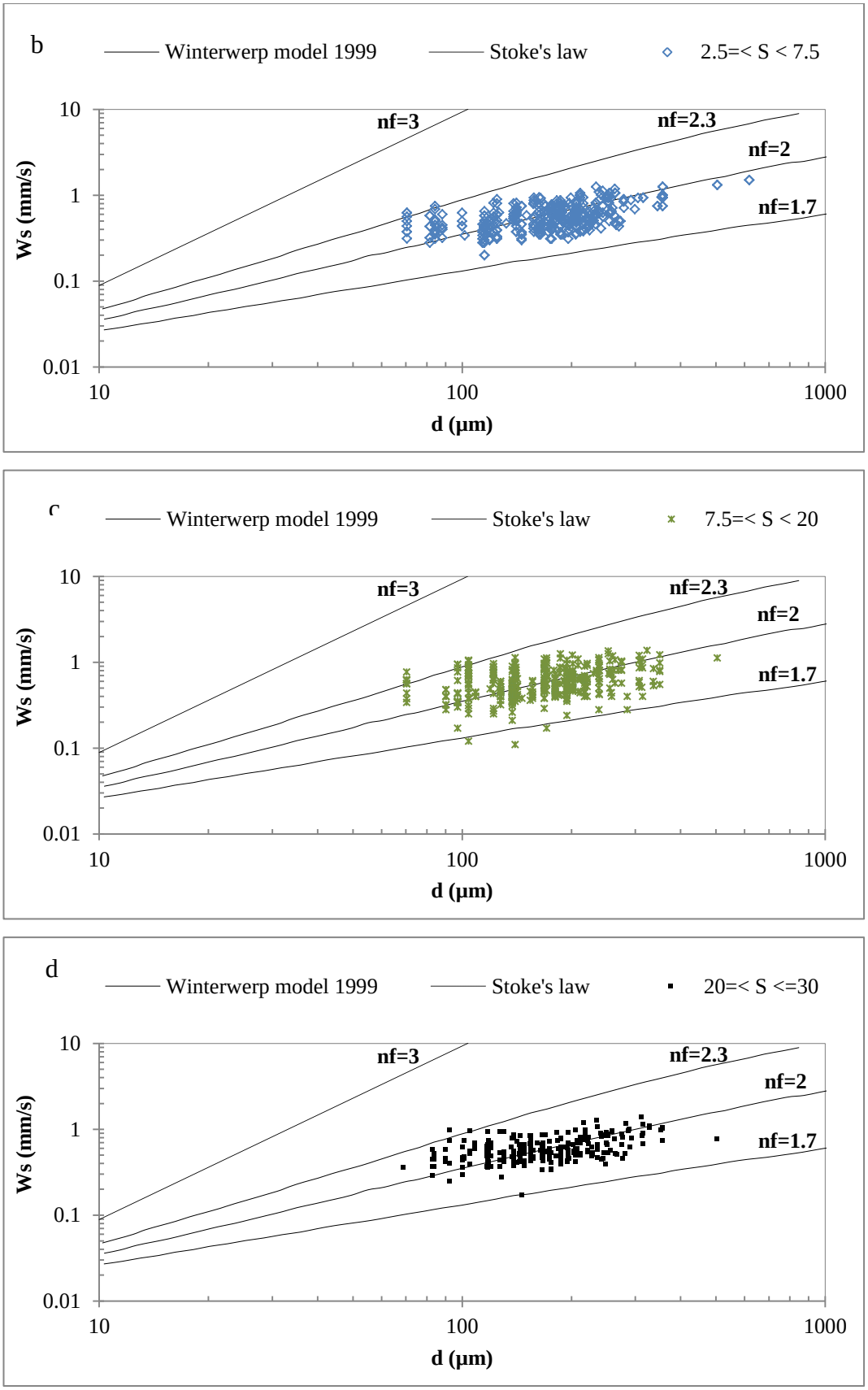

Figure 3.20 The relationship between settling velocity and floc size at different salinity ranges

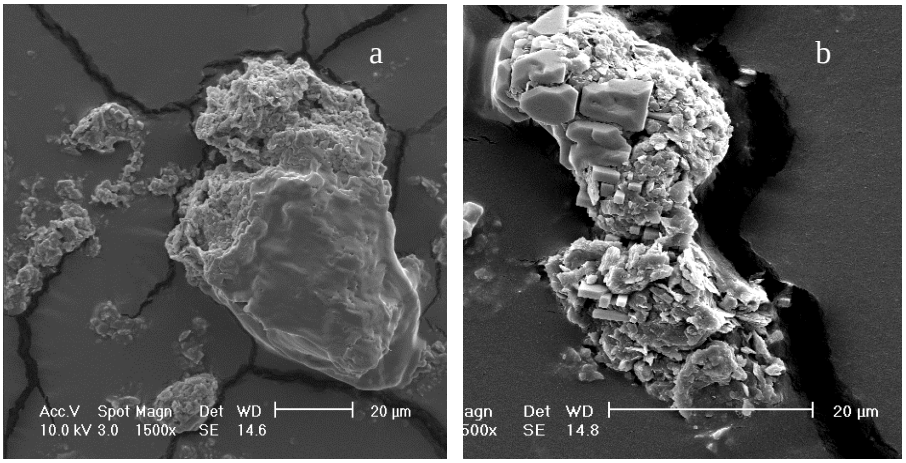

Figure 3.21 A selection of SEM photographs of flocs at a) S=2, b) S=20

For different sediment concentration, the fractal dimension (n_f) value was found to be increased from 2.1 to 2.3 with increasing SSC at low S of 2.5 ppt (Figure 3.22 a). This can be explained as described previously in section 3.5.5.2, with increasing SSC at low salinity, the flocs are more likely to bump into each other more frequently which subsequently can cause flocs' breakdown and the flocs became more dense. However, the situation was reversed at S of 20 ppt; the n_f value decreases with increasing SSC (Figure 3.22 b). This result is shown in the scanning electron microscope (SEM) photographs provided in Figure 3.23 a, b. This figure shows the scanning electronic microscope (SEM) photographs of flocs at S=20 and turbulence of 0.57 N/m^2 for SSC of 100 and 200 g/m^3. The flocs at sediment concentration of 200 g/m^3 become unstable and more fragile (less dense) as they grow and the flocs at low SSC of 100 g/m^3 are more dense. Therefore, it was expected that the settling velocity would decrease with increasing sediment concentration for this range of salinity (20).

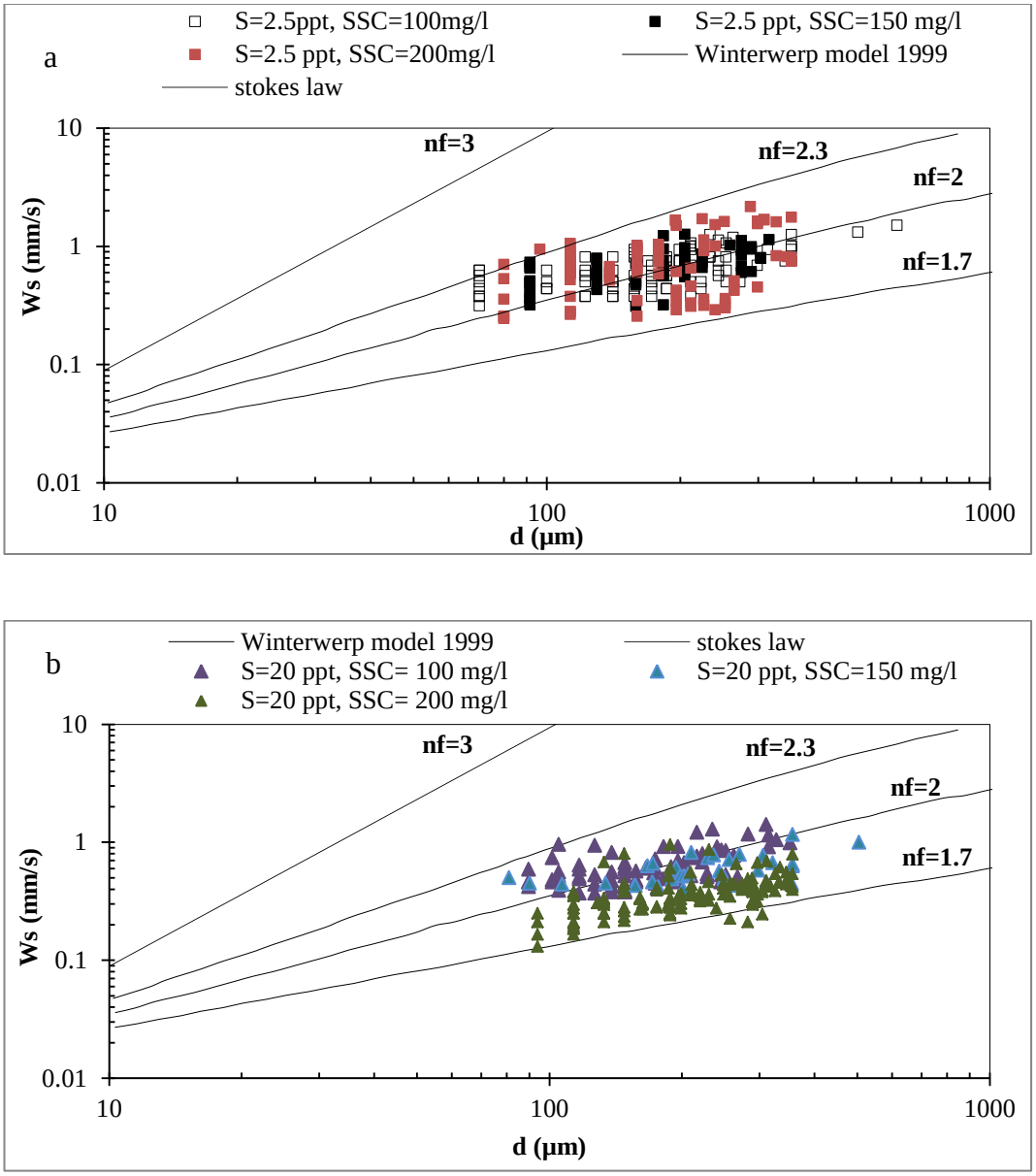

Figure 3.22 The relationship between settling velocity and floc size at different SSC a) S=2.5 ppt and b) S=20 ppt

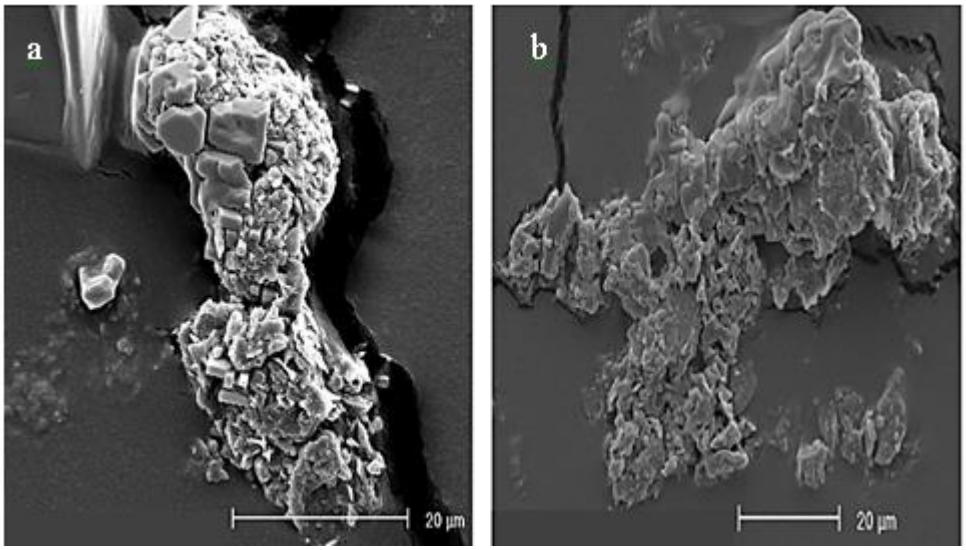

Figure 3.23 A selection of SEM photographs of flocs at S=20, different SSC, a=100 and b=200 mg l^{-1}

For different turbulent shear stresses, the fractal dimension (n_f) value was found to be between 2–2.3 for a T_s of more than 6 N/m^2. However, the situation was reversed at low turbulence; the flocs became bigger and less dense, with n_f values between 1.7–2.3 (Figure 3.24). This result indicates that high shear stresses break macroflocs down into microflocs, and the flocs increase in density. As turbulent shear stress increases, the flocs are more likely to collide more frequently. When comparing the experimental finding with the field data, (Dyer and Manning 1999) found that the n_f values ranged from 1.5–2.36 for the 28 field samples that were measured at Portishead on the Severn Estuary. These results indicate that more fragile (n_f =1.5) and stronger flocs (n_f =2.36) were observed in the field study by Dyer and Manning (1999) compared with the n_f ranges that were found in this laboratory study, which were 1.6–2.35.

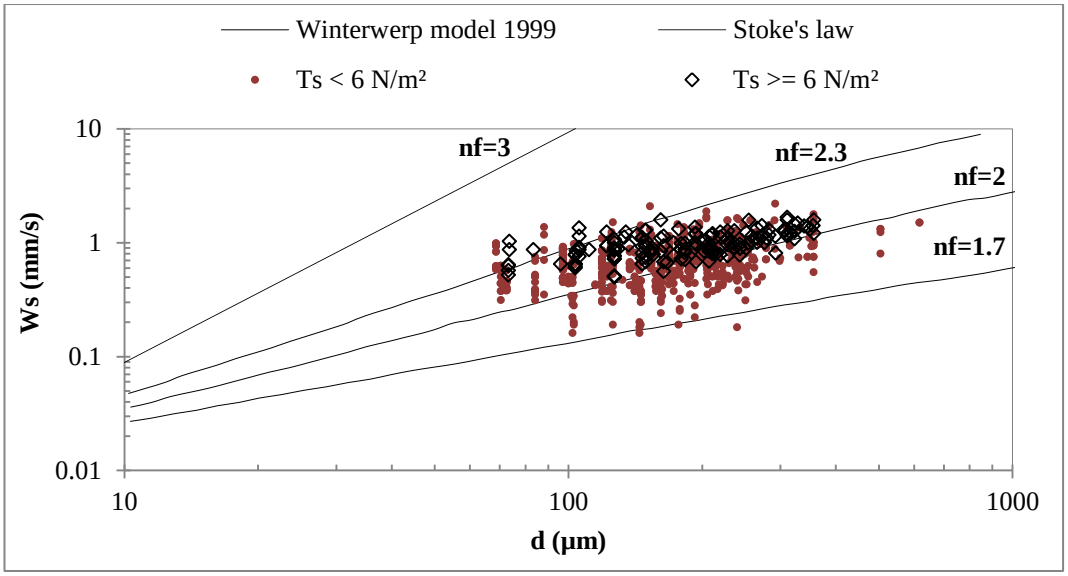

Figure 3.24 The relationship between settling velocity and floc size at different turbulent shear stress

Knowing the settling velocity of flocculated mud sediment aids in calculating the mass settling flux. This is the rate at which mud sediment is either deposited towards the river bed or resuspended into the water column (Geyer et al. 2004; Soulsby et al. 2013; Keyvani and Strom 2014). This study showed that the sedimentation of cohesive sediment is substantially slowed down by the increasing water salinity of more than 2.5 ppt (Figure 3.20). Sedimentation did not noticeably increase in water once salinity exceeded 10 ppt. In previous studies, such as those by Verney et al. (2009) and Sutherland et al. (2015), this was observed for estuarine waters when salinity did not exceed 20 ppt.

Increasing SSCs in high saline waters can slow down the sedimentation of cohesive sediment (Figure 3.22). Increased sediment concentrations at high salinity can cause the formation of less dense flocs, which means that there is more sediment in suspension than what is being deposited in the river bed. The situation is reversed when increasing sediment concentration at low salinity. Increasing settling velocity can affect the accumulation of sediment particles, especially in the region of the estuary turbidity maximum (ETM). This region's ETM was defined in Chapter 1. In addition to the effects of salinity and sediment concentration on mud deposition and resuspension, turbulent shear stress also plays a dominant role in sediment deposition; more mud sediment can be observed during high turbulence intensity.

Therefore, it can be assumed that the occurrence of mud sedimentation is affected by salinity, SSC and turbulent shear stress.

3.5.9 **Analysis of floc density**

Floc effective density was theoretically calculated based on and Winterwerp (1999) model (Equation 2.5), which states that effective density is a function of the diameter and the density of the primary particle, floc size and fractal dimension. The diameter and density of the primary particle were measured in the laboratory (see the result in section 3.5.2). The flocs' fractal dimension (n_f) was also determined theoretically using Winterwerp's model (Winterwerp 1999), which is discussed in greater detail in the following subsection. The effective density as a function of floc size is presented in Figure 3.25. The floc effective densities found in this study range from 30 kg/m^3 to 350 kg/m^3. The effective density decreases with increasing diameter. This relationship has been observed by different authors (e.g. Krone 1962, Winterwerp 1999, Winterwerp et al. 2006). Dyer and Manning (1999) found that large floc size with diameter of 800 µm has a low density and high and low density was observed at small flocs size of 150 µm, based on 28 field samples at Portishead on the Severn Estuary.The aggregates formation at S of 2.5 ppt demonstrates an increase of effective density with a constant floc size as SSC increases. This observation has been reported previously by Gratiot and Manning (2004). In contrast, at high S of 20 ppt the ρ_e decreases with a constant floc size as SSC increases. This can be explained by a decrease in the floc density meaning an increase in the porosity, which leads to an increase in the water content that forces the density of the floc towards the density of the water and tends to reduce the settling velocity (Droppo et al. 1997).

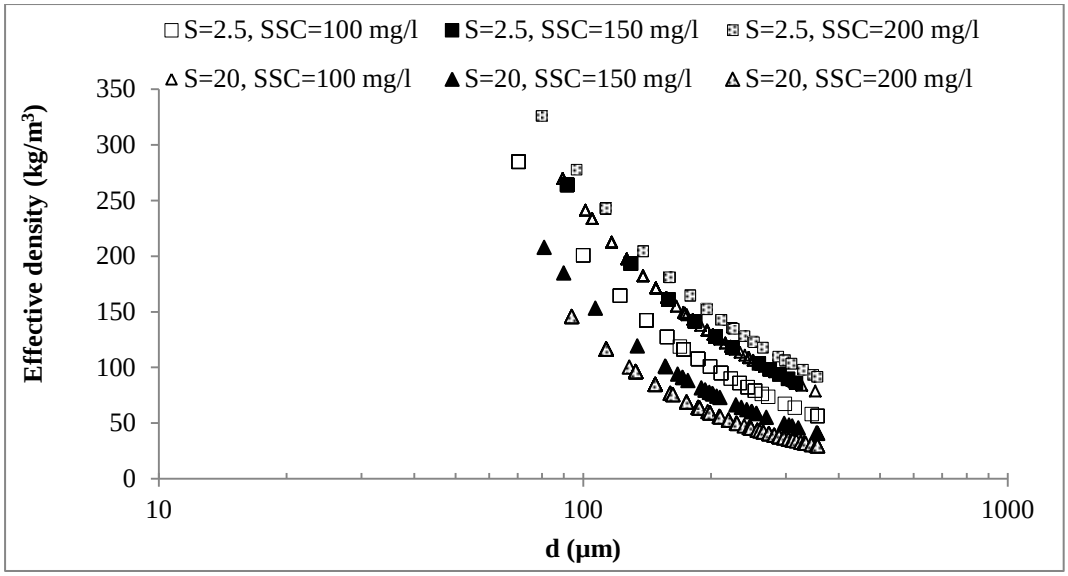

Figure 3.25 The relationship of the flocs size to the effective density for different S and SSC

3.6 Summary

In this chapter, the potential effects of the hydrodynamic parameters (i.e. salinity, suspended sediment concentration and turbulence) on the floc size and settling velocity were assessed using suspended sediment samples collected from the Severn Estuary under controlled laboratory experiments.

The main conclusions are as follows:

- The maximum floc size increased by 62% as S increased from fresh water to S 2.5 ppt. However, as S increased higher than 2.5 ppt, the maximum floc size decreased by 50%.
- Turbulent shear stresses ranging from 0.57–8.5 N/m^2 caused a breakdown of almost 67.6% of the floc structure.
- The percentage of large flocs increased by 3% as sediment concentration increased at high salinity. However, the situation was reversed at lower salinity when the percentage of large flocs decreased by nearly 7% as sediment concentrations increased from 100 to 200 g/m^3.

- The settling velocity was found to increased or decreased upon increasing the SSC, and it was further controlled by the salinity. Faster settling velocity occurred when sediment concentration was higher and salinity of 2.5 ppt. By contrast, at salinities of 20, in addition to increasing SSC, it was found that the situation was reversed (i.e. the lower the sediment concentration, the faster the settling velocity).
- The relationships between floc size and turbulent shear stresses and between floc size and salinity were independent of the history of the floc formation.
- The floc size and settling velocity were controlled by the interaction between turbulence and salinity at less than 10 ppt. At salinity equal to and more than 10 ppt, the floc size and settling velocity were functions of only turbulent shear stress.
- A favourable comparison between flocculation features (floc size and settling velocity) from different experimental studies confirmed that the method used in this study was successful measuring and analysing the floc size and settling velocity.

4 The numerical modelling system

4.1 Introduction

In numerical models, different scenarios can be developed to simulate and predict the flow, water quality and sediment transport characteristics in river and estuaries, and complex problems can be solved. The hydrodynamic computer model used in this study is Delft3D. This chapter describes the Delft3D program and the governing equations of flow and sediment modules that have been used in this study; however, Delft3D has several modules and features for used in different modelling scenarios. Further explanation and description of Delft3D program and full mathematical descriptions, can be found in the user manuals (WL|Delft Hydraulics 2014).

4.2 Delft 3D model

Delft3D is an open source software which means that the extendable software is completely free. Also, it is a three-dimensional, finite-difference model for wave, currents, sediment and contaminant transport. Delft3D is developed by WL/Delft Hydraulics in close cooperation with the Delft University of Technology, the Netherland (WL|Delft Hydraulics 2014). This package has several modules coupled together to provide a complete process for simulating two or three dimensional flow, sediment transport, water quality, morphological development and ecology of water systems, including coastal, river and estuarine waters. The Delft3D model can simulate various flow control structures, such as bridges, culverts, porous plates and weirs. Delft3D also includes pre-processing and post-processing programs (Figure 4.1). The main purpose of the two pre-process programs Delft3D-RGFGRID and Delft3D-QUICKIN are that Delft3D-RGFGRID generates and modifies curvilinear or orthogonal grids and Delft3D-QUICKIN allows creating, editing and visualising bathymetric data. Delft3D-FLOW, the computer program, generates input definition files and executes actual simulations. Delft3D-QUICKPLOT, the post-process program, allows the visualisation and animation of numerical results.

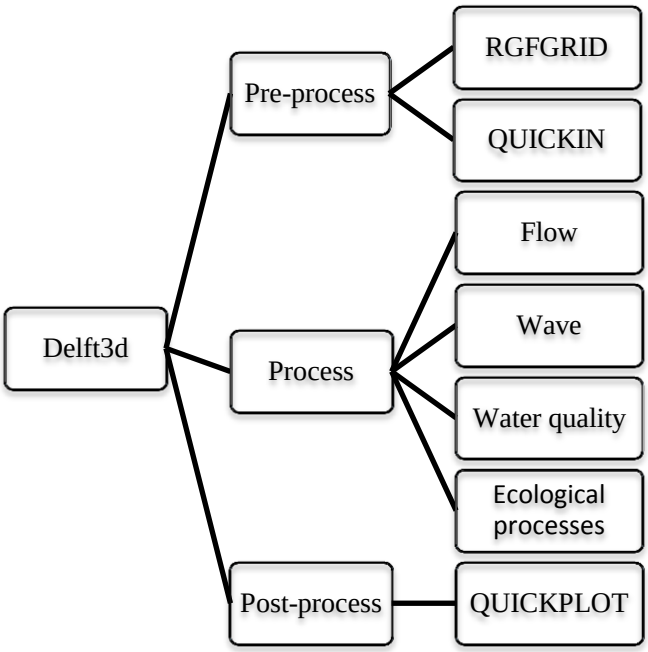

Figure 4.1 Overview of software tools of Delft3D

4.3 Hydrodynamic equations

The Delft3D-FLOW module is based on finite-difference solutions of the two- (depth-averaged) or three dimensional unsteady shallow water equations. The shallow water equations are derived from the Navier-Stokes equation in the vertical direction. Several assumptions have been made to derive these equations. One of the main assumptions is that the vertical length scale is much smaller than the horizontal length scale. This assumption contributes to reducing the vertical momentum equation to a hydrostatic pressure equation.

The main equations which were used in this study are: continuity equation, momentum equations, turbulence closure model and transport equation. As mentioned before, Delft3D has many other modules and features. Further information including the governing equations for other modules and full mathematical descriptions, refer to the user manuals (WL|Delft Hydraulics 2014).

4.3.1 **Vertical σ-coordinate system**

The vertical direction is defined as the sigma coordinate (σ-coordinate) system that can be defined by the following equation:

$$\sigma = \frac{z - \zeta}{H} \tag{4.1}$$

in which z is the vertical coordinate in physical space ζ is the water depth above the reference planes and H is the total water depth. This system is scaled as $\sigma = 0$ for the free surface and the bottom corresponds to $\sigma = -1$ (Figure 4.2).

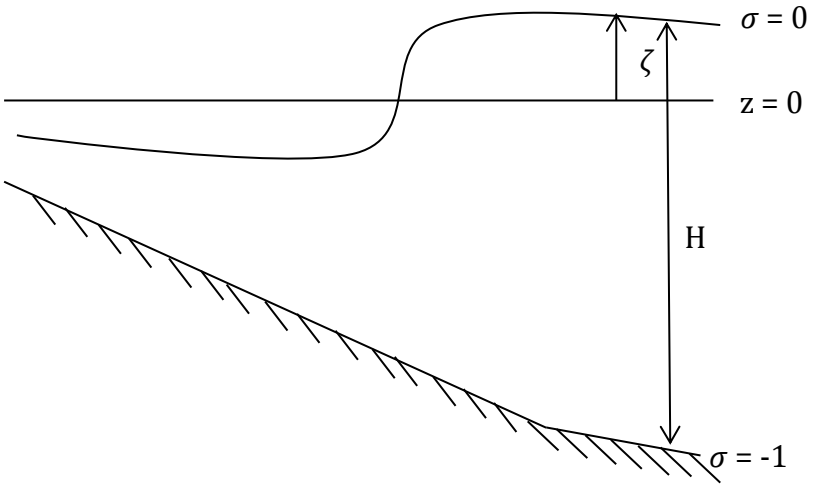

Figure 4.2 Model geometry

4.3.2 **Continuity and momentum equations**

The main two equations of the fluid dynamics model are related to continuity and momentum equation. The continuity equation can be written as follows:

$$\frac{\partial \zeta}{\partial t} + \frac{\partial [(H)U]}{\partial x} + \frac{\partial [(H)V]}{\partial y} = Q \tag{4.2}$$

in which Q represents the contributions per unit area due to the discharge or withdrawal of water, evaporation and precipitation. U and V are the depth averaged velocities.

The horizontal momentum equations can be written as follows:

$$\frac{\partial u}{\partial t} + u\frac{\partial u}{\partial x} + v\frac{\partial u}{\partial y} + \frac{w}{H}\frac{\partial u}{\partial \sigma} - f_v = -\frac{1}{\rho}P_u + F_u + \frac{1}{(H)^2}\frac{\partial}{\partial \sigma}\left(\nu_V \frac{\partial u}{\partial \sigma}\right) + M_u \tag{4.3}$$

$$\frac{\partial v}{\partial \mathrm{t}} + \mathrm{u}\frac{\partial \mathrm{v}}{\partial x} + \mathrm{v}\frac{\partial \mathrm{v}}{\partial y} + \frac{\mathrm{w}}{\mathrm{H}}\frac{\partial \mathrm{v}}{\partial \sigma} + f_u = -\frac{1}{\rho}P_v + F_v + \frac{1}{(\mathrm{H})^2}\frac{\partial}{\partial \sigma}\left(\nu_V \frac{\partial \mathrm{v}}{\partial \sigma}\right) + M_v \qquad \textbf{(4.4)}$$

where u, v and w are the flow velocity components in the x, y and z directions, respectively. t is the time. ρ is the fluid density ν_V is the vertical eddy coefficient. M_u and M_v represent the contributions due to external sources or sinks of momentum. F_u and F_v are the turbulent momentum flux in x and y directions. P_u and P_v represent the hydrostatic pressure gradients in x and y directions.

The vertical momentum equation is reduced to the hydrostatic pressure relation and Boussinesq approximation because vertical accelerandation is assumed to be small compared to gravitational acceleration, which can be written as follows:

$$\frac{\partial P}{\partial \sigma} = -\rho \mathrm{gH} \qquad \textbf{(4.5)}$$

where ρ is the water density, g is the acceleration due to gravity and H is the total water depth. This assumption makes the Delft3D-FLOW model suitable for predicting the flow of shallow seas, coastal areas, estuaries, lagoons, rivers and lakes.

4.3.3 **Turbulence model**

In Delft3D-FLOW, four turbulence closure models are included:

- Constant coefficient;
- Algebraic Eddy viscosity closure Model (AEM);
- K-L turbulence closure model and
- K-ε turbulence closure model.

The K-ε turbulence closure model is used in the simulations presented in this thesis, which commonly recommended for sigma model (WL|Delft Hydraulics 2014). This turbulence model was also selected because the turbulent shear stress in the laboratory was calibrated using the K-ε turbulence closure model (see section 3.4.2).

In addition, the K-ε turbulence closure model has been successfully applied elsewhere (e.g. Mikes et al. 2004, Violeau et al. 2002, Winterwerp 2002) for studying modelling floc size and settling velocity as it was found to represent the turbulence best.

In the K-ε turbulence closure mode, transport equations must be solved for both the turbulent kinetic energy K and the energy dissipation ε. The mixing length L can then be determined as follows:

$$\mathrm{L} = \mathrm{C_v}\frac{\mathrm{K}\sqrt{\mathrm{K}}}{\varepsilon} \tag{4.6}$$

where $\mathrm{C_v}$ is a K- ε closure constant, ε is the energy dissipation and K is the turbulent kinetic energy and can be calculated from Equation (3.2).

4.3.4 **Sediment transport model**

Sediments play an active role in hydromorphological processes and in the nutrient adsorption and desorption processes in the aquatic environment and may remove or release pollution from or to the overlying water, thereby affecting the quality of coastal waters (Wang et al. 2009; Etemad-Shahidi et al. 2010). In the Delft3D model, up to five sediment fractions can be defined. Each fraction must be classified as cohesive or non-cohesive because different formulations are used for erosion, sedimentation and settling of these different types of sediments. Both cohesive and non-cohesive sediment were implemented in this study.

The three dimensional advection and diffusion of suspended sediment transport particles can be written as follows:

$$\frac{\partial c^{(l)}}{\partial t} + \frac{\partial \mathrm{u}c^{(l)}}{\partial x} + \frac{\partial \mathrm{v}c^{(l)}}{\partial y} + \frac{\partial (\mathrm{w}-\mathrm{Ws})c^{(l)}}{\partial z} - \frac{\partial}{\partial x}\left(\varepsilon_{s,x}^{(l)}\frac{\partial c^{(l)}}{\partial x}\right) - \frac{\partial}{\partial y}\left(\varepsilon_{s,y}^{(l)}\frac{\partial c^{(l)}}{\partial y}\right) - \frac{\partial}{\partial z}\left(\varepsilon_{s,z}^{(l)}\frac{\partial c^{(l)}}{\partial z}\right) = 0 \tag{4.7}$$

where $c^{(l)}$ is the mass concentration of sediment fraction (l) (kg/m3), u, v and w are the flow velocity components in x, y and z directions (m/s), $\varepsilon_{s,xyz}$ is the eddy

diffusivity of the sediment fraction and Ws is the settling velocity of sediment fraction.

4.3.4.1 **Cohesive sediment**

Cohesive sediment settling velocity

Settling velocity is defined as one of the important parameters when modelling the sediment transport processes (Johansen 1998). The settling velocity of cohesive sediment can be defined as a single constant value by the user. For modelling sediment transport where flocculation occurs, the settling velocity of cohesive sediment is modelled as a function of salinity. To model this salinity dependency, the user has to supply two settling velocities and a maximum salinity. The first velocity, W_{Sf}, is the settling velocity of the sediment fraction in fresh water, at salinity = 0. The second velocity, W_{Smax}, is the settling velocity of the fraction in water having a maximum salinity (S_{max}). The settling velocities of the sediment flocs are calculated as follows:

$$Ws^{(l)} = \begin{cases} \frac{W^{l}_{Smax}}{2}\left(1-\cos\left(\frac{\pi S}{S_{max}}\right)\right)+\frac{W^{l}_{Sf}}{2}\left(1+\cos\left(\frac{\pi S}{S_{max}}\right)\right), & \text{when } S \le S_{max} \\ W^{l}_{Smax}, & \text{when } S > S_{max} \end{cases} \quad \textbf{(4.8)}$$

where $Ws^{(l)}$ is the settling velocity of sediment fraction (l), W^{l}_{Smax} is the settling velocity of sediment fraction (l) at salinity concentration Smax, W^{l}_{Sf} is the settling velocity of sediment fraction (l) at fresh water, S is salinity and S_{max} is the maximum salinity at which W_{Smax} is specified.

If the influence of flocculation is disregarded, then $W_{Smax} = W_{Sf}$ can be specified.

Cohesive sediment erosion and deposition

For cohesive sediment, the evaluation of the resuspension rate between the water phase and the bed are given by Partheniades-Krone formulations (Partheniades 1965) as:

$$E^{(l)} = M^{(l)} \mathrm{S}\,(\mathrm{T_{cw}}, \mathrm{T_{cr,e}^{(l)}}), \tag{4.9}$$

$$D^{(l)} = \mathrm{Ws}^{(l)} c_b^l \mathrm{S}\,(\mathrm{T_{cw}}, \mathrm{T_{cr,d}^{(l)}}), \tag{4.10}$$

$$c_b^{(l)} = c^{(l)}(z = \tfrac{\Delta_{zb}}{2}, \mathrm{t}) \tag{4.11}$$

$$\mathrm{S}\,(\mathrm{T_{cw}}, \mathrm{T_{cr,e}^{(l)}}) = \begin{cases} \left(\dfrac{\mathrm{T_{cw}}}{\mathrm{T_{cr,e}^{(l)}}} - 1\right), \text{when } \mathrm{T_{cw}} > \mathrm{T_{cr,e}^{(l)}}, \\ 0, \qquad \text{when } \mathrm{T_{cw}} \leq \mathrm{T_{cr,e}^{(l)}} \end{cases} \tag{4.12}$$

$$\mathrm{S}\,(\mathrm{T_{cw}}, \mathrm{T_{cr,d}^{(l)}}) = \begin{cases} \left(\dfrac{\mathrm{T_{cw}}}{\mathrm{T_{cr,d}^{(l)}}} - 1\right), \text{when } \mathrm{T_{cw}} > \mathrm{T_{cr,d}^{(l)}}, \\ 0, \qquad \text{when } \mathrm{T_{cw}} \leq \mathrm{T_{cr,d}^{(l)}} \end{cases} \tag{4.13}$$

where $E^{(l)}$ is the erosion flux (kg.m^{-2}s^{-1}), $M^{(l)}$ is the user-defined erosion parameter EROUNI (kg.m^{-2}s^{-1}), S ($\mathrm{T_{cw}}$, $\mathrm{T_{cr,e}^{(l)}}$) is the erosion step function, $D^{(l)}$ is the deposition flux (kg.m^{-2}s^{-1}), $W_S^{(l)}$ is the settling velocity (hindered) (m/s), $c_b^{(l)}$is the average sediment concentration in the near bottom computational layer, S ($\mathrm{T_{cw}}$, $\mathrm{T_{cr,d}^{(l)}}$) is the deposition step function, $\mathrm{T_{cw}}$ is the maximum bed shear stress due to current and waves as calculated by the wave- current interaction model selected by the user, $\mathrm{T_{cr,d}^{(l)}}$is the user- defined critical deposition shear stress (N/m^2) and $\mathrm{T_{cr,e}^{(l)}}$is the user-defined critical erosion shear stress (N/m^2). Superscript (l) implies that this quantity applies to sediment fraction (l).

4.3.4.2 **Non-cohesive sediment**

Non-cohesive sediment settling velocity

The settling velocity of non-cohesive sediment is calculated using the method given by Van Rijn (1993) based on the representative diameter and the relative density of sediment particles.

$$\mathrm{Ws}^{(l)} = \begin{cases} \dfrac{(\rho^{(l)} - 1) g D_s^{(l)2}}{18\nu} & 65\ \mu\mathrm{m} < D_s \leq 100\ \mu\mathrm{m} \\ \dfrac{10\upsilon}{D_s}\left(\sqrt{1 + \dfrac{0.01(\rho^{(l)} - 1) g D_s^{(l)3}}{\nu^2}} - 1\right) & 100\ \mu\mathrm{m} < D_s \leq 1000\ \mu\mathrm{m} \\ 1.1\sqrt{(\rho^{(l)} - 1) g D_s^{(l)}} & 1000\ \mu\mathrm{m} < D_s \end{cases} \quad \textbf{(4.14)}$$

where $\rho^{(l)}$ is the relative density $\rho_s^{(l)}/\rho_w$ of sediment fraction (l), $D_s^{(l)}$ is the representative diameter of sediment fraction (l) and υ is the kinematic viscosity coefficient of water (m^2/s).

Non-cohesive sediment erosion and deposition

The transfer of sediment between the bed and the water column is modelled using sink and source terms acting on the near-bottom layer that is entirely above Van Rijn's reference height. This layer is identified as the reference layer and for brevity is referred to as the kmx layer, (Figure 4.3). A sink term is solved implicitly in the advection-diffusion equation, whereas a source term is solved explicitly. In order to determine the required sink and source terms for the kmx layer, the concentration and concentration gradient at the bottom of the kmx layer need to be approximated. In Delft3D model, a standard Rouse profile is assumed between the reference level a and the centre of the kmx layer (see Figure 4.3).

$$C^{(l)} = C_a^{(l)} \left[\frac{a(h-Z)}{Z(h-a)}\right]^{A^{(l)}} \quad \textbf{(4.15)}$$

where $C^{(l)}$ is the concentration of sediment fraction (l), $C_a^{(l)}$ is the reference concentration of sediment fraction (l), a is Van Rijn's reference height, Z is the elevation above the bed and $A^{(l)}$ is the Rouse number.

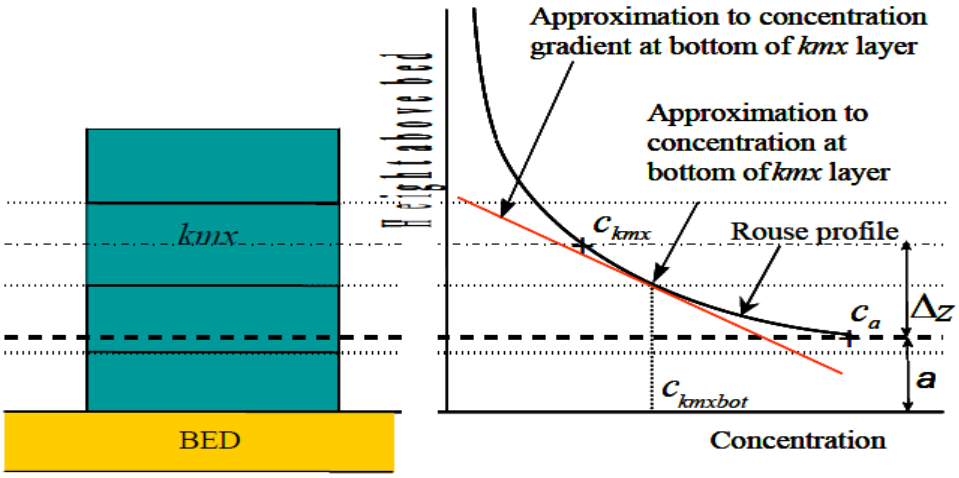

Figure 4.3 Approximation of concentration and concentration gradient at the bottom of kmx Layer, adopted from (WL|Delft Hydraulics 2014).

Erosive flux due to upward diffusion is given by the expression:

$$E^{(l)} = \alpha_2^{(l)} \varepsilon_s^{(l)} \left(\frac{C_a^{(l)} - C_{kmx}^{(l)}}{\Delta z}\right) \quad \textbf{(4.16)}$$

$$\Delta z = \text{zkmx} - \text{a} \quad \textbf{(4.17)}$$

Deposition flux due to sediment settling is expressed as:

$$D^{(l)} = \alpha_1^{(l)} \text{Ws}^{(l)} C_{kmx}^{(l)} \quad \textbf{(4.18)}$$

where $\alpha_1^{(l)}, \alpha_2^{(l)}$ is the correction factor for sediment concentration, $\varepsilon_s^{(l)}$ is the sediment diffusion coefficient evaluated at the bottom of the kmx cell of sediment fraction (l), $C_a^{(l)}$ is the reference concentration of sediment fraction (l), $C_{kmx}^{(l)}$ is the average concentration of the kmx cell of sediment fraction (l), Δz is the difference in the elevation between the centre of the kmx cell and Van Rijn's reference height, z_{kmx} is the elevation at the centre of the kmx cell and a is Van Rijn's reference height.

4.4 Summary

The equations governing water flow and sediment transport processes in Delft3D have been outlined in this chapter. The continuity and momentum equations are presented, and are followed by descriptions of the turbulence model and sediment transport equation. The settling velocity for the cohesive sediment is presented, including a link to the flocculation model as a function of salinity. These equations form the basis of the hydro-environmental modelling tools used and refined in this study.

5 Suspended sediment transport and flocculation modelling using refined settling velocity formulations

5.1 Introduction

The flocculation processes of cohesive sediments in estuarine waters play an important role in governing the suspended sediment concentrations (SSCs) in the water column. Modelling turbulence-induced flocculation or the breakup of sediment flocs is not included in existing models like the Delft3D commercial model (WL|Delft Hydraulics 2014). In the Delft3D model, the settling velocity of cohesive sediment is a function of salinity only.

The objectives of this chapter are as follows:

1. To refine a numerical model to include new settling velocity equations as a function of turbulent shear stress and salinity developed from experimental laboratory presented in Chapter 3.

2. To apply and test the refined numerical model in simulating the flocculation phenomenon in the Severn Estuary.

The details of the setup, sensitivity analysis and calibration of the model and the results of validation are presented in sections 5.2, 5.3 and 5.4. The refinement and application of the model are presented in section 5.5, and the model results and discussion are presented in section 5.6.

5.2 Model setup

5.2.1 Study area and model domain

The Delft3D model was set up for the Severn Estuary as a case study site with the aim to implement and validate a new settling velocity formula for cohesive sediment taking account of flocculation processes. The computational domain and the bathymetry are shown in Figure 5.1. The bathymetry file was obtained from Sea Zone (http://www.seazone.com/marine-maps/type/bathymetry-data). The domain covers the Severn Estuary and the Bristol Channel from an imaginary line between Milford Haven (West Wales) and Hartland Head (Southwest England). The stability of the model and the accuracy of the results were determined by the scale (time and space) and grid size of the model.

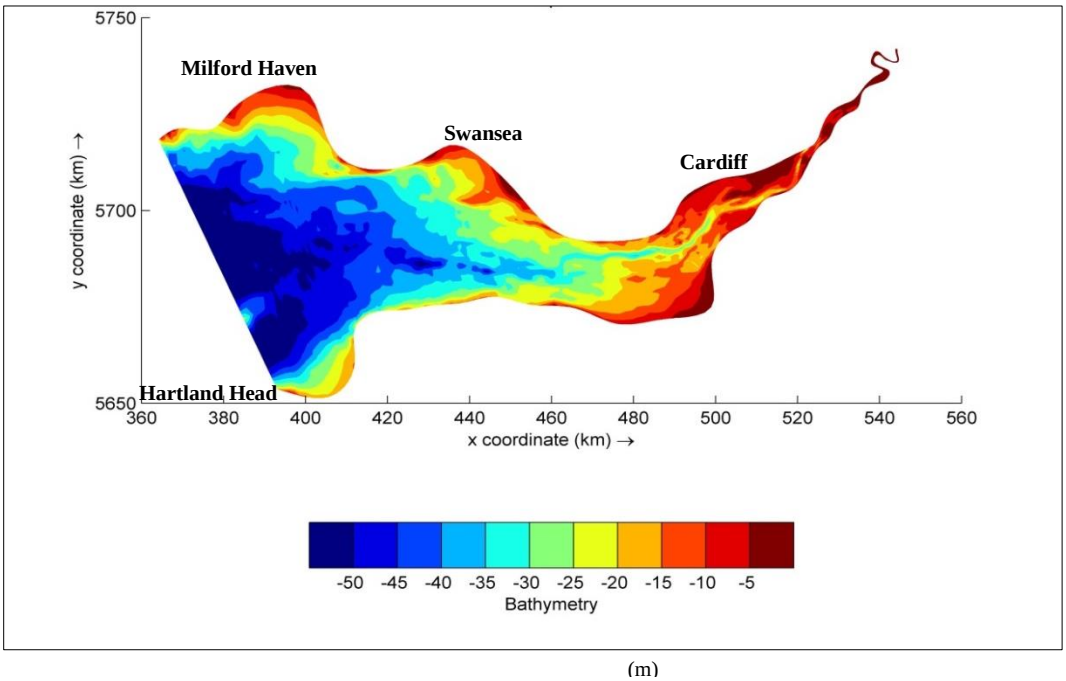

Figure 5.1 The model domain and bathymetry

The curvilinear grid that covers this domain (Figure 5.2) was generated by Delft3D-RGFGRID, with a high grid resolution in the areas of main interest. The total number of grids was (29 X 461); the average grid spacing was approximately 500 m, with its maximum being 2.5 km at the downstream end of the model domain and the minimum of 80 m being located at the upstream end of the domain. The model was divided vertically into three layers and the layer thickness was assumed to be uniform.

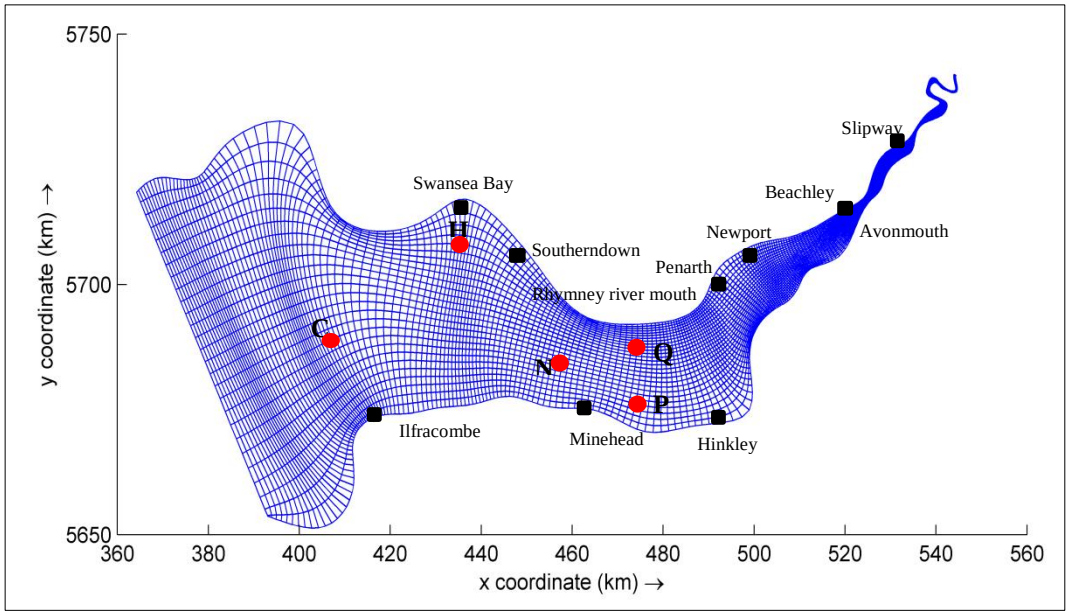

Figure 5.2 Curvilinear grid for the Severn Estuary and Bristol Channel, red circles indicate to calibration and validation points of the velocity and black squares indicate to calibration and validation points of water level, salinity and sediment transport models

5.2.2 Characteristics of suspended sediment

Knowing the grain size distribution of the suspended sediment (SS) is essential to model the suspended sediment transport processes and the flocculation phenomenon and the median grain size (d_{50}) is a good description of it (Winterwerp 1998). SS consists of cohesive and non-cohesive sediment. However, sediment flocculation affects only the fine particles (cohesive sediment). Table 5.1 gives the percentage of cohesive sediment and the suspended sediment median grain size based on field samples collected at upstream sampling points with the suspended sediment size distribution being determined at Cardiff School of Engineering using a Malvern Master Sizer 3000 as described previously in section 3.3.5 (see Figure 3.7 for the grain size distribution results) and in studies by Al-Enezi (2011) and Stapleton et al. (2007). Table 5.1 shows that the median grain size is finest at the Minehead site, followed by Slipway and Penarth with d_{50} values of 10.6, 11.4 and 11.5, respectively. SS becomes almost 57% bigger at the Porthcawl site (24.8 μm); however, this SS is still classified as cohesive sediment (92% < 63 μm).

Table 5.1 Medium grain size of suspended sediment

Location	d_{50}	% of cohesive sediment
Slipway (this study)	11.4	95
Penath (Al-Enezi 2011)	11.5	94
Beachley (this study)	13.0	97
Porthcawl / Southerndown (Stapleton et al. 2007)	24.8	92
Minehead (Stapleton et al. 2007)	10.6	97

5.2.3 Initial conditions

Simulations of flow, salinity and sediment transport are conducted in this study using the Delft3D model. The simulation starts by applying a uniform value for the water level of 4 m. The initial cohesive and non-cohesive sediment concentrations were both set to 0.02 kg/m^3. The spatially varied salinity was defined in the flow model by creating the initial file based on the field sample analysed in Chapter 3. In that file, the values of salinity were gradually changed from upstream to downstream. The model time step was set to 15 s based on satisfying the Courant number (Cr) criterion.

5.2.4 Boundary conditions

Two types of hydrodynamic open boundary conditions were adopted. The first type uses the water level downstream. The open boundaries were extracted from the Delft Dashboard. Delft Dashboard is a part of Open Earth Tools and is a standalone MATLAB based graphical user interface that allows users to set up a new model or alter an existing model. A large number of toolboxes are coupled with Delft Dashboard, such as bathymetry data, tidal data and observation stations, which make for fast and easy generation of input files. After generating the necessary grid and bathymetry files, as mentioned in section 5.2.1, these two files and other physical parameters were uploaded in Delft Dashboard. Next, the downstream location boundary condition was defined in Delft Dashboard as the line between Milford

Haven and Hartland Head (Figure 5.3) and was generated as water level astronomic constituents. With this type of boundary condition, the water downstream was treated as saline water with salinity (S) of 35 ppt (Zhou et al. 2014a). The upstream boundary condition at Gloucester was treated as a uniform flow discharge time series varying between 60 m^3/s and 106 m^3/s (Ahmadian and Falconer 2012). The upstream boundary condition was considered to be fresh water; therefore, salinity levels were set to zero at this boundary.

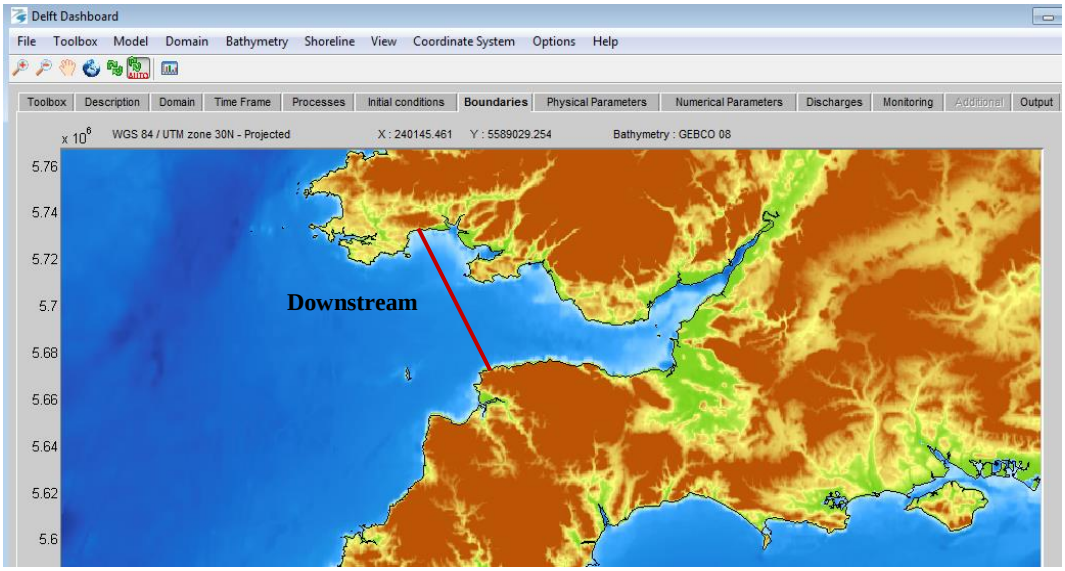

Figure 5.3 Delft Dashboard screen menu

5.3 Sensitivity analysis

The sensitivity tests of the hydrodynamic model were carried out by applying the Manning and Chezy formulae. The model was run for 14 days from 1st March 2009 to 14th March 2009. Four different sensitivity scenarios were carried out the bottom friction of Manning n of 0.025 and 0.03 and Chezy C of 53 and 65. These friction ranges were chosen because they were used by Ahmadian et al. (2010) and Gao et al. (2011) in previous studies of the Severn Estuary. Figure 5.4 shows the effect of varying the bottom friction equations on the current speed at point C (see Figure 5.2 for the location). Figure 5.4 indicates that the prediction of velocity is independent of the bottom friction equation, although the velocity magnitude changes with the friction value. It was decided that the model be calibrated using the Manning formula, as this formula is often successfully used in similar studies. Many

sensitivity tests were carried out to calibrate for velocities, water depths, salinities and suspended sediment concentrations by adjusting the layer thickness, grid resolution and the initialisation parameters of (time step, water level, salinity, friction value, horizontal and vertical viscosity and diffusivity, cohesive and non-cohesive sediment concentration, sediment concentration up and down stream and critical bed shear stress for erosion and deposition). After determining the model's sensitivity, the model was considered to be working satisfactorily for calibration and then validation.

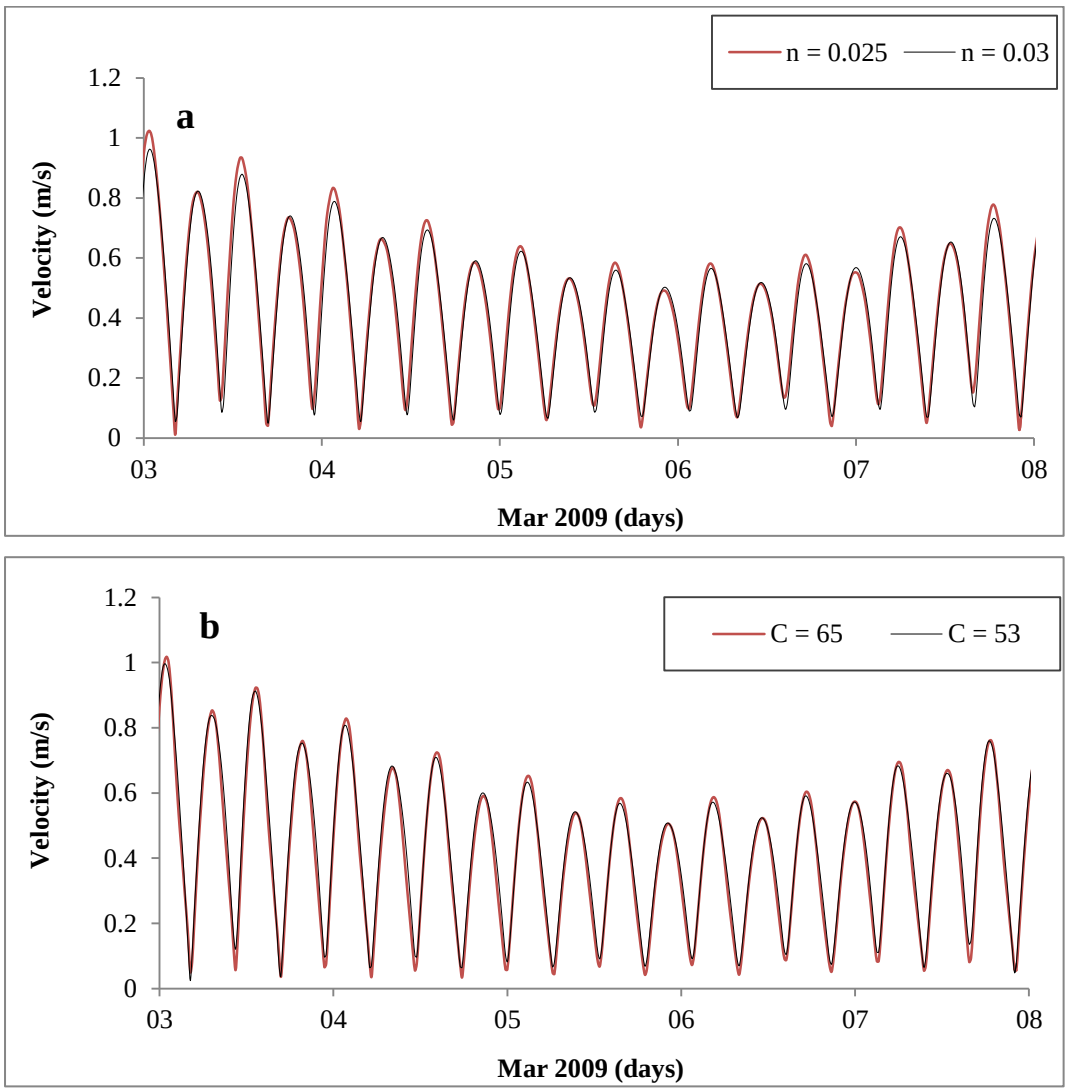

Figure 5.4 Current velocities at point C (see Figure 2 for the location) using (a) the Manning formula and (b) the Chezy formula

5.4 Model calibration and validation

There is no standard procedure for carrying out calibration and validation. However, achieving the hydrodynamic model calibration can be achieved by comparing water level or predicted velocity with field data measured over a short time period (Cheng et al. 1993). The model can then be validated for water levels and velocities at other locations. Next, the model was validated before being modified to include the flocculation processes. In terms of predicted and measured data, the model performance was evaluated using the relative mean absolute error (RMAE), as defined by Sutherland (2001). The qualification of RMAE is given in Table 5.2, as suggested by Sutherland (2001). Further evaluation of the relationship between measurements and predictions was carried out using the root mean square (RMS) to measure the difference between values predicted and values actually observed. The analysis using (RMS) is widely used in the literature (e.g. Zhou et al. 2014, Dias and Lopes 2006) and was selected to be applied in this study too as shown in sections 5.4.1 to 5.4.3 and section 5.6.

Table 5.2 Qualification of model performance

Qualification	RMAE
Excellent	< 0.2
Good	0.2–0.4
Reasonable / fair	0.4–0.7
Poor	0.7–1
Bad	> 1

5.4.1 Hydrodynamics modelling

The model was run for a period of 29 days from 1st March 2009 to 30th March 2009, over a neap-spring tidal cycle. Several tests were carried out by changing the initial water level, time step and the bottom friction, which was represented by the Manning formulation (as decided after the sensitivity analysis 5.3), to get the best possible match between the predicted and measured water level and current speed

data at a number of locations throughout the computational domain. The evaluation of predicted and measured data was carried out using the RMAE and the RMS, as mentioned above. Figure 5.5 shows a typical comparison of the tidal levels between March 8 and March 14, 2009 at Hinckley and Ilfracombe, with the computed water level being predicted by Delft3D for the two Manning values of 0.025 and 0.03 and the measurement data provided by the British Oceanographic Data Centre (UK National Tide Gauge Network, 2009).

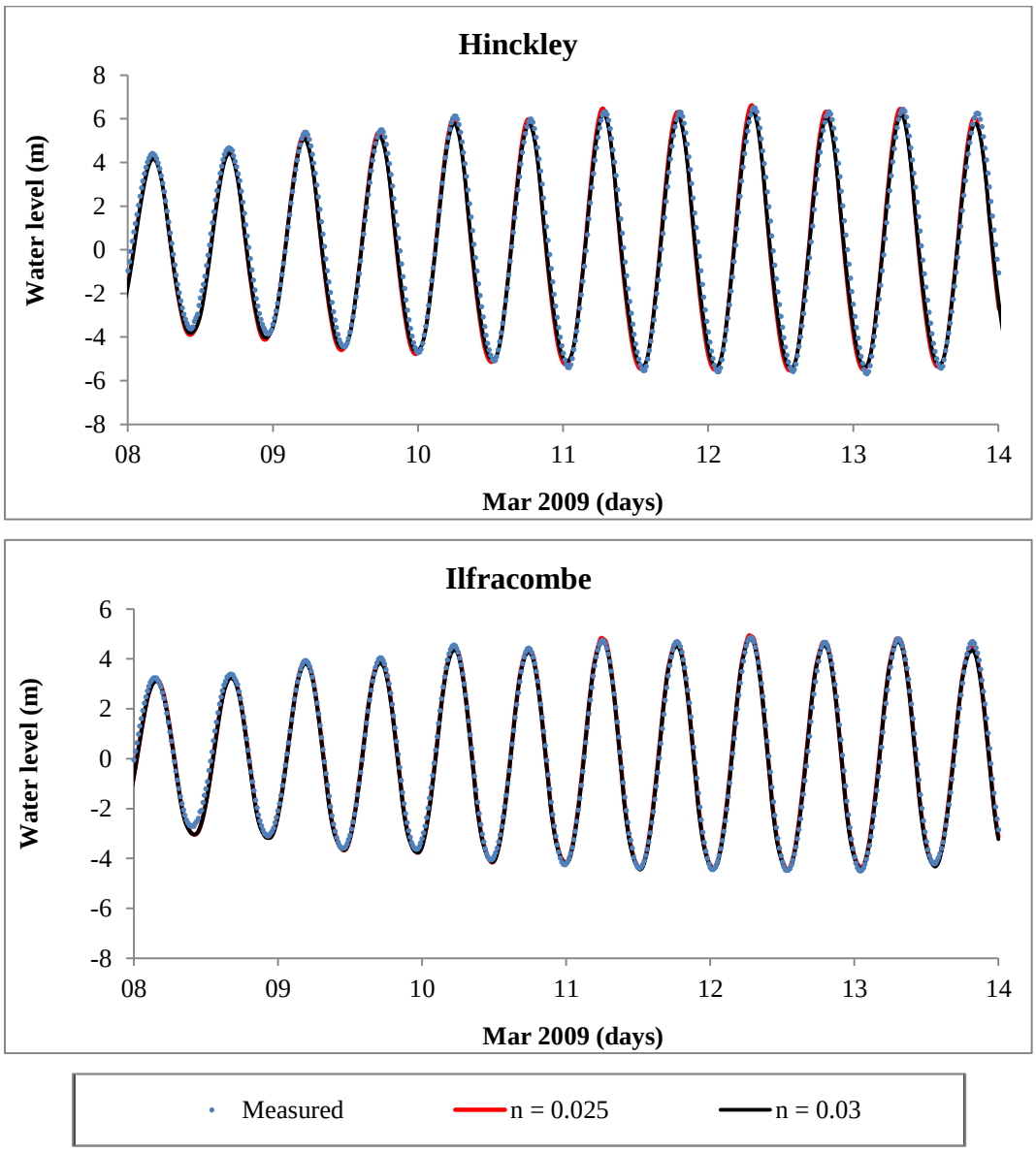

Figure 5.5 Comparison between the Delft3D model predictions and observed water levels at Hinckley and Ilfracombe for model calibration

A comparison of the water level results shows excellent agreement (in relation to the qualification given in Table 5.2) with the statistical analysis in Table 5.3 in terms of the magnitude and phases for both sites at both Manning values of 0.025 and 0.03. The RMS ranges from 0.349 to 0.470. These high values are related to slight phase shift (Figure 5.5). However, a close examination of the water level comparisons at Hinckley and Ilfracombe shows that using the Manning value of 0.025 predicts the peak tidal level differences of 20 cm and 13 cm, respectively. However, using the Manning value of 0.03 leads to a decrease in the difference of the peak tidal level to 11 cm and 9 cm at Hinckley and Ilfracombe, respectively.

Table 5.3 RMAE and RMS values for the difference between the predicted and measured tidal elevations at Hinckley and Ilfracombe

Site	**Hinckley**		**Ilfracombe**	
Manning value	**0.025**	**0.03**	**0.025**	**0.03**
RMAE	0.204	0.164	0.132	0.131
RMS (m)	0.367	0.349	0.470	0.460

The current speed and direction data for spring and neap tides were calibrated and then validated against Admiralty chart data (number 1179) at five locations, as shown in Figure 5.2 (indicated by red circle). The current speed and direction were calibrated first at sites C and H by adjusting the Manning value. Typical comparisons of the Admiralty chart data and predicted current speeds for spring and neap tides and directions at calibration sites C and H are shown in Figure 5.6 and 5.7. Once again, the comparisons show good agreement between the model predictions and tidal stream data provided by the Admiralty chart for Manning's values of 0.025 and 0.03, except for some noticeable differences in the flow direction observed at location H for n = 0.025 (Figure 5.7 c) which could be due to local bathymetry differences between real bed level and bathymetrical data used in the model. The differences between the predicted and field data were calculated, and the

corresponding RMAE and RMS values for currents are listed in Table 5.4. In general, the use of both friction values produces an RMAE ranging between 0.126 and 0.290 (Table 5.4), which indicates excellent agreement between measurements and predictions (Table 5.2); the neap tide at n = 0.025 provides good agreement with the RMAE of 0.29. In addition, an examination of RMS values in Table 5.4 shows that both Manning values of 0.025 and 0.03 provide reliable hydrodynamic predictions of the velocities, with RMS ranging between 0.056 m/s and 0.168 m/s.

Table 5.4 RMAE and RMS values for the difference between the predicted and measured speed and direction at points C and H

Site		**C**		**H**	
Manning value	**Tide type**	**0.025**	**0.03**	**0.025**	**0.03**
RMAE	Spring tide	0.170	0.171	0.129	0.126
	Neap tide	0.290	0.195	0.210	0.199
	Direction	0.167	0.172	0.174	0.133
RMS (m/s)	Spring tide	0.168	0.168	0.063	0.063
	Neap tide	0.125	0.087	0.056	0.057

The model calibration for the water levels and velocities reveals that the best correlation between measured and predicted data was for the Manning value of 0.03. This value will be used for the model validation.

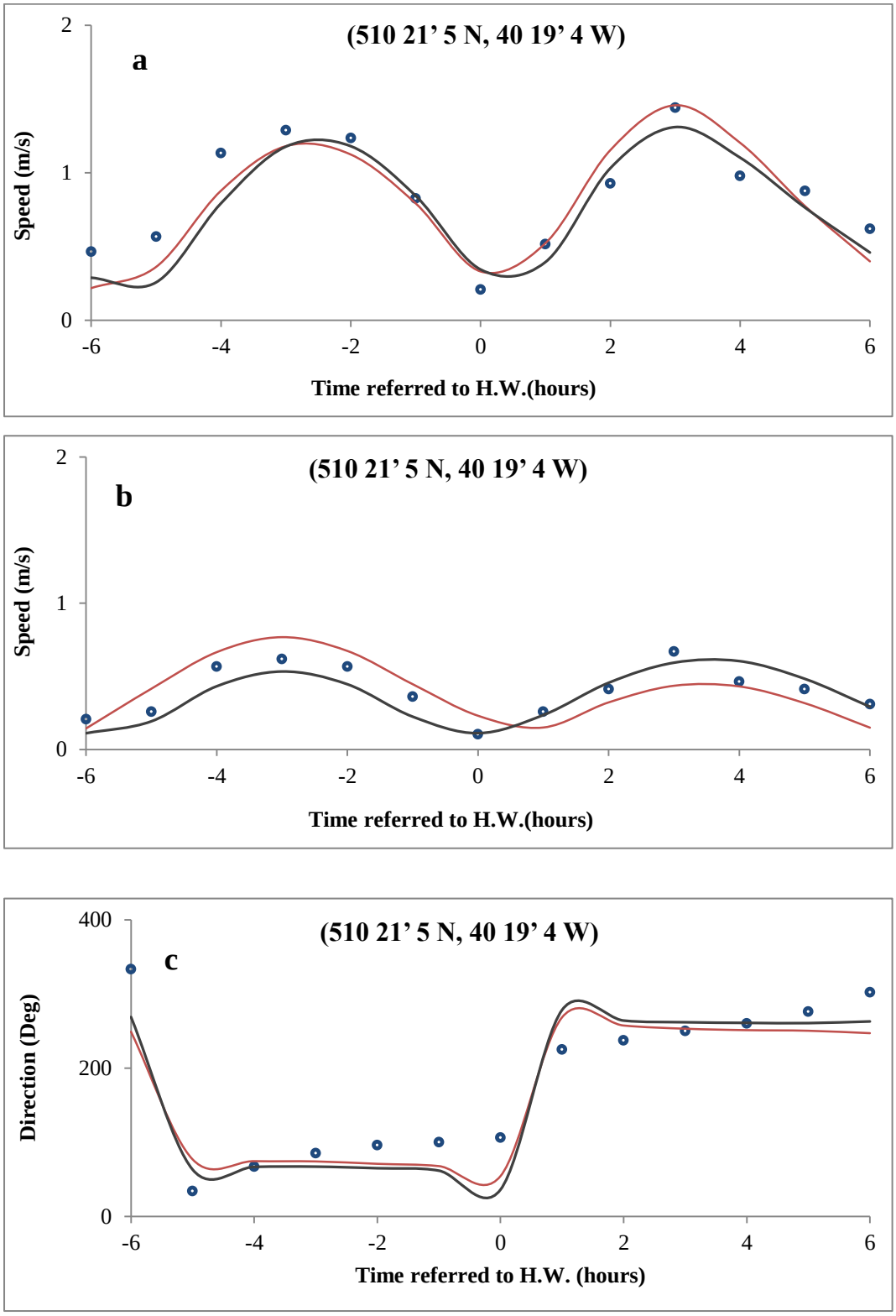

Figure 5.6 Calibration of tidal current for site C: (a) velocities at spring tide, (b) velocities at neap tide and (c) current direction

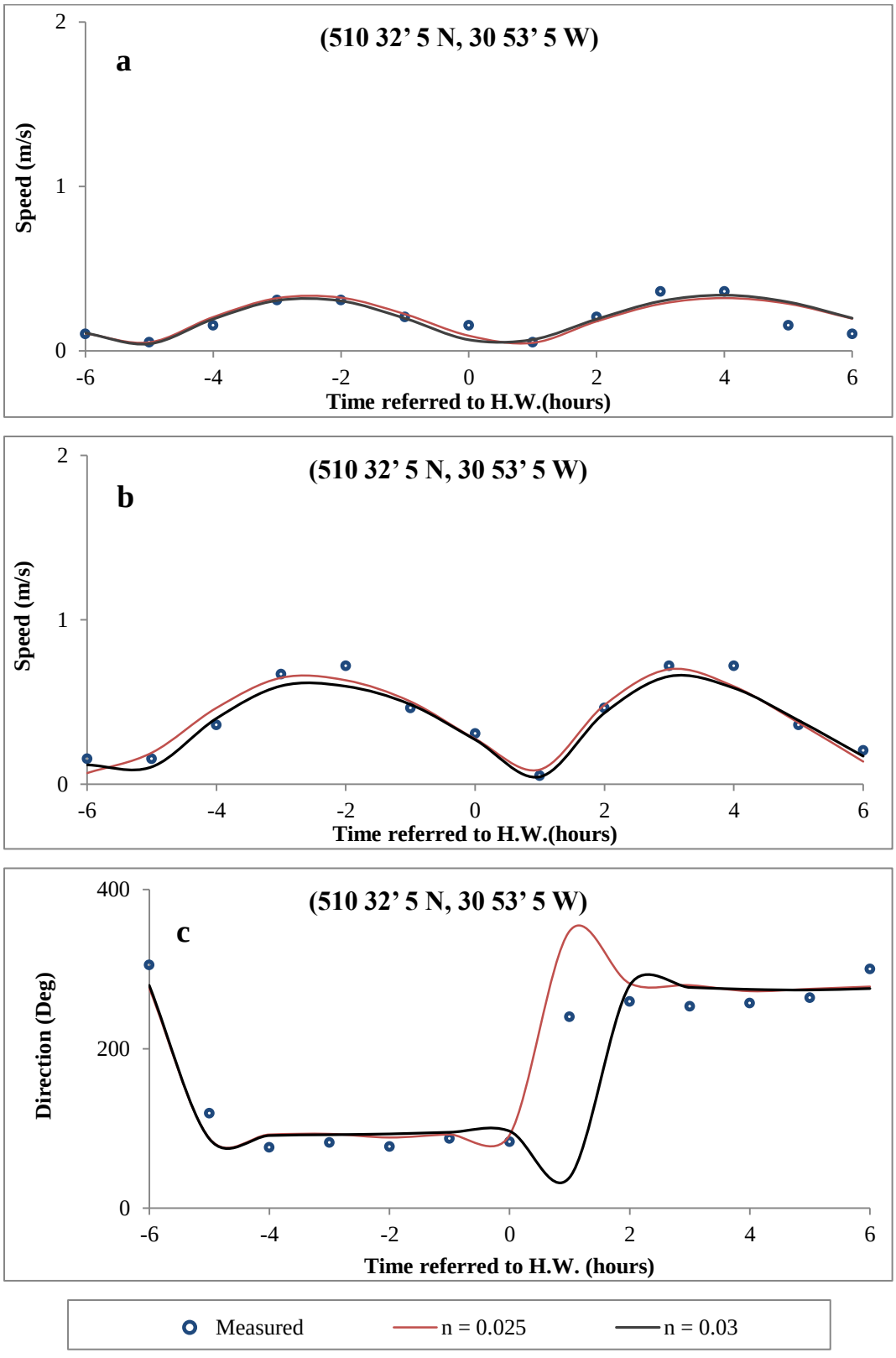

Figure 5.7 Calibration of currents for site H: (a) velocities at spring tide, (b) velocities at neap tide and (c) current direction

After calibration, the model is validated for water levels and velocities. The water levels are validated against data measured at the Newport and Avonmouth stations (Figure 5.8). The water level comparisons at Newport and Avonmouth stations reveal that the Delft3D model predicting of water levels agree well with the measured data. The model predicts the peak tidal levels at these two sites with a very small difference of approximately 10 and 8 cm. This is possibly due to the complex geometry surrounding these locations (Zhou et al. 2014b). This result could be further improved by varying roughness along the modelling domain. The correlation between the model predictions and the measured water level data can be evaluated with the statistical analysis of errors provided in (Table 5.5). It was found that the RMAE values were less than 0.2. In relation to the qualification of RMAE suggested as shown in Table 5.2 means that the model still provides an excellent prediction of the water level.

Table 5.5 RMAE and RMS values for the difference between the predicted and measured tidal elevations

Location	Newport	Avonmouth
RMAE	0.185	0.186
RMS (m)	0.384	0.383

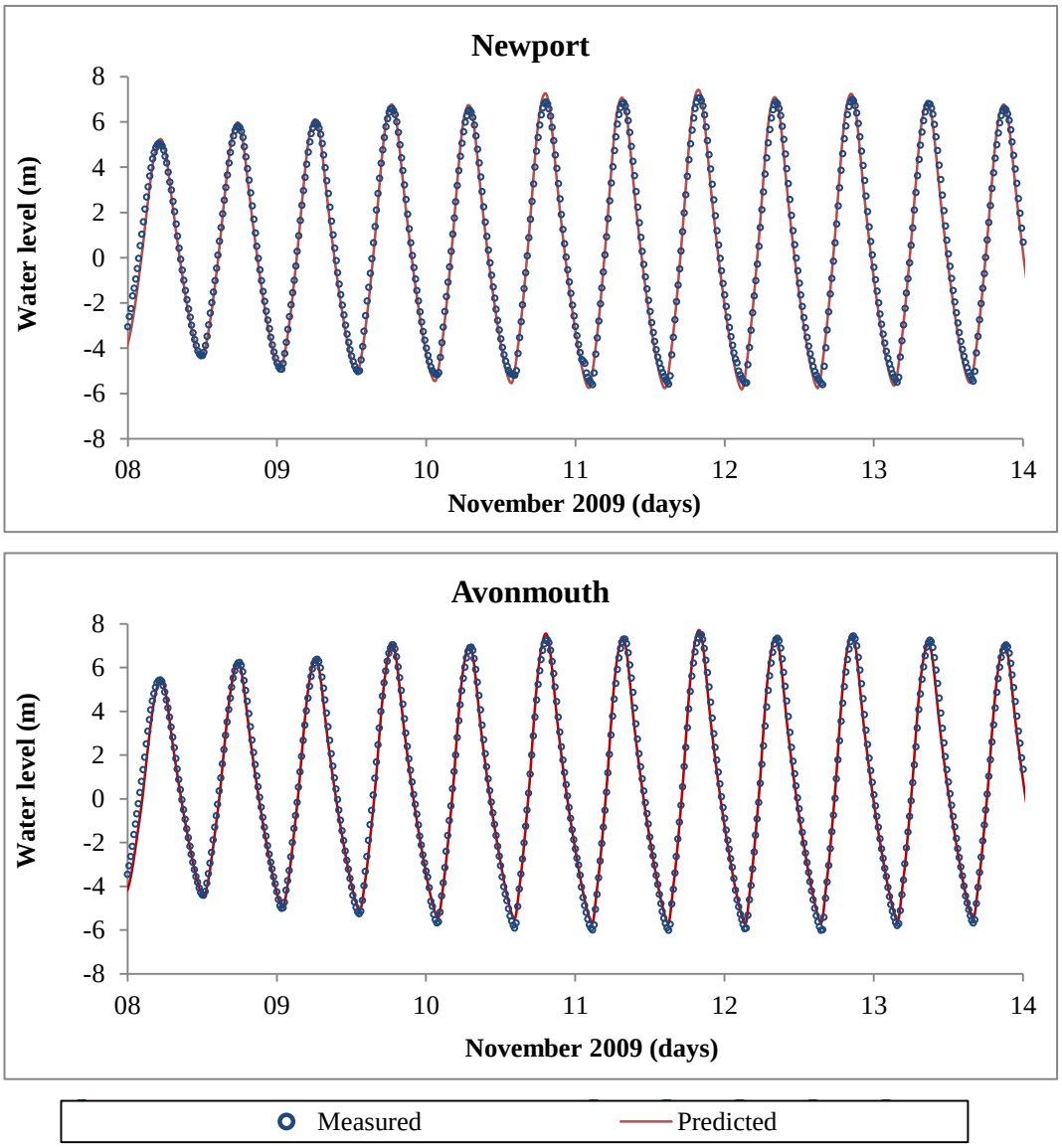

Figure 5.8 Comparison between predicted and observed water levels at Newport and Avonmouth for model validation

The current speeds were validated at sites N, P and Q as shown in Figures 5.9, 5.10 and 5.11. The RMAE and RMS values are listed in Table 5.6 and indicate a good level of agreement. In general, comparisons of the tidal currents with the measured data show that the model can provide an excellent prediction for the current speed, with an RMAE of less than 0.2. The maximum RMS = 0.256 m/s is obtained when comparing the predicted and measured data at both spring and neap tides, indicating the tidal currents agree well with the field measurements. As in the literature, the

maximum RMS of the tidal current in the Severn Estuary and the Bristol Channel can be 0.33 m/s, which is an acceptable value as shown by Zhou et al. (2014c). Therefore, using the Delft Dashboard boundary conditions for the Delft3D model is found to be satisfactory for the Severn Estuary as setup in this study.

Table 5.6 RMAE and RMS values for the difference between the predicted and measured speeds

Locations	Tide type	Site N	Site P	Site Q
RMAE	Spring tide	0.181	0.140	0.151
	Neap tide	0.146	0.135	0.176
	Direction	0.046	0.044	0.038
RMS (m/s)	Spring tide	0.220	0.165	0.256
	Neap tide	0.093	0.089	0.156

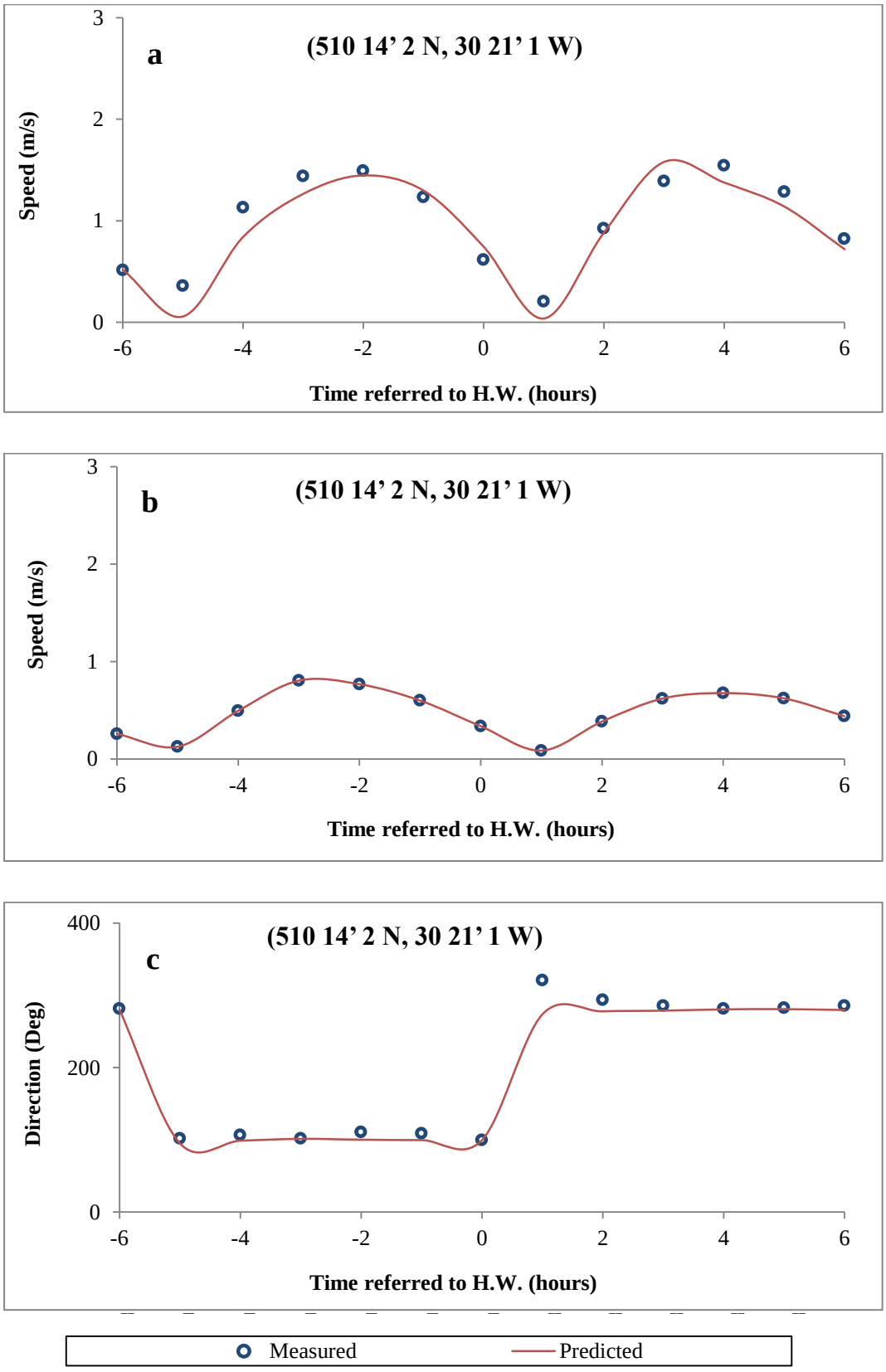

Figure 5.9 Comparison between predicted and observed tidal currents for site P: (a) velocities at spring tide, (b) velocities at neap tide and (c) current direction for model validation

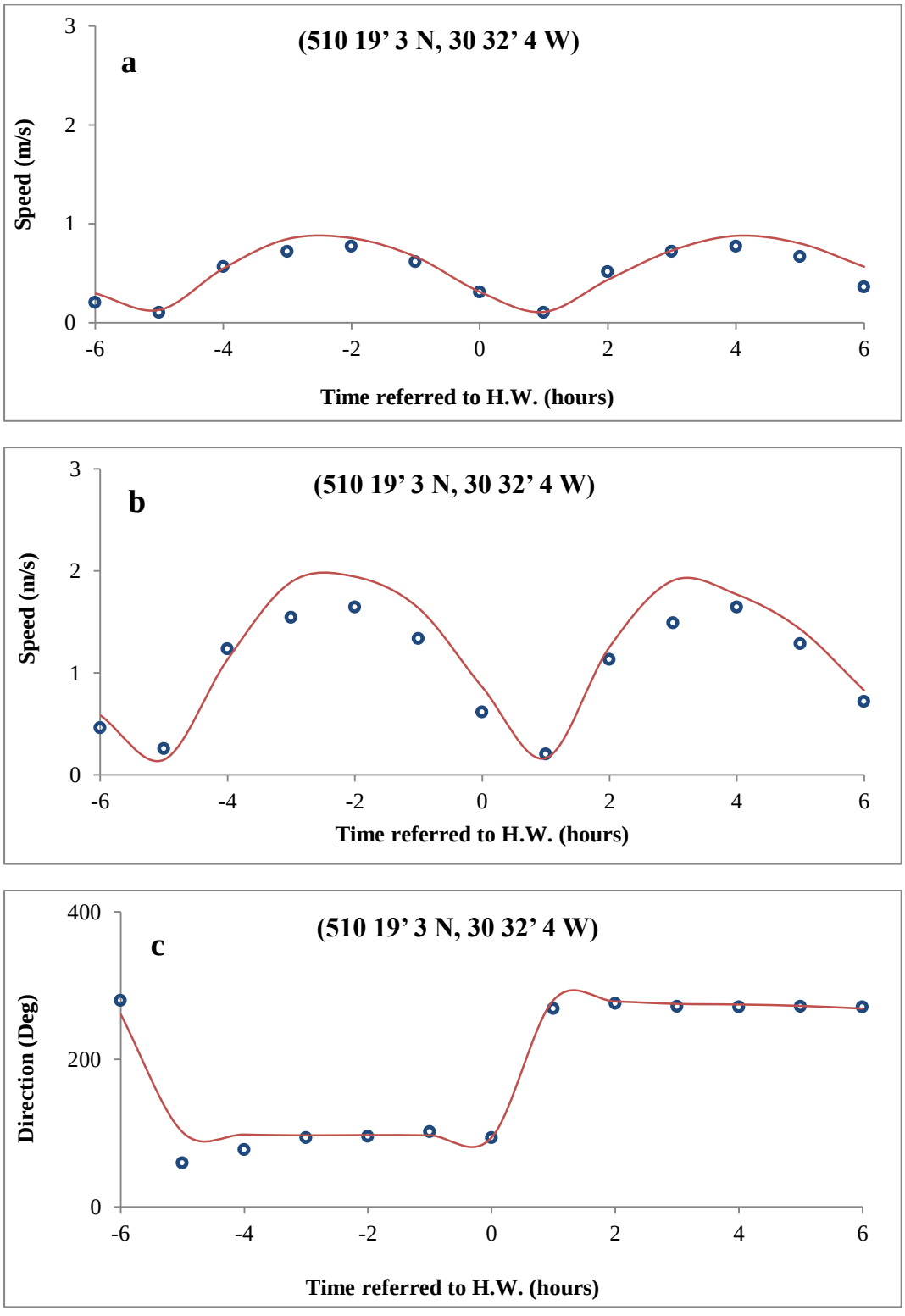

Figure 5.10 Comparison between predicted and observed tidal currents for site N: (a) velocities at spring tide, (b) velocities at neap tide and (c) current direction for model validation

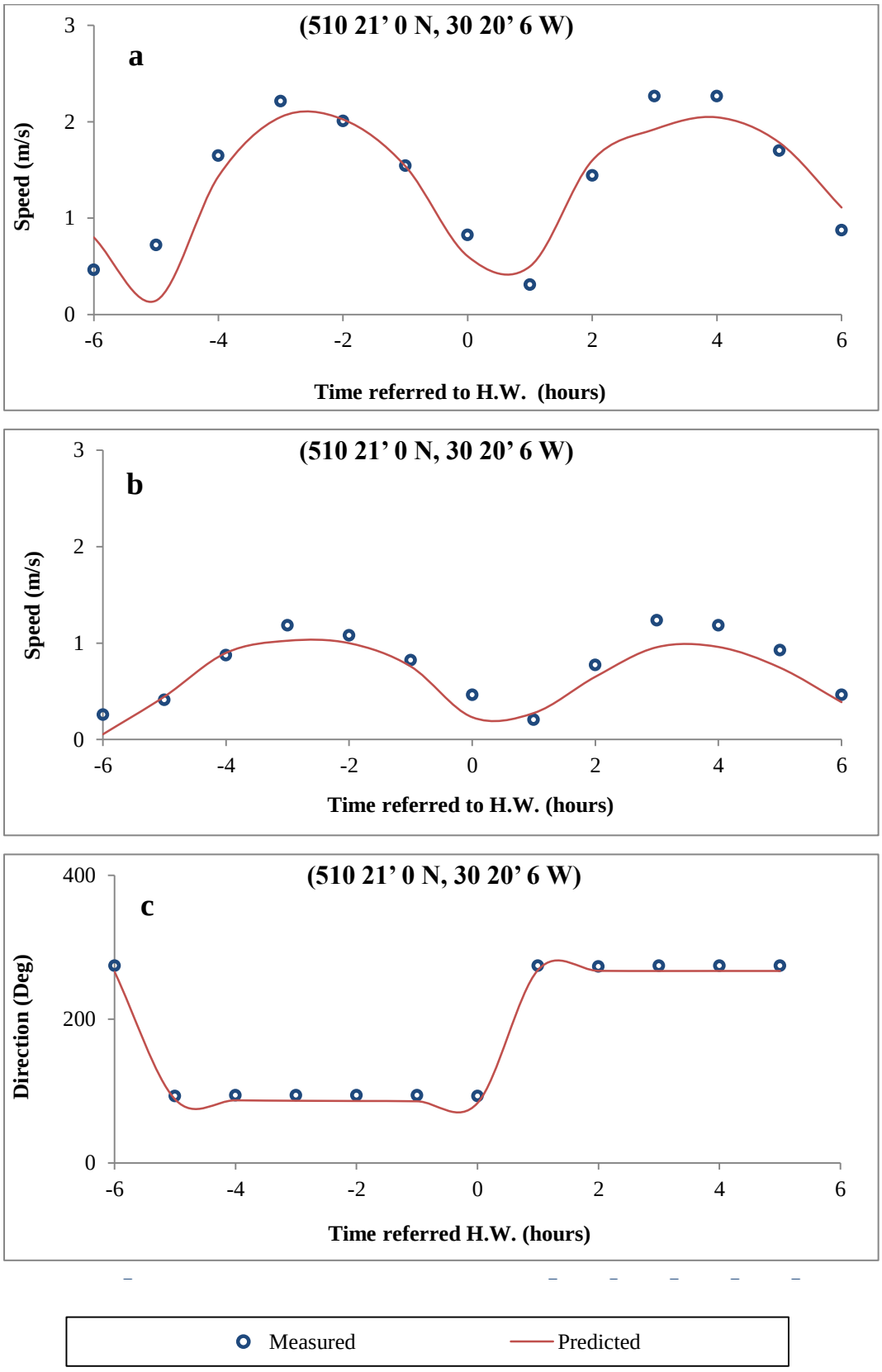

Figure 5.11 Comparison between predicted and observed tidal currents for site Q: (a) velocities at spring tide, (b) velocities at neap tide and (c) current direction for model validation

5.4.2 **Salinity**

Salinity distributions were initially calibrated using field data from Swansea Bay by adapting the initial salinity value (Figure 5.12). The field data for Swansea Bay was obtained from Natural Resources Wales. The model was first run with an initial salinity value of 15 ppt (Figure 5.12), the water downstream was treated as saline water with salinity (S) of 35 ppt and the upstream boundary condition was considered to be fresh water with salinity levels set to zero. It was noted that the salinity values take a long time to reach equilibrium across the domain. Therefore, a spatially varied salinity distribution file was defined in the flow model by creating an initial salinity file based on field samples analysed in Chapter 3. In that file, the salinity values gradually change from upstream to downstream.

The salinity was then validated against field data from two other sites, namely the Rhymney River mouth and Penarth (Figure 5.13). The field data for Penarth was obtained from a previous study (Al-Enezi 2011) and the field data for Rhymney River mouth site was obtained from Natural Resources Wales. The RMAE and RMS values are listed in Table 5.7 and indicate a good level of agreement. In general, comparisons of the predicted with the measured data show that the model can provide an excellent prediction for the salinity level, with an RMAE of less than 0.2. The maximum RMS = 5 ppt is obtained when comparing the predicted and measured data at Penarth. This difference value between predicted and measured could be a result of not including the discharge of fluvial tributaries in the model.

Table 5.7 RMAE and RMS values for the difference between the predicted and measured salinities

Locations	**Swansea Bay**	**Rhymney River mouth**	**Penarth**
RMAE	0.050	0.010	0.191
RMS (ppt)	1.747	0.330	5.010

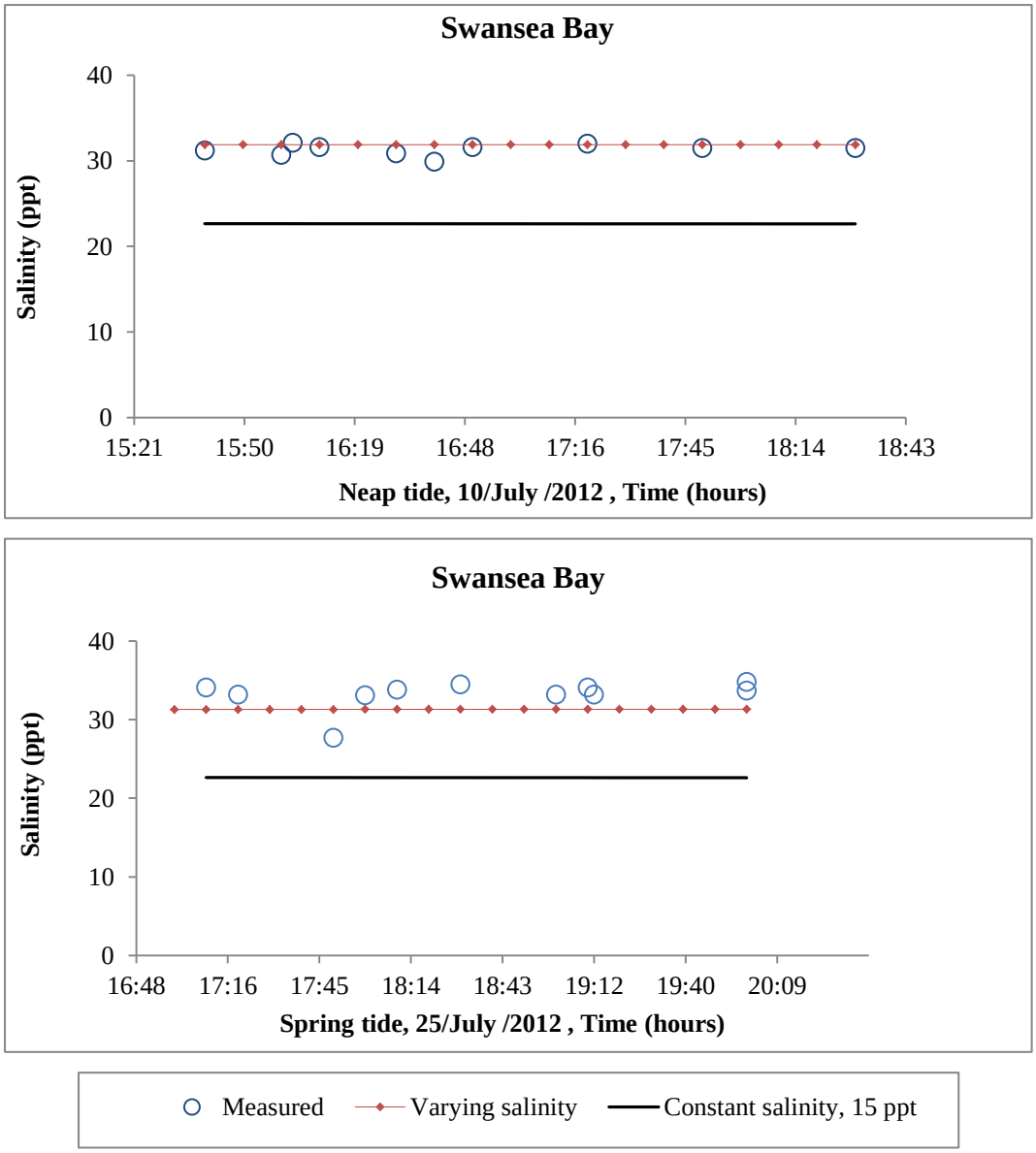

Figure 5.12 Comparison of modelled and predicted salinities for Swansea Bay

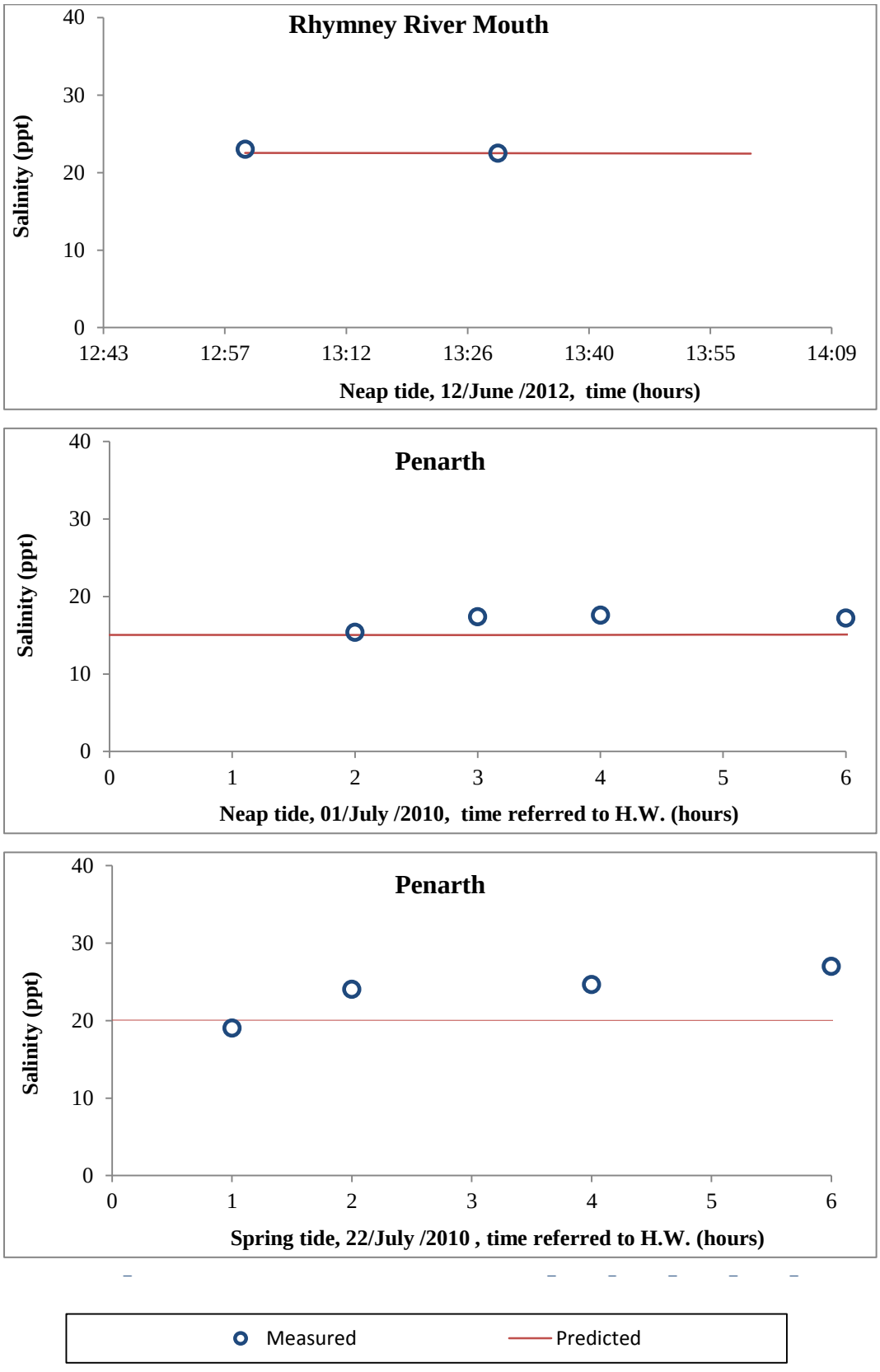

Figure 5.13 Comparison between predicted and observed salinities at Rhymney River mouth and Penarth for model validation

5.4.3 **Sediment transport**

Data collected at different events were used for model calibration and validation of suspended sediment transport processes. These were from events in June, July and September 1991; July 2001; July and November 2009 and November 2010 for which field data are available from different studies (Stapleton et al. 2007; Mclntosh 2010; Waite 2010; Al-Enezi 2011). The SSC calibration was carried out by comparing the computed against observed SSC at Porthcawl / Southerndown. The sediment calibrations were carried out by changing the sensitive parameters that the critical shear stress of cohesive sediment is sensitive for, both for erosion ($T_{cr,e}$) and deposition ($T_{cr,d}$). These two parameters are defined as the values at which cohesive sediment erodes from the bed or settles to the bed. The variability of the critical shear stress of cohesive sediment for erosion is in the range of 1 N/m^2 to 2 N/m^2 (Moody et al. 2005) and for sedimentation it is 0.05 N/m^2 to 0.2 N/m^2 (Berlamont et al. 1993).

In this study, the calibration was carried out by changing the critical shear stress of cohesive sediment for the erosion from 1 N/m^2, to 1.5 N/m^2 and to 2 N/m^2 and by changing the critical shear stress of cohesive sediment for deposition between 0.06 N/m^2 and 0.1 N/m^2 (Figure 5.14). Based on the statistical analysis of RMAE and RMS (Table 5.8) during the calibration of the model, the best results are acquired by setting the critical shear stress for the erosion and deposition of the cohesive particles to 2 N/m^2 and 0.1N/m^2, respectively. These values are also used by Ahmadian et al. (2010) and Gao et al. (2011) in previous studies of the Severn Estuary.

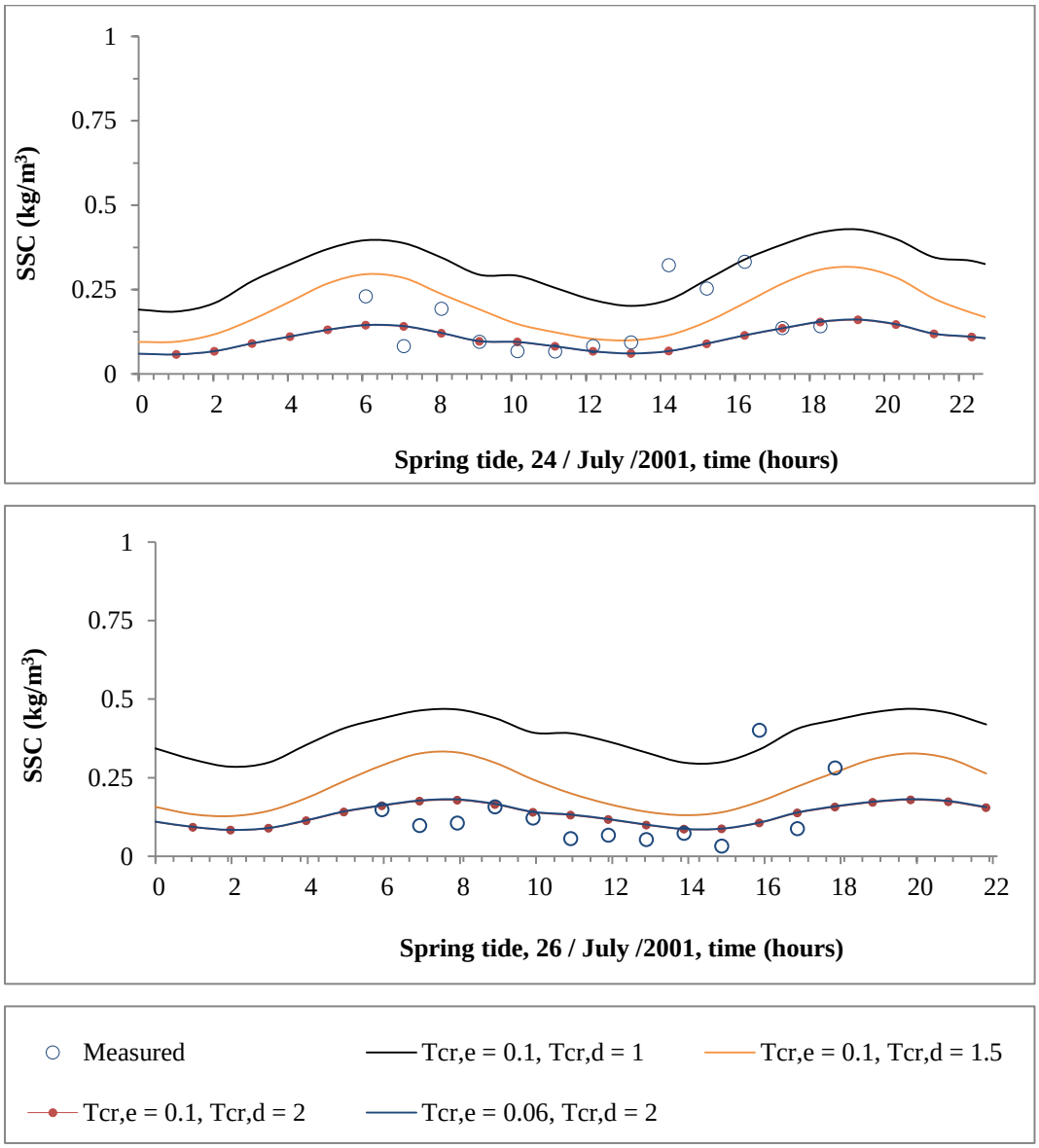

Figure 5.14 Comparison of predicted and measured sediment concentrations at Porthcawl / Southerndown for model calibration

Table 5.8 RMAE and RMS values for the difference between the predicted and measured suspended sediment concentrations at Porthcawl / Southerndown

$T_{cr,e}$, $T_{cr,d}$	0.10, 1.0	0.10, 1.5	0.1, 2.0	0.06, 2.0
RMAE	1.559	0.828	0.495	0.5011
RMS (kg/ m^3)	0.234	0.132	0.105	0.106

Next, the model was validated for SSCs at Newport, Penarth and Slipway (Figure 5.15, 5.16 and 5.17). The statistical analysis of RMS values shows that the maximum RMS is 0.060 kg/m3 at Penarth (Table 5.9). The RMAE values at Newport, Penarth and Slipway are 0.077, 0.253 and 0.131, respectively. In relation to the qualification of RMAE suggested by Walstra et al. (2001) (see Table 5.2), these values mean that the model provides an excellent prediction of the SSC at Newport and Slipway and is a good prediction of the SSC at Penarth. Based on the calibration and validation results, it is thought that the hydrodynamic numerical model for the Severn Estuary could be successfully used for the assessment of using the refined settling velocity equation.

Table 5.9 RMAE and RMS values for the difference between the predicted and measured suspended sediment concentrations

Locations	**Newport**	**Penarth**	**Slipway**
RMAE	0.077	0.253	0.131
RMS (kg/m3)	0.018	0.060	0.052

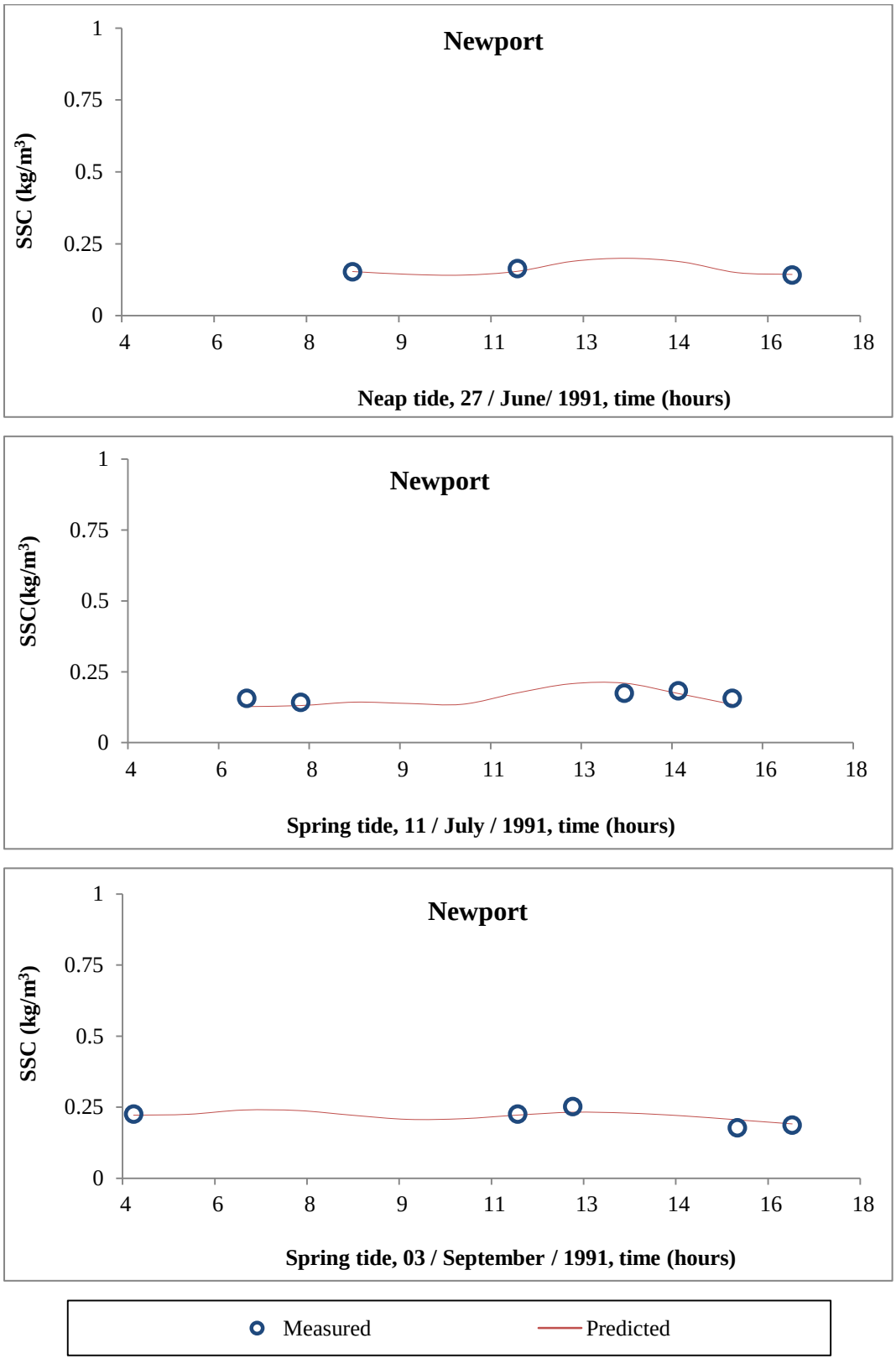

Figure 5.15 Comparison between predicted and observed suspended sediment concentration at Newport for model validation

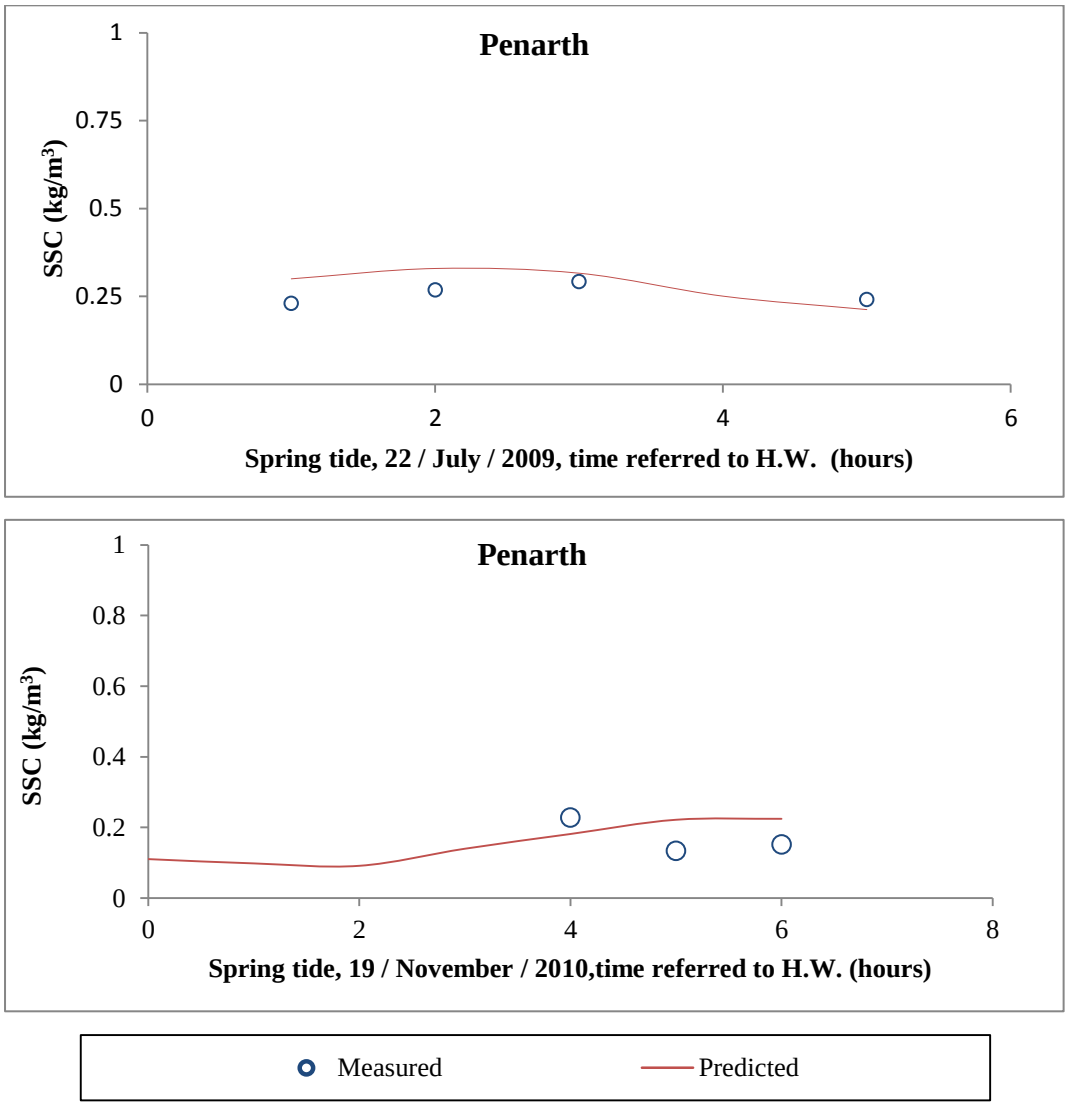

Figure 5.16 Comparison between predicted and observed suspended sediment concentration at Penarth for model validation

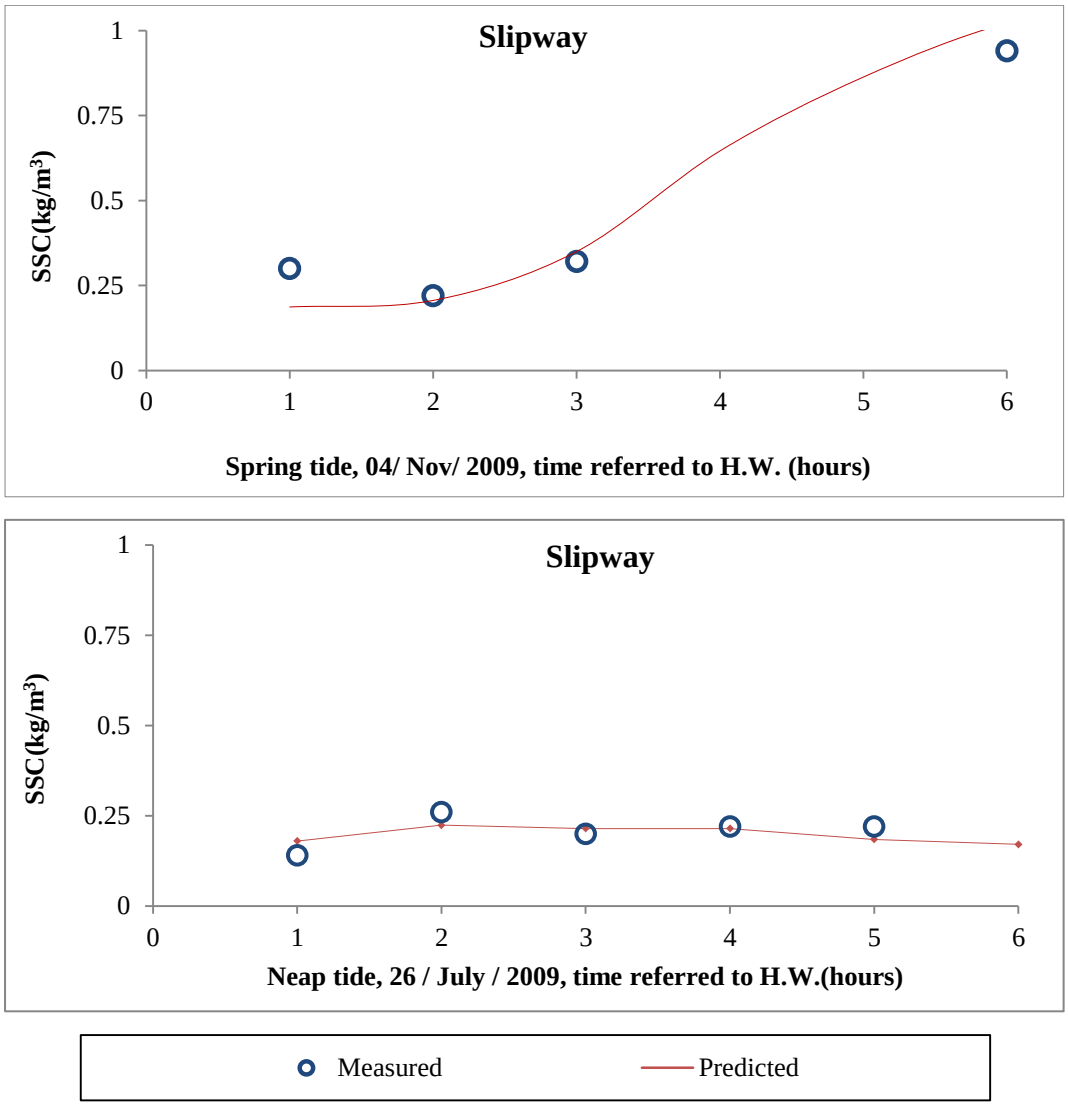

Figure 5.17 Comparison between predicted and observed suspended sediment concentration at Slipway for model validation

5.5 Model refinement and application

After the series of calibration and validation steps carried out across the whole domain (Figure 5.2), the model can be assumed to be ready for simulating the hydrodynamic and suspended sediment transport processes in the Severn Estuary. It was then used in this study to simulate the flocculation processes of cohesive sediment in a more realistic manner by using a refined settling velocity equation derived in laboratory experiments presented in Chapter 3. To do this, the original Delft3D model code was modified to include new settling velocity equations for cohesive sediment, equations (3.13) and (3.16), which were produced via experimental work, as described, shown and discussed in Chapter 3. The model was run for three different scenarios: without flocculation, with the existing flocculation model in Delft3D and with the newly refined flocculation model.

- **Scenario (S1): Modelling excluding flocculation effect**

The model was used without taking account of flocculation processes, and by treating the settling velocity as a constant with a value of 0.1 mm/s. This value was based on experimental results gained by field sample analysis in the laboratory (see Table 3.3).

- **Scenario (S2): Modelling including the existing Delft3D flocculation model**

The model was run with the existing Delft3D flocculation model. However, this model can not be directly used. The settling velocity value at fresh water, the settling velocity value at maximum saline water and a maximum salinity have to be defined first. Laboratory experiment are required first to define these values. The laboratory experiment has been conducted at freshwater of S=0 and at high salinity of 30 ppt. The settling velocity values of sediment at both salinities have been measured using ImageJ software (experiment was presented in Chapter 3). The formulation of the settling velocity as a function of the salinity equation (4.8) was used to predict the settling velocity of flocculated sediment.

- **Scenario (S3): Modelling including the newly refined flocculation model**

The model was run with the new flocculation model implemented in the Delft3D model to represent the settling velocity of the flocculation of cohesive sediment, as observed in the laboratory experiments. The formulation of settling velocity as a function of the salinity and turbulence equations, (3.13) and (3.16), was used to predict the settling velocity.

5.6 Model results and discussion

The first assessment of the refined settling equations model compared computed SSC against observed data. The comparison stage is important to demonstrate that the new equations are sufficiently robust for general application. The assessment of the new settling equation model involved comparing computed SSC from three different scenarios (S1, S2 and S3) with observation data. The computed SSCs were compared against the field data given in Stapleton et al. (2007). The comparisons of modelled SSC values with and without flocculation against observed SSC for the Severn Estuary for the Minehead and Beachley sites are shown in Figure 5.18. There is close agreement between the observed and predicted SSCs. The SSC predicted without flocculation was higher than the observed SSC at the Minehead and Beachley sites, meaning that using a constant settling velocity value gives an overestimation of SSC. The results of the new model at Beachley and Minehead were generally good; a part from for the maximum and minimum observed points (Figure 5.18) but were close to the median values. This is possibly a result of the new flocculation model being developed based on the average settling velocity as discussed in section 3.5.6.

Table 5.10 Comparison of sediment concentrations for three different scenarios (S1: modelling excluding flocculation effect, S2: modelling including the existing Delft3D flocculation model and S3: modelling including the newly refined flocculation model)

Sites	**Minehead**			**Beachley**		
No of obs*.	**26**			**4**		
Scenarios	**S1**	**S2**	**S3**	**S1**	**S2**	**S3**
RMAE	2.210	0.700	0.725	0.609	0.511	0.473
RMS (kg/m3)	0.261	0.109	0.113	0.262	0.292	0.260

* Number of observation points

At Minehead, the new flocculation model (S3) predicted almost 80.2% of sediment concentration compared with 35% for S1 and 80.3 % for S2. The evaluation of predicted and field data was carried out using the RMAE and the RMS analysis (Table 5.10). The RMS values at Minehead ranged from 0.109 kg/m3 to 0.113 kg/m3 in the S2 and S3 scenarios, respectively, where the flocculation model was included. The RMS value at Minehead was 0.261 kg/m3 in the worst scenario, S1, which excluded the flocculation model (Table 5.10). The RMAE values for the three different scenarios indicate that S1 provides a bad prediction of SSC with a RMAE of 2.210, and the S2 and S3 scenarios provide a poor prediction with RMAEs of 0.700 and 0.725. Despite the new and the original flocculation models providing poor predictions of SSC, in relation to the qualification of RMAE suggested by Sutherland (2001) (Table 5.2) the predictions are still much better than the predicted SSC in S1.

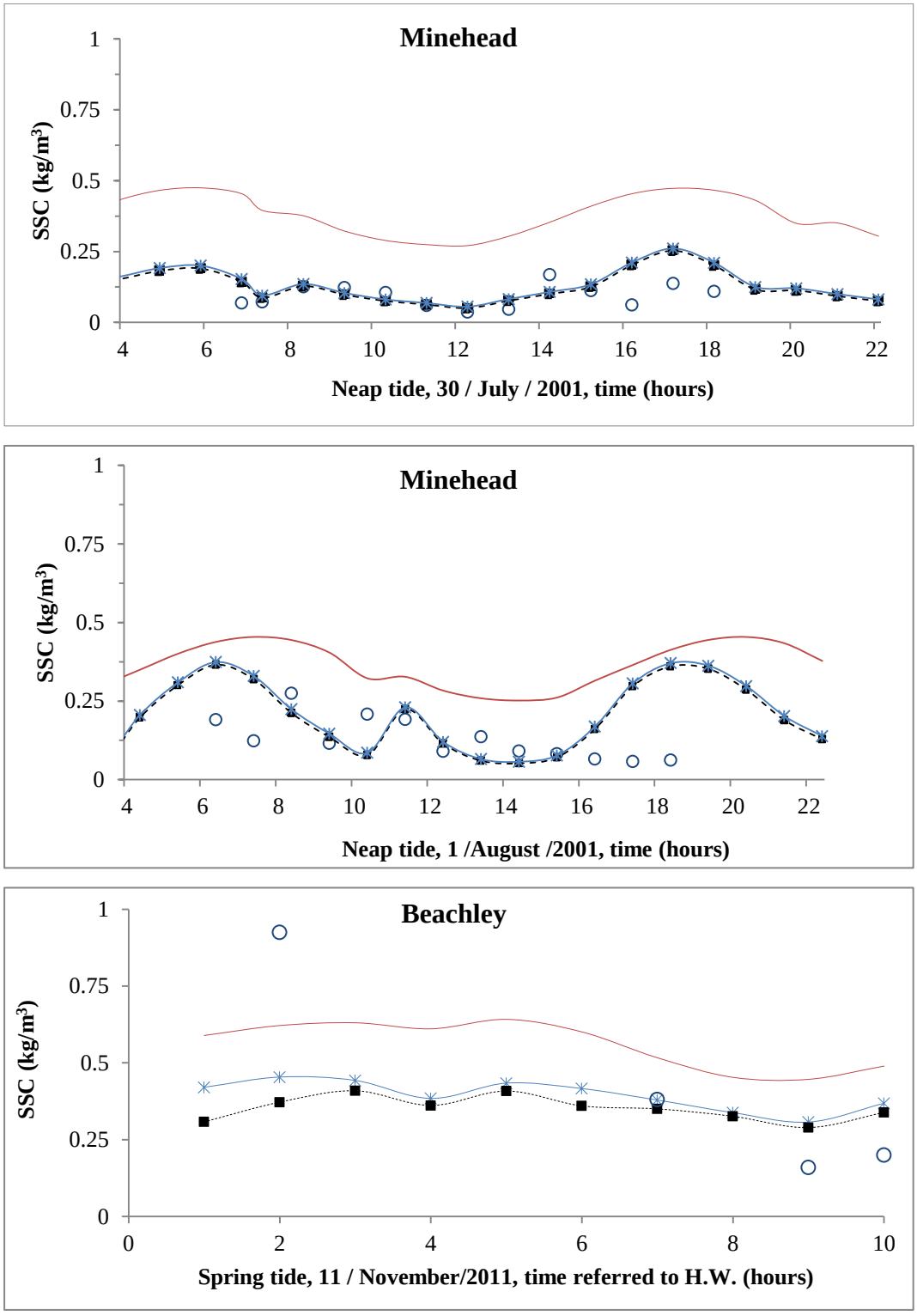

Figure 5.18 Comparison of measured and predicted suspended sediment concentrations at Minehead, Penarth and Beachley for three different scenarios (S1, S2, and S3)

At Beachley, The new flocculation model (S3) predicted almost 88% of suspended sediment concentrations compared with 85% for S1 and 87% for S2. The RMAE values for the three different scenarios indicated that S1, S2 and S3 provide a reasonable prediction of SSC, with RMAEs of 0.609, 0.511 and 0.473. The predicted sediment concentrations when the new flocculation model was included (S3) are more accurate than the case excluding the new flocculation model (S1) and the case including the original flocculation model (S2).

The predicted SSC levels across the Severn Estuary and Bristol Channel with and without the flocculation model are shown in Figure 5.19. It can be seen that the SSC levels are reduced after including the effect of flocculation for both the original and the new flocculation models. The main impacts of flocculation primarily occur in the regions upstream. For example, the predicted SSC at the Beachley site is predicted to decrease from 1.03 kg/m3 for S1 to 0.59 kg/m3 for S3 and to 0.58 kg/m3 for S2. Also, the predicted SSCs close to Newport are 0.82 kg/m3, 0.19 kg/m3 and 0.2 kg/m3 for the three scenarios, respectively. In the Severn Estuary, the predicted SSCs decrease from 0.42 kg/m3 for S1 to 0.34 kg/m3 for S2 and S3 (Figure 5.20).

The sediment concentration that included the effect of flocculation was lower than that not taking into account the effect of flocculation. This occurred because the sediment under different salinity and turbulence conditions flocculated to form biger particles that have a larger settling velocity and thus settle out onto the bed more quickly. This study produced results which corroborate the findings of previous work in this field. Winterwerp (2002) simulated using a flocculation model as a result of turbulence processes for the Ems Estuary, the Netherland. The author concluded that suspended sediment concentration can not be accurately simulated using constant settling velocity value. Also, finding of this study corroborate results of the flocculation model by Baugh and Manning (2007), who found that using a constant settling velocity value in the numerical model can not represent any of the observed SSC at Tamar Estuary (UK).

The new flocculation model agrees best with the measured suspended sediment concentration in the field. Consequently, it can be stated that the new settling velocity equations are a more reliable representation of suspended sediment settling

processes and can be used to more accurately simulate the SSCs including the effects of flocculation in future studies.

The quality of the water environment and cohesive sediment concentrations are closely related. Any under- or overestimation of the SSC levels can impact on water quality predictions for future scenarios like climate change impacts and from tidal renewable energy projects like the Severn Barrage and other tidal renewable energy schemes. As discussed in previous studies, Zhou et al. (2014a) indicated that the proposed Severn Barrage across the Bristol Channel and Severn Estuary could significantly affect the water quality, sediment transport concentration, salinity level and the hydrodynamic parameters e.g flow velocity and water level.

The simulation results indicate that the turbulence effect on flocculation should not be neglected in suspended sediment modelling studies, as observed by Winterwerp (2002) and Baugh and Manning (2007). Although the difference between the new flocculation model and the existing flocculation model in Delft3D is small, the new refined Delft3D model should be used. The main advantage of the new flocculation model is that it can be directly used to simulate the flocculation processes. The disadvantage of using the existing flocculation model in Delft3D is that this model does not include the turbulence processes and the model is only function of salinity. Also, the existing flocculation model in Delft3D can not be directly used, the user has to define the settling velocity value at fresh water, the settling velocity value at maximum saline water and a maximum salinity and laboratory experiment are required first to define these values.

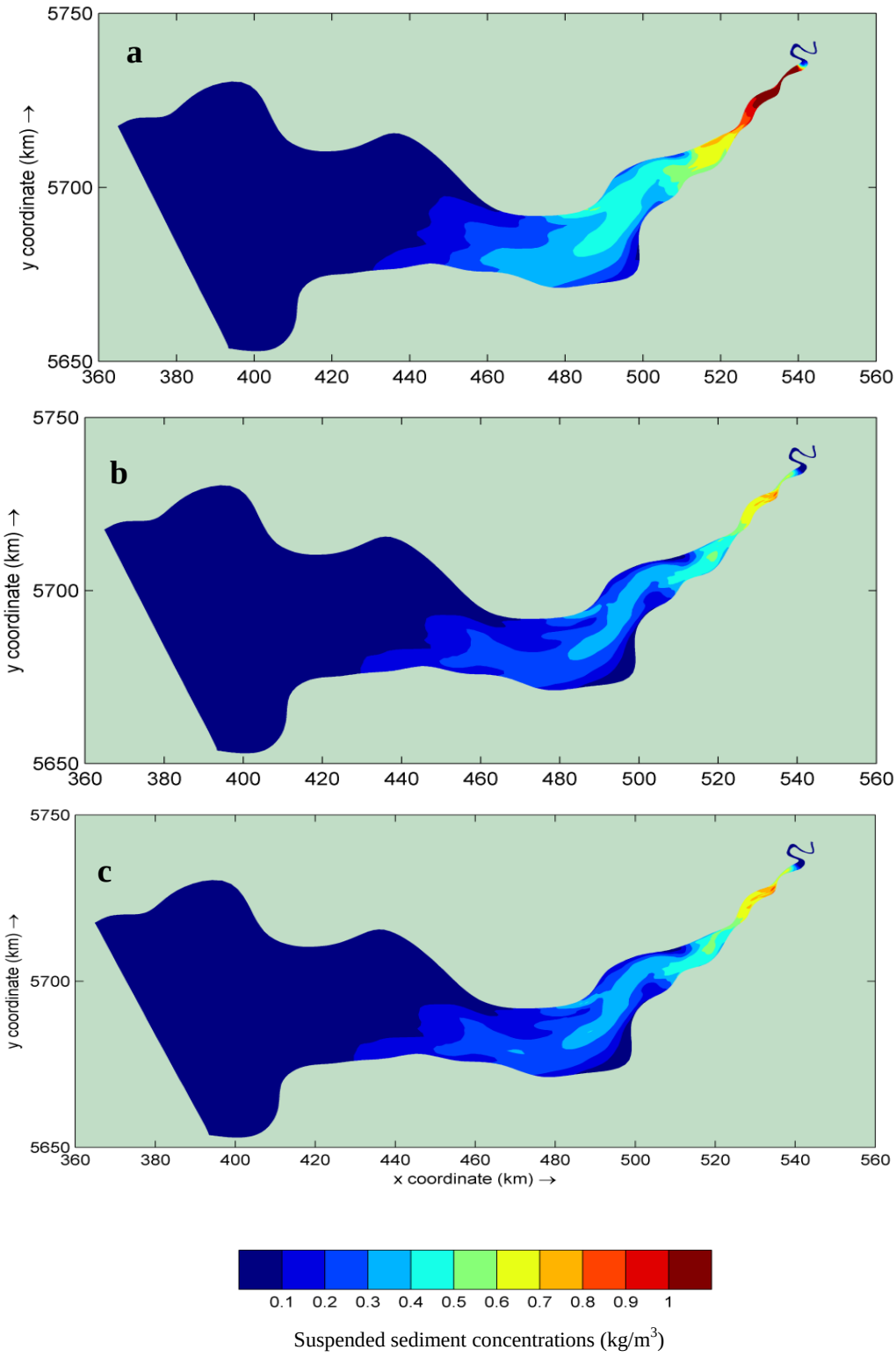

Figure 5.19 Predicted suspended sediment levels at high water spring tide for scenario: (a) S1, (b) S2 and (c) S3

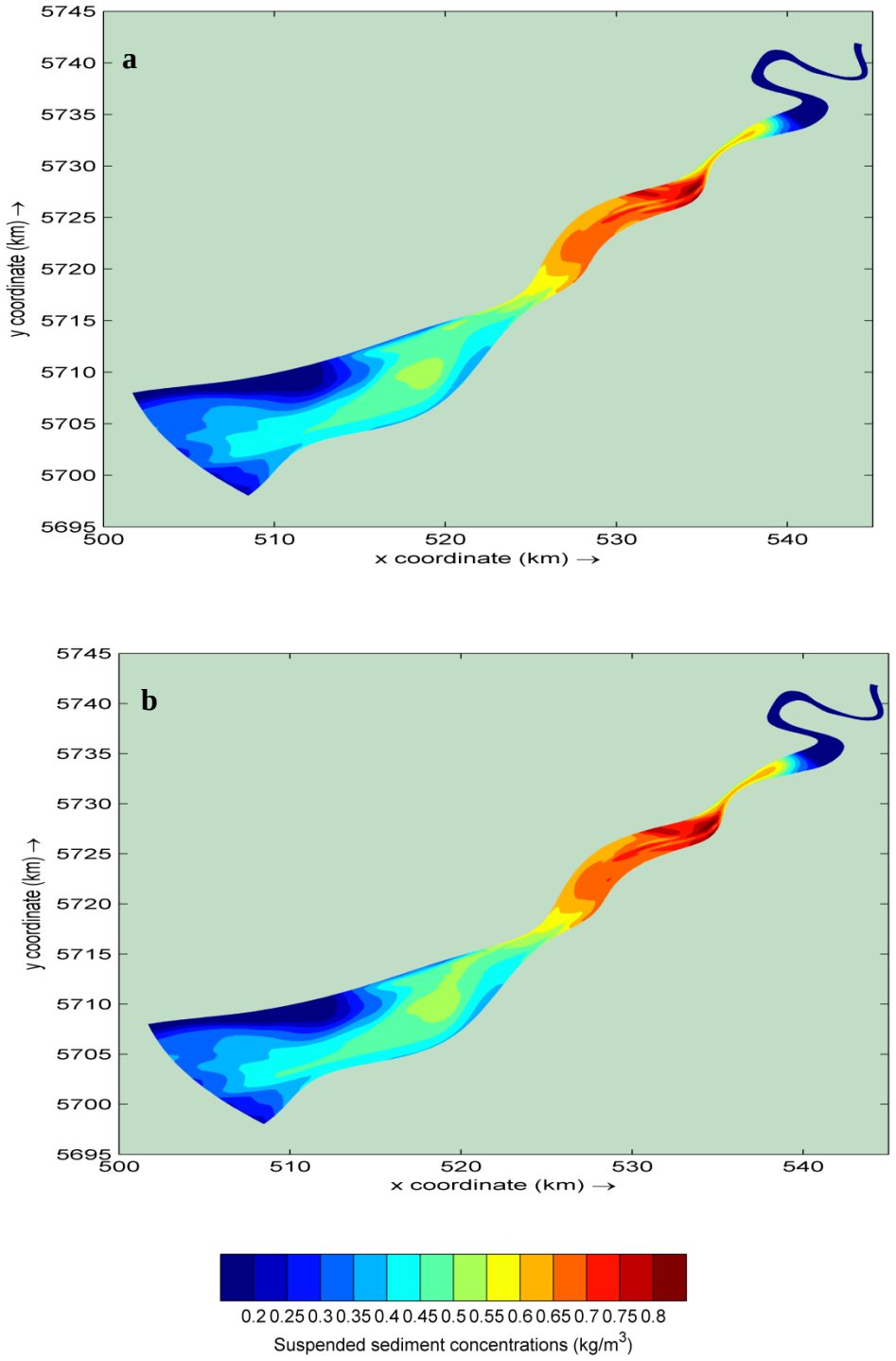

Figure 5.20 Predicted suspended sediment levels at high water spring tide for scenarios :(a) S2 and (b) S3, a zoomed in version of Figure 5.19

5.7 Summary

Based on Delft3D-FLOW, a 3D hydrodynamic and sediment transport model for the Severn Estuary has been set up. In this model the suspended sediment concentration within the water column was linked to the flocculation processes, i.e. suspended sediment concentrations are affected by flocculation of fine sediment particles. The model was applied to predict the suspended sediment concentrations in the Severn Estuary. The model predictions were encouraging, with reasonably good agreement with field measurements at various sites along the estuary. The model results were then compared to the flocculation modelling approach in Delft3D, wherein modelling turbulence induced flocculation or the break-up of sediment flocs is not included. The results showed the new turbulence model's predictions to be in closer agreement with the field data when sediment flocculation processes were included in predicting the suspended sediment concentration in the water column. Thus, for the studies applied to the Severn Estuary the results show that the effects of flocculation of fine sediment were significant when trying to predict the suspended sediment concentrations in the water column. In general, including the new flocculation model successfully better represents the observed suspended sediment distribution throughout the estuary. Overall, the model developed in this study can be regarded as a basic tool for managing the water quality of the Severn Estuary and assessing the impact of human interferences on the system. The model can also be the platform for the fundamental research about the hydro-environmental impact of tidal energy projects and the base for further modelling studies on water quality.

6 Conclusions and recommendations for future work

6.1 Conclusions

The aim of the present study was to assess the potential effects of the hydrodynamic parameters (i.e. salinity, SSC and turbulence) on both floc size and settling velocity under controlled laboratory experiments using suspended sediment samples that were collected from the Severn Estuary. The Severn Estuary was chosen because there is still a lack of understanding regarding the flocculation phenomenon in this estuary (Manning et al. 2010a), which is one of the highly dynamic estuaries in the world. Simple equations were developed from the laboratory experiments to describe the settling velocity of flocs of cohesive sediment in the Severn Estuary as a function of the hydrodynamic and physicochemical parameters (i.e. the turbulent shear stress and the salinity). These equations were implemented into a widely used three dimensional hydrodynamic model, namely Delft3D. The refined numerical model was applied and tested to simulate the flocculation phenomenon in the Severn Estuary.

Although the literature review presented cohesive sediment equations as a function of turbulence, suspended sediment and floc size, which were developed from studies of estuaries around the world, the applicability of these equations may vary from one estuary to another due to different availability and composition of suspended sediment, estuary topography and mineralogy and biological properties of the particles.

The main conclusions of this research can be summarised as follows:

- Floc size and settling velocity are controlled by the interaction between turbulence and salinity at less than 10 ppt. At a salinity either equal to or more than 10 ppt, the floc size and settling velocity were found to be functions only of the turbulent shear stress.
- The maximum floc size increased by 62% as S increased from fresh water to S 2.5 ppt. However, as S increased higher than 2.5 ppt, the maximum floc size decreased by 50%.
- Turbulent shear stresses ranging from 0.57–8.5 N/m^2 caused a breakdown of 67.6% of the floc structure.

- The percentage of large flocs increased by 3% as sediment concentration increased at high salinity of 20 ppt. However, the situation was reversed at lower salinity of 2.5 ppt when the percentage of large flocs decreased by nearly 7% as sediment concentrations increased from 100 to 200 g/m^3
- The settling velocity was found to increased or decreased upon increasing the SSC, and it was further controlled by the salinity. Faster settling velocity occurred when sediment concentration was higher and salinity of 2.5 ppt. By contrast, at salinities of 20, in addition to increasing SSC, it was found that the situation was reversed (i.e. the lower the sediment concentration, the faster the settling velocity).
- The relationships between floc size and turbulent shear stresses and between floc size and salinity were found to be independent of the history of the floc formation.
- Although the experimental results compared favourably with experimental studies from different estuaries, they also confirmed that the method used in this study was successful at both measuring and analysing the floc size and settling velocity, and the developed equations should be considered to more accurately predict both the transport and fate of cohesive sediments than previously understood.
- Delft3D model for the Severn Estuary and Bristol Channel is considered successfully calibrated and validated and can be used for predicting the hydrodynamics and sediment parameters, including water levels, velocities, salinities and SSCs.
- The model predictions were encouraging, with reasonably good agreement being obtained with field measurements at various sites along the Severn Estuary and Bristol Channel.
- The new settling velocity equations derived in laboratory experiments were successfully implemented in Delft3D via FORTRAN DLL.
- Comparisons of predicted suspended sediment levels with measured data showed further improvements in the predictions, when compared with the models both for scenarios with and without flocculation.

- The new turbulence model's predictions were in close agreement with the field data when sediment flocculation processes were included in predicting the suspended sediment concentration in the water column.
- The new flocculation model successfully represents the observed suspended sediment distribution by 86% throughout the estuary.
- The developed model can be regarded as a basic tool for managing the water quality of the Severn Estuary and assessing the impact of human interferences on the system. The model can also be the platform for the fundamental research about the impact of climate change and hydro-environmental impact of tidal energy projects and the base for further modelling studies on water quality.

6.2 Recommendations for future work

This section suggests further future works which would logically follow on from works presented in this study to help improve understanding the flocculation phenomenon in estuaries, and particularly the Severn Estuary. The laboratory experiment in this study was conducted at a turbulence level of 0.57-8.5 N/m^2 and higher, and the equations were developed based on these ranges. However, the intensity was high due to limitation of agitator speed in the laboratory. Therefore, future experimental work should explore the effect of floc size and settling velocity of suspended sediment of the Severn Estuary at low turbulence levels of 0.1–0.5 N/m^2, which are more typical for the estuary. Larger flocs will probably occur, and as the aggregation processes will be instigated in this range.

Floc sizes smaller than 60 μm are not included in the analysis due to light limitations. Therefore, the instrumentation should be improved for future study by using a strong enough light to both detect smaller particles and give the ability to use higher sediment concentrations in the experiment, which will better mimic the field sediment concentration in the Severn Estuary. Also, the biological processes are important parameters in the flocculation processes. More studies are required to determine the impacts of biological activity (e.g. organic matter) on flocculation processes and improve new equations to include its effect. Particular emphasis would be placed on adding bacteria with different levels to provide a significant difference on both floc size and settling velocity

The mixing jar experiments (small scale) should be compared with large-scale flocculation experiments (settling column). Pollutants, including nutrients and heavy metals, can accumulate in sediments after recycling due to physical, chemical and biological processes. Therefore, future studies should investigate a way to link the flocculation and nutrient processes using a numerical model. The suspended sediment was validated using the available sediment concentration from the sampled upstream sections of the Severn Estuary, which resulted in a lack of measured downstream data; therefore, further validation is required for the sediment concentration against data collected at downstream sections.

The discharge of fluvial tributaries should be included in the numerical model to more realistically present salinities values and therefore the flocculation processes. The new settling equations were implemented in Delft3D via FORTRAN DLL. However, floc size is currently not a quantity in Delft3D; therefore, it should be included. This parameter would have offered a better understanding of the flocculation processes in both estuarine and coastal waters. The present model should be tested in other hypotidal estuaries (e.g. the Humber Estuary) before being adopted.

References

Ackroyd, D. R., Bale, A. J., Howland, R. J. M., Knox, S., Millward, G. E. and Morris, A. W. 1986. Distributions and behaviour of dissolved Cu, Zn and Mn in the Tamar Estuary. *Estuarine Coastal and Shelf Science* 23(5), pp. 621-640.

Agrawal, Y. C. and Pottsmith, H. C. 2000. Instruments for particle size and settling velocity observations in sediment transport. *Marine Geology* 168(1–4), pp. 89-114.

Ahmadian, R., Falconer, R. and Lin, B. 2010. Hydro-environmental modeling of proposed Severn barrage, UK. *Proceedings of the Institution of Civil Engineers - Energy* 163(3), pp. 107-117.

Ahmadian, R. and Falconer, R. A. 2012. Assessment of array shape of tidal stream turbines on hydro-environmental impacts and power output. *Renewable Energy* 44(Supplement C), pp. 318-327.

Al-Enezi, E. 2011. *Modelling of phosphorus adsorption processes in estuarine and coastal waters.* PhD Thesis, Cardiff University (UK).

Allen, J. R. L. 1990. The Severn Estuary in southwest Britain: its retreat under marine transgression, and fine-sediment regime. *Sedimentary Geology* 66(1–2), pp. 13-28.

Allersma, E., Hoekstra, A. and Bijker, E. 1967. Transport patterns in the Chao Phya Estuary. *Coastal Engineering*, pp. 632-650.

Baugh, J. V. and Manning, A. J. 2007. An assessment of a new settling velocity parameterisation for cohesive sediment transport modeling. *Continental Shelf Research* 27(13), pp. 1835-1855.

Berhane, I., Sternberg, R. W., Kineke, G. C., Milligan, T. G. and Kranck, K. 1997. The variability of suspended aggregates on the Amazon Continental Shelf. *Continental Shelf Research* 17(3), pp. 267-285.

Berlamont, J., Ockenden, M., Toorman, E. and Winterwerp, J. 1993. The characterisation of cohesive sediment properties. *Coastal Engineering* 21(1–3), pp. 105-128.

Bryant, R. and Williams, D. J. A. 1983. Characteristics of suspended cohesive sediment of the Severn Estuary, U.K. *Canadian Journal of Fisheries and Aquatic Sciences* 40(S1), pp. s96-s101.

Bungartz, H. and Wanner, S. C. 2004. Significance of particle interaction to the modelling of cohesive sediment transport in rivers. *Hydrological Processes* 18(9), pp. 1685-1702.

Burban, P. Y., Lick, W. and Lick, J. 1989. The flocculation of fine-grained sediments in estuarine waters. *Journal of Geophysical Research: Oceans* 94(C6), pp. 8323-8330.

Burchard, H. and Baumert, H. 1998. The formation of estuarine turbidity maxima due to density effects in the salt wedge. A hydrodynamic process study. *Journal of Physical Oceanography* 28(2), pp. 309-321.

Cai, W. J. 2011. Estuarine and coastal ocean carbon paradox: CO2 sinks or sites of terrestrial carbon incineration? *Annual Review of Marine Science* 3, pp. 123-145.

Carpenter, S. R., Caraco, N. F., Correll, D. L., Howarth, R. W., Sharpley, A. N. and Smith, V. H. 1998. Nonpoint pollution of surface waters with phosphorus and nitrogen. *Ecological Applications* 8(3), pp. 559-568.

Cheng, R. T., Casulli, V. and Gartner, J. W. 1993. Tidal, residual, intertidal mudflat (TRIM) model and its applications to San Francisco Bay, California. *Estuarine, Coastal and Shelf Science* 36(3), pp. 235-280.

Cheviet, C., Violeau, D. and Guesmia, M. 2002. Numerical simulation of cohesive sediment transport in the Loire estuary with a three-dimensional model including new parameterisations. *Proceedings in Marine Science* 5, pp. 529-543.

Collins, M. B. 1983. Supply, distribution and transport of suspended sediment in a macrotidal environment: Bristol Channel, U.K. *Canadian Journal of Fisheries and Aquatic Sciences* 40 (S1), pp. s44-s59.

Cross, J., Nimmo-Smith, W. A. M., Torres, R. and Hosegood, P. J. 2013. Biological controls on resuspension and the relationship between particle size and the Kolmogorov length scale in a shallow coastal sea. *Marine Geology* 343, pp. 29-38.

Davies, E. J., Brandvik, P. J., Leirvik, F. and Nepstad, R. 2017. The use of wide-band transmittance imaging to size and classify suspended particulate matter in seawater. *Marine Pollution Bulletin* 115(1), pp. 105-114.

Dobereiner, C. and McManus, J. 1983. Turbidity maximum migration and harbour siltation in the Tay Estuary. *Canadian Journal of Fisheries and Aquatic Sciences* 40(S1), pp. s117-s141.

Dorich, R. A., Nelson, D. W. and Sommers, L. E. 1984. Algal availability of phosphorus in suspended stream sediments of varying particle size. *Journal of Environmental Quality* 13(1), pp. 82-86.

Droppo, I. G. 2001. Rethinking what constitutes suspended sediment. *Hydrological Processes* 15(9), pp. 1551-1564.

Droppo, I. G., Leppard, G. G., Flannigan, D. T. and Liss, S. N. 1997. The freshwater floc: A functional relationship of water and organic and inorganic floc constituents affecting suspended sediment properties. *Water, Air, and Soil Pollution* 99(1-4), pp. 43-54.

Droppo, I. G. and Ongley, E. D. 1994. Flocculation of suspended sediment in rivers of southeastern Canada. *Water Research* 28(8), pp. 1799-1809.

Dunn, I. S., Anderson, L. R. and Kiefer, F. W. 1980. *Fundamentals of geotechnical analysis*. New York: John Wiley & Sons Inc.

Dyer, K. R. 1986. *Coastal and Estuarine Sediment Dynamics,* . John Wiley & Sons.

Dyer, K. R. 1989. Sediment processes in estuaries: future research requirements. *Journal of Geophysical Research: Oceans* 94(C10), pp. 14327-14339.

Dyer, K. R., Cornelisse, J., Dearnaley, M. P., Fennessy, M. J., Jones, S. E., Kappenberg, J., McCave, I. N., Pejrup, M., Puls, W., Van Leussen, W. and Wolfstein, K. 1996. A comparison of in situ techniques for estuarine floc settling velocity measurements. *Journal of Sea Research* 36(1-2), pp. 15-29.

Dyer, K. R. and Manning, A. J. 1999. Observation of the size, settling velocity and effective density of flocs, and their fractal dimensions. *Journal of Sea Research* 41(1–2), pp. 87-95.

Eisma, D. 1986. Flocculation and de-flocculation of suspended matter in estuaries. *Netherlands Journal of Sea Research* 20(2–3), pp. 183-199.

Eisma, D., Bernard, P., Cadée, G. C., Ittekkot, V., Kalf, J., Laane, R., Martin, J. M., Mook, W. G., van Put, A. and Schuhmacher, T. 1991. Suspended-matter particle size in some west-European estuaries; Part II: A review on floc formation and break-up. *Netherlands Journal of Sea Research* 28(3), pp. 215-220.

Eisma, D., Boon, J., Groenewegen, R., Ittekkot, V., Kalf, J. and Mook, W. G. 1983. Observations on macro-aggregates, particle size and organic composition of suspended matter in the Ems estuary. *Mitt. Geol. Paläontol. Inst. Univ. Hamburg* 55, pp. 295-314.

Eisma, D., Schuhmacher, T., Boekel, H., Van Heerwaarden, J., Franken, H., Laan, M., Vaars, A., Eijgenraam, F. and Kalf, J. 1990. A camera and image-analysis system for in situ observation of flocs in natural waters. *Netherlands Journal of Sea Research* 27(1), pp. 43-56.

Etemad-Shahidi, A., Shahkolahi, A. and Liu, W. C. 2010. Modeling of hydrodynamics and cohesive sediment processes in an estuarine system: study case in Danshui river. *Environmental Modeling & Assessment* 15(4), pp. 261-271.

Fennessy, M. J. 1994. *Development and testing of an instrument to measure estuarine floc size and settling velocity in-situ.* PhD Thesis, University of Plymouth.

Fennessy, M. J., Dyer, K. R. and Huntley, D. A. 1994. INSSEV: An instrument to measure the size and settling velocity of flocs in situ. *Marine Geology* 117(1-4), pp. 107-117.

Flory, E. N., Hill, P. S., Milligan, T. G. and Grant, J. 2004. The relationship between floc area and backscatter during a spring phytoplankton bloom. *Deep Sea Research Part I: Oceanographic Research Papers* 51(2), pp. 213-223.

Gao, G., Falconer, R. A. and Lin, B. 2011. Numerical modelling sediment-bacteria interaction processes in the Severn Estuary. *Journal of Water Resource and Protection* 3(1), pp. 22-31.

Gebhardt, A. C., Schoster, F., Gaye-Haake, B., Beeskow, B., Rachold, V., Unger, D. and Ittekkot, V. 2005. The turbidity maximum zone of the Yenisei River

(Siberia) and its impact on organic and inorganic proxies. *Estuarine, Coastal and Shelf Science* 65(1), pp. 61-73.

Geyer, W. R., Hill, P. S. and Kineke, G. C. 2004. The transport, transformation and dispersal of sediment by buoyant coastal flows. *Continental Shelf Research* 24(7), pp. 927-949.

Gibbs, R. J. 1985. Estuarine flocs: their size, settling velocity and density. *Journal of Geophysical Research: Oceans* 90(C2), pp. 3249-3251.

Gibbs, R. J. and Konwar, L. 1986. Coagulation and settling of Amazon River suspended sediment. *Continental Shelf Research* 6(1-2), pp. 127-149.

Gratiot, N. and Manning, A. J. 2004. An experimental investigation of floc characteristics in a diffusive turbulent flow. *Journal of Coastal Research*, pp. 105-113.

Harries, T., Brammer, J., Bockelmann-Evans, B. N. and Kwan, A. S. K. 2013. Quantification and visualisation of blockage effects for a savonius type turbine using particle image velocimetry. In: *35th IAHR World Congress. Presented at the IAHR World Congress, Chengdu, China.*

Harrison, R. M. 2007. *Principles of Environmental Chemistry*. Royal Society of Chemistry.

Hjulström, F. 1935. *Studies of the morphological activity of rivers as illustrated by the river Fyris.* PhD Thesis, University of Uppsala.

Ittekkot, V. 1988. Global trends in the nature of organic matter in river suspensions. *Nature* 332(6163), pp. 436-438.

Johansen, C. 1998. *Dynamics of cohesive sediment.* PhD Thesis, University of Aalborg.

Jonas, P. J. C. and Millward, G. E. 2010. Metals and nutrients in the Severn Estuary and Bristol Channel: Contemporary inputs and distributions. *Marine Pollution Bulletin* 61(1–3), pp. 52-67.

Kadiri, M., Bockelmann-Evans, B., Zhou, J. and Falconer, R. 2014. Water quality impacts of a tidal barrage in the Severn Estuary,UK. In: *10th International Symposium on Ecohydraulics.* Trondheim, Norway.

Keyvani, A. and Strom, K. 2014. Influence of cycles of high and low turbulent shear on the growth rate and equilibrium size of mud flocs. *Marine Geology* 354(Supplement C), pp. 1-14.

Kirby, R. 2010. Distribution, transport and exchanges of fine sediment, with tidal power implications: Severn Estuary, UK. *Marine pollution bulletin* 61(1-3), pp. 21-36.

Knowles, S. C. and Wells, J. T. 1998. In situ aggregate analysis camera (ISAAC): A quantitative tool for analyzing fine-grained suspended material. *Limnology and Oceanography* 43(8), pp. 1954-1962.

Kolmogorov, A. N. 1991. Dissipation of Energy in the locally isotropic turbulence. *Proceedings: Mathematical and Physical Sciences* 434(1890), pp. 15-17.

Kranck, K., Petticrew, E., Milligan, T. G. and Droppo, I. G. 1993. In situ particle size distributions resulting from flocculation of suspended sediment. In: Mehta, A.J. ed. *Nearshore and Estuarine Cohesive Sediment Transport*.

Kranenburg, C. 1994. The fractal structure of cohesive sediment aggregates. *Estuarine, Coastal and Shelf Science* 39(6), pp. 451-460.

Krone, R. B. 1962. *Flume studies of the transport of sediment in estuarial shoaling processes; final report. Hydraulic Engineering Laboratory and Sanitary Engineering Research Laboratory*. California: University of Berkeley.

Lafite, R. 2001. *Impact de la dynamique tidale sur le transfert de sédiments fins.* PhD Thesis, Université de Rouen.

Lang, G., Schubert, R., Markofsky, M., Fanger, H. U., Grabemann, I., Krasemann, H. L., Neumann, L. J. R. and Riethmüller, R. 1989. Data interpretation and numerical modeling of the mud and suspended sediment experiment 1985. *Journal of Geophysical Research: Oceans* 94(C10), pp. 14381-14393.

Le Bris, H. and Glémarec, M. 1996. Marine and brackish ecosystems of south Brittany (Lorient and Vilaine Bays) with particular reference to the effect of the turbidity maxima. *Estuarine, Coastal and Shelf Science* 42(6), pp. 737-753.

Le Hir, P., Ficht, A., Silva Jacinto, R., Lesueur, P., Dupont, J. P., Lafite, R., Brenon, I., Thouvenin, B. and Cugier, P. 2001. Fine sediment transport and accumulations at the mouth of the Seine estuary (France). *Estuaries* 24(6), pp. 950-963.

Liang, D., Wang, X., Bockelmann-Evans, B. N. and Falconer, R. A. 2013. Study on nutrient distribution and interaction with sediments in a macro-tidal estuary. *Advances in Water Resources* 52, pp. 207-220.

Lick, W., Huang, H. and Jepsen, R. 1993. Flocculation of fine-grained sediments due to differential settling. *Journal of Geophysical Research: Oceans* 98(C6), pp. 10279-10288.

Lintern, D. G. 2003. *Influences of flocculation on bed properties for fine-grained cohesive sediment.* PhD Thesis, Oxford University.

Maggi, F. 2005. *Flocculation dynamics of cohesive sediment.* PhD Thesis, University of Technology, Delft.

Maggi, F., Mietta, F. and Winterwerp, J. C. 2007. Effect of variable fractal dimension on the floc size distribution of suspended cohesive sediment. *Journal of Hydrology* 343(1), pp. 43-55.

Maldiney, M. A. and Mouchel, J. M. 1996. In situ video recording of suspended flocs. *Journal of Sea Research* 36(1–2), pp. 87-91.

Manning, Langston, W. J. and Jonas, P. J. C. 2010a. A review of sediment dynamics in the Severn Estuary: Influence of flocculation. *Marine Pollution Bulletin* 61(1), pp. 37-51.

Manning, A., Martens, C., De Mulder, T., Vanlede, J., Winterwerp, J., Ganderton, P. and Graham, G. 2007. Mud floc observations in the turbidity zone of the Scheldt estuary during neap tides. *Journal of Coastal Research* (Special issue 50), pp. 832-836

Manning, A. J. 2001. *A study of the effect of turbulence on the properties of flocculated mud.* PhD Thesis, University of plymouth.

Manning, A. J. 2004a. *The development of new algorithms to parameterise the mass settling flux of flocculated estuarine sediments. HR Wallingford Ltd (UK) Technical Report No.TR 145*

Manning, A. J. 2004b. Observations of the properties of flocculated cohesive sediment in three western European estuaries. *Journal of Coastal Research*, pp. 70-81.

Manning, A. J. 2004c. The observed effects of turbulence on estuarine flocculation. *Journal of coastal research*, pp. 90-104.

Manning, A. J., Baugh, J. V., Spearman, J. R. and Whitehouse, R. J. S. 2010b. Flocculation settling characteristics of mud: sand mixtures. *Ocean Dynamics* 60(2), pp. 237-253.

Manning, A. J. and Dyer, K. R. 1999. A laboratory examination of floc characteristics with regard to turbulent shearing. *Marine Geology* 160(1–2), pp. 147-170.

Manning, A. J. and Dyer, K. R. 2007. Mass settling flux of fine sediments in Northern European estuaries: Measurements and predictions. *Marine Geology* 245(1–4), pp. 107-122.

Manning, A. J., Dyer, K. R., Lafite, R. and Mikes, D. 2004. Flocculation measured by video based instruments in the Gironde Estuary during the European commission SWAMIEE project. *Journal of Coastal Research*, pp. 58-69.

Manning, A. J. and Schoellhamer, D. H. 2013. Factors controlling floc settling velocity along a longitudinal estuarine transect. *Marine Geology* 345, pp. 266-280.

Manning, A. J., Schoellhamer, D. H., Mehta, A. J., Nover, D. and Schladow, S. G. 2010c. Video measurements of flocculated sediment in lakes and estuaries in the USA. In: *Proceedings of the Joint Federal Interagency Conference on Sedimentation and Hydrologic Modeling, Riviera Hotel, Las Vegas, Nevada.* USA, 27th June–1st July 2010.

Mantovanelli, A. and Ridd, P. V. 2008. SEDVEL: An underwater balance for measuring in situ settling velocities and suspended cohesive sediment concentrations. *Journal of Sea Research* 60(4), pp. 235-245.

Markussen, T. N. and Andersen, T. J. 2013. A simple method for calculating in situ floc settling velocities based on effective density functions. *Marine Geology* 344, pp. 10-18.

McCave, I. N. 1984. Size spectra and aggregation of suspended particles in the deep ocean. *Deep Sea Research Part A. Oceanographic Research Papers* 31(4), pp. 329-352.

Mclntosh, H. 2010. *Sediment nutrient interaction in estuarine waters.* Master Thesis, Cardiff university.

Mehta, A. J. 2014. *An introduction to hydraulics of fine sediment transport*. World Scientific.

Mhashhash, A., Bockelmann-Evans, B. and Pan, S. 2017. Effect of hydrodynamics factors on sediment flocculation processes in estuaries. *Journal of Soils and Sediments*.

Mhashhash, A., Bockelmann-Evans, B. and Pan, S. 2018. A new settling velocity equation for cohesive sediment based on experimental analysis. *Journal of Ecohydraulics*.

Mhashhash, A., Bockelmann-Evans, B. N. and Pan, S. 2016. Effect of hydrodynamics factors on flocculation processes in estuaries. In: *4th IAHR European Congress.* Liege, Belgium, 27-29 July 2016.

Mietta, F., Chassagne, C., Manning, A. J. and Winterwerp, J. C. 2009. Influence of shear rate, organic matter content, pH and salinity on mud flocculation. *Ocean Dynamics* 59(5), pp. 751-763.

Migniot, C. 1968. Etude des propriétés physiques de différents sédiments très fins et de leur comportement sous des actions hydrodynamiques. . *La houille blanche* 7, pp. 591-620.

Mikes, D., R. Verney, R. Lafite and M. Belorgey. 2004. Controlling factors in estuarine flocculation processes : experimental results with material from the Seine Estuary, Northwestern France. *Journal of Coastal Research*, pp. 82-89.

Mikkelsen, O. and Pejrup, M. 2001. The use of a LISST-100 laser particle sizer for in-situ estimates of floc size, density and settling velocity. *Geo-Marine Letters* 20(4), pp. 187-195.

Mikkelsen, O. A., Hill, P. S. and Milligan, T. G. 2007. Seasonal and spatial variation of floc size, settling velocity, and density on the inner Adriatic Shelf (Italy). *Continental Shelf Research* 27(3), pp. 417-430.

Milligan, T. G. 1996. In situ particle (floc) size measurements with the benthos 373 plankton silhouette camera. *Journal of Sea Research* 36(1–2), pp. 93-100.

Mitchell, S. B. 2013. Turbidity maxima in four macrotidal estuaries. *Ocean & Coastal Management* 79, pp. 62-69.

Mohapatra, P., Chandra, V. and Nestmann, F. 2012. Effect of flow depth, ions, and salinity on suspended sediment concentration. *Journal of Hydraulic Engineering* 138(4), pp. 348-352.

Moody, J. A., Smith, J. D. and Ragan, B. W. 2005. Critical shear stress for erosion of cohesive soils subjected to temperatures typical of wildfires. *Journal of Geophysical Research: Earth Surface* 110(F1).

Morris, A. W., Allen, J. I., Howland, R. J. M. and Wood, R. G. 1995. The estuary plume zone: source or sink for land-derived nutrient discharges? *Estuarine, Coastal and Shelf Science* 40(4), pp. 387-402.

Nasser, M. S. and Twaiq, F. A. 2011. An experimental study of the relationship between settling flocs and eroded flocs of kaolinite in aqueous media. *Chemical Engineering Research and Design* 89(6), pp. 768-776.

Neill, S. P. 2009. A numerical study of lateral grain size sorting by an estuarine front. *Estuarine, Coastal and Shelf Science* 81(3), pp. 345-352.

Nichols, M. M. 1984. Fluid mud accumulation processes in an estuary. *Geo-Marine Letters* 4(3), pp. 171-176.

Owen, M. W. 1976. *Determination of the settling velocities of cohesive muds*. Report no. IT 161, Hydraulics Research Station, Wallingford, UK.

Parker, W. R. and Kirby, R. 1982. Sources and transport patterns of sediment in the inner Bristol Channel and Severn Estuary. In: *Severn Barrage: Proceedings of a symposium organized by the Institution of Civil Engineers.* Thomas Telford, London, 8-9 October 1981 pp. 181–194.

Partheniades, E. 1965. Erosion and deposition of cohesive soils. *Journal of the Hydraulics Division* 91(1), pp. 105–139.

Partheniades, E. 1971. Erosion and deposition of cohesive materials. *River mechanics* 2, pp. 25-91.

Pejrup, M., Larsen, M. and Edelvang, K. 1997. A fine-grained sediment budget for the Sylt-Rømø tidal basin. *Helgoländer Meeresuntersuchungen* 51, pp. 253–268.

Pejrup, M. and Mikkelsen, O. A. 2010. Factors controlling the field settling velocity of cohesive sediment in estuaries. *Estuarine, Coastal and Shelf Science* 87(2), pp. 177-185.

Portela, L. I., Ramos, S. and Teixeira, A. T. 2013. Effect of salinity on the settling velocity of fine sediments of a harbour basin. *Journal of Coastal Research* 65(2), pp. 1188-1193.

Robins, P. E., Lewis, M. J., Simpson, J. H., Howlett, E. R. and Malham, S. K. 2014. Future variability of solute transport in a macrotidal estuary. *Estuarine, Coastal and Shelf Science* 151(Supplement C), pp. 88-99.

Robins, P. E., Neill, S. P. and Giménez, L. 2012. A numerical study of marine larval dispersal in the presence of an axial convergent front. *Estuarine, Coastal and Shelf Science* 100(Supplement C), pp. 172-185.

Robins, P. E., Skov, M. W., Lewis, M. J., Giménez, L., Davies, A. G., Malham, S. K., Neill, S. P., McDonald, J. E., Whitton, T. A., Jackson, S. E. and Jago, C. F. 2016. Impact of climate change on UK estuaries: A review of past trends and potential projections. *Estuarine, Coastal and Shelf Science* 169(Supplement C), pp. 119-135.

Serra, T. and Casamitjana, X. 1998. Structure of the aggregates during the process of aggregation and breakup under a shear flow. *Journal of Colloid and Interface Science* 206(2), pp. 505-511.

Serra, T., Colomer, J. and Casamitjana, X. 1997. Aggregation and breakup of particles in a shear flow. *Journal of Colloid and Interface Science* 187(2), pp. 466-473.

Shi, Z., Zhou, H. J., Eittreim, S. L. and Winterwerp, J. C. 2003. Settling velocities of fine suspended particles in the Changjiang Estuary, China. *Journal of Asian Earth Sciences* 22(3), pp. 245-251.

Smithson, P., Addison, K. and Atkinson, K. 2002. *Fundamentals of the physical environment*. Routledge, London.

Soulsby, R. 1997. *Dynamics of marine sands: a manual for practical applications*. Thomas Telford.

Soulsby , R. L., Manning , A. J., Spearman , J. and Whitehouse , R. J. 2013. Settling velocity and mass settling flux of flocculated estuarine sediments. *Marine Geology* 339, pp. 1-12.

Spearman, J. R., Manning, A. J. and Whitehouse, R. J. S. 2011. The settling dynamics of flocculating mud and sand mixtures: part 2—numerical modelling. *Ocean Dynamics* 61(2), pp. 351-370.

Stapleton, C. M., Wyer, M. D., Kay, D., Bradford, M., Humphrey, N., Wilkinson, J., Lin, B., Yang, Y., Falconer, R. A., Watkins, J., Francis, C. A., Crowther, J., Paul, N. D., Jones, K. and & McDonald, A. T. 2007. Fate and transport of particles in estuaries, Volume IV: Numerical modelling for bathing water enterococci estimation in the Severn estuary. Environment Agency Science Report SC000002/SR4, Bristol.

Sternberg, R. W., Berhane, I. and Ogston, A. S. 1999. Measurement of size and settling velocity of suspended aggregates on the northern California continental shelf. *Marine Geology* 154(1–4), pp. 43-53.

Sutherland, B. R., Barrett, K. J. and Gingras, M. K. 2015. Clay settling in fresh and salt water. *Environmental Fluid Mechanics* 15(1), pp. 147-160.

Sutherland, J. 2001. COSMOS modeling and the development of model performance statistics. *TR121-EC MAST Project no MAS3–CT97–0086,HR Wallingford, UK*.

Syvitski, J. P. M., Asprey, K. W. and Leblanc, K. W. G. 1995. In-situ characteristics of particles settling within a deep-water estuary. *Deep Sea Research Part II: Topical Studies in Oceanography* 42(1), pp. 223-256.

Thill, S., Moustier, S., Garnier, J. M., Estournel, C., Naudin, J. J. and Bottero, J. Y. 2001. Evolution of particle size and concentration in the Rhône river mixing zone : influence of salt flocculation. *Continental Shelf Research* 21, pp. 2127-2140.

Thompson, J., Cassidy, R., Doody, D. G. and Flynn, R. 2014. Assessing suspended sediment dynamics in relation to ecological thresholds and sampling strategies in two Irish headwater catchments. *Science of the Total Environment* 468, pp. 345-357.

Thomsen, L. and Gust, G. 2000. Sediment erosion thresholds and characteristics of resuspended aggregates on the western European continental margin. *Deep Sea Research Part I: Oceanographic Research Papers* 47(10), pp. 1881-1897.

Thouy, R. and Jullien, R. 1996. Structure factors for fractal aggregates built off-lattice with tunable fractal dimension. *Journal de Physique I* 6(10), pp. 1365-1376.

Tombácz, E. and Szekeres, M. 2004. Colloidal behavior of aqueous montmorillonite suspensions: the specific role of pH in the presence of indifferent electrolytes. *Applied Clay Science* 27(1), pp. 75-94.

Tsai, C.-H., Iacobellis, S. and Lick, W. 1987. Flocculation of fine-grained lake sediments due to a uniform shear stress. *Journal of Great Lakes Research* 13(2), pp. 135-146.

Uncles, R. J. and Stephens, J. A. 1993. The freshwater-saltwater interface and its relationship to the turbidity maximum in the Tamar Estuary, United Kingdom. *Estuaries* 16(1), pp. 126-141.

Uncles, R. J., Stephens, J. A. and Smith, R. E. 2002. The dependence of estuarine turbidity on tidal intrusion length, tidal range and residence time. *Continental Shelf Research* 22(11), pp. 1835-1856.

Van der Lee, W. T. B. 2000. Temporal variation of floc size and settling velocity in the Dollard estuary. *Continental Shelf Research* 20(12), pp. 1495-1511.

Van Leussen, W. 1988. Aggregation of particles, settling velocity of mud flocs a review.*Physical processes in estuaries*. Berlin, Heidelberg: Springer Berlin Heidelberg, pp. 347-403.

Van Leussen, W. 1994. *Estuarine macroflocs and their role in fine-grained sediment transport.* PhD Thesis, University of Utrecht.

Van Leussen, W. 1996. The RWS field settling tube. *Journal of Sea Research* 36(1-2), pp. 83-86.

Van Leussen, W. 1997. The Kolmogorov microscale as a limiting value for the floc sizes of suspended fine-grained sediments in estuaries. *Cohesive Sediments*, pp. 45-62.

Van Leussen, W. 1999. The variability of settling velocities of suspended fine-grained sediment in the Ems estuary. *Journal of Sea Research* 41(1–2), pp. 109-118.

Van Leussen, W. and Cornelisse, J. M. 1993. The determination of the sizes and settling velocities of estuarine flocs by an underwater video system. *Netherlands Journal of Sea Research* 31(3), pp. 231-241.

Van Leussen, W. and Cornelisse, J. M. 1996. The underwater video system VIS. *Journal of Sea Research* 36(1–2), pp. 77-81.

Van Rijn, L. C. 1993. *Principles of sediment transport in rivers, estuaries, and coastal seas*. Aqua publications Amsterdam.

Verney, R. 2006. *Processus de controle de la dynamique des sediments cohesifs; mesures in situ, experimentales et modelisation; application a l'estuaire de la Seine.* PhD thesis, Université de Rouen.

Verney, R., Lafite, R. and Brun-Cottan, J. C. 2009. Flocculation potential of estuarine particles: The importance of environmental factors and of the spatial and seasonal variability of suspended particulate matter. *Estuaries and Coasts* 32(4), pp. 678-693.

Villaret, C. and Davies, A. G. 1995. Modeling Sediment-Turbulent Flow Interactions. *Applied Mechanics Reviews* 48(9), pp. 601-609.

Violeau, D., Bourban, S., Cheviet, C., Markofsky, M., Petersen, O., Roberts, W., Spearman, J., Toorman, E., Vested, H. J. and Weilbeer, H. 2002. Numerical simulation of cohesive sediment transport : intercomparison of several numerical models.*Proceedings in Marine Science*. Vol. 5. Elsevier, pp. 75-89.

Waite, R. 2010. *Phosphorus in the Severn estuary and the environmental implications of the proposed Severn barrage.* MSc Thesis, cardiff university.

Walstra, D. J., Van Rijn, L. C., Blogg, H. and Van Ormondt, M. 2001. Evaluation of a hydrodynamic area model based on the Coast3D data at Teignmouth 1999. In: *Proceedings of coastal dynamics 2001 conference.* pp. 1-D4.

Wang, D., Wu, R., Jiang, Y. and Chow, C. W. K. 2011. Characterization of floc structure and strength: Role of changing shear rates under various coagulation mechanisms. *Colloids and Surfaces A: Physicochemical and Engineering Aspects* 379(1–3), pp. 36-42.

Wang, X. H. and Andutta, F. P. 2013. Sediment transport dynamics in ports, estuaries and other coastal environments.*Sediment Transport Processes and Their Modelling Applications*. Rijeka: InTech.

Wang, Y., Shen, Z., Niu, J. and Liu, R. 2009. Adsorption of phosphorus on sediments from the Three-Gorges Reservoir (China) and the relation with sediment compositions. *Journal of Hazardous Materials* 162(1), pp. 92-98.

Wellershaus, S. 1981. Turbidity maximum and mud shoaling in the Weser estuary. *Archiv fur Hydrobiologie* 92(2), pp. 161–198.

Whitehead, P. G., Wilby, R. L., Battarbee, R. W., Kernan, M. and Wade, A. J. 2009. A review of the potential impacts of climate change on surface water quality. *Hydrological Sciences Journal* 54(1), pp. 101-123.

Whitehouse, R., Soulsby, R. L., Roberts, W. and Mitchener, H. 2000. *Dynamics of estuarine muds*. London: Thomas Telford.

Winterwerp, J. C. 1998. A simple model for turbulence induced flocculation of cohesive sediment. *Journal of Hydraulic Research* 36(3), pp. 309-326.

Winterwerp, J. C. 1999. *On the dynamics of high-concentrated mud suspension.* PhD Thesis, University of Technology.

Winterwerp, J. C. 2002. On the flocculation and settling velocity of estuarine mud. *Continental Shelf Research* 22(9), pp. 1339-1360.

WL|Delft Hydraulics. 2014. *User manual Delft-3D flow*. Delft, the Netherlands.

Wollast, R. 1988. The Scheldt Estuary.*Pollution of the North Sea: an Assessment*. Berlin, Heidelberg: Springer, pp. 183-193.

Xu, B., Burnett, W., Dimova, N., Diao, S., Mi, T., Jiang, X. and Yu, Z. 2013. Hydrodynamics in the Yellow River Estuary via radium isotopes: Ecological perspectives. *Continental Shelf Research* 66(Supplement C), pp. 19-28.

Zhou, J., Falconer, R. A. and Lin, B. 2014a. Refinements to the EFDC model for predicting the hydro-environmental impacts of a barrage across the Severn Estuary. *Renewable Energy* 62, pp. 490-505.

Zhou, J., Pan, S. and Falconer, R. A. 2014b. Effects of open boundary location on the far-field hydrodynamics of a Severn Barrage. *Ocean Modelling* 73, pp. 19-29.

Zhou, J., Pan, S. and Falconer, R. A. 2014c. Optimization modelling of the impacts of a Severn Barrage for a two-way generation scheme using a Continental Shelf model. *Renewable Energy* 72(Supplement C), pp. 415-427.

Zhu, Z., Yu, J., Wang, H., Dou, J. and Wang, C. 2015. Fractal dimension of cohesive sediment flocs at steady state under seven shear flow conditions. *Water* 7(8), p. 4385.